

Estimation of Microwave Power Margin Losses Due to Earth's Atmosphere and Weather in the Frequency Range of 3–30 GHz

Prepared for the United States Air Force Spectrum Efficient Technologies for Test and Evaluation Advanced Range Telemetry Edwards Air Force Base, California

Christian M. Ho, Charles Wang, Kris Angkasa, and Kelly Gritton

January 20, 2004

Abstract:

This is the final report for the Air Force contract "Estimation of Microwave Power Margin Losses due to Earth's Atmosphere and Weather in the Frequency Range of 3–30 GHz " (JPL task plan No. 81-6775). The goal of this study has been to perform an evaluation of radio wave propagation losses at SHF band by using available propagation models and several benchmark scenarios. The Department of Defense is exploring the possibility of occupying the microwave range of 3–30 GHz to increase bandwidth. As frequency increases, crucial changes to link power margins must be examined. Dominantly responsible for additional losses to the free space loss in the transmitted signal are atmospheric absorption, clouds, fog, and precipitation, as well as scintillation/multipath at low elevation angles. All of these losses due to the atmosphere at the studied frequency range cannot be neglected. The free space Friis Equation has been modified to add an additional term, which includes all atmospheric attenuation and fading effects. First, we completed an extensive literature search on SHF band propagation studies. Microwave propagation models from the International Telecommunication Union (ITU) are employed for this study. All attenuation figures are estimated as a function of weather condition (percent of time) and radio wave frequencies. Through detailed calculation and case study, analysis of the microwave attenuations propagating in both line of sight and trans-horizon are performed. There are significant differences in anomalous mode (ducting) propagation features between the east and the west coastal receiving stations. Terrain profiles along all directions of interest within the coastal areas and inland areas for four benchmark cases, have been analyzed in detail. Through this study, we find that at high elevation angles, atmospheric gaseous absorption and rain attenuation are the two dominant factors at SHF band. While the atmospheric gaseous absorption plays a significant role under a clear weather, heavy rainfalls can cause several tens of dB loss for a 100-km path through the rain. At very low elevation angles ($< 5^\circ$), atmospheric scintillation/multipath fading becomes a very important factor. At about 50% of time, radio signals can propagate through an elevated ducting layer above the ocean up to thousand kilometers to the Pt. Mugu receiving stations. All results from this study have been plotted and tabulated as figures in this final report.

Report Contents

This report will contain the following sections:

- I. Introduction
 - 1.1 Background
 - 1.2 Objectives
- II. Analysis
 - 2.1 General Propagation Theory
 - 2.1.1 Free Space Loss: Friis Equation
 - 2.1.2 Modification of Friis Equation
 - 2.1.3 Elevation Angle Dependence
 - 2.2 Microwave Propagation Models through the Atmospheric Medium
 - 2.2.1 Atmospheric Absorption
 - 2.2.2 Attenuation by Rainfall
 - 2.2.3 Attenuation due to Clouds and Fog
 - 2.2.4 Attenuation due to Scintillation/Multipaths at Low Elevation Angles
 - 2.2.5 Anomalous Propagation Modes
- III. Benchmark Case Study
 - 3.1 Benchmark Case Scenarios
 - 3.2 Terrain Profile Analysis
 - 3.3 Radio Parameters and Calculation
- IV. Summary of Study Results
- V. Potential Follow-on Study
- VI. Figure Captions and Plots
- VII. Appendixes

I. Introduction

1.1 Background:

The Department of Defense (DoD) has tasked the Advanced Range Telemetry Project (ARTP) to study the impact of augmenting some aeronautical telemetry (AT) operations from one frequency range to another. Most AT links operate in the frequency range of 1.4–2.4 GHz. The DoD is considering moving to the super high frequency (SHF) band in a range of 3–30 GHz. It is important to determine the changes to link power margins as the frequency increases. It is also necessary to identify any other propagation variances in the range of interest.

In order to increase transmission bandwidth, the military aeronautical telemetry (AT) operations are upgrading their operating frequency from below 3 GHz to a range of 3–30 GHz. Microwave signals in the new frequency band are expected to have higher propagation losses than in the 1.4–2.4 GHz (L and S bands) band due to atmospheric attenuation and terrain interference. The impact on microwave power link margin due to the frequency increase will be assessed through this contract work with JPL.

The atmospheric and weather effects on 3–30 GHz frequency band becomes more significant and is not negligible as at the 1.4–2.4 GHz frequency band which the military is using now. There are mainly two types of attenuations that will affect the power margin at higher frequencies. One is the atmospheric gaseous absorption, while another is the rain attenuation when microwave signals pass through the rain. Additional environmental phenomena, such as, cloud, fog, ice, snow, aerosol, dust, etc., can also cause severer signals impairment as increasing operating frequency. Several anomalous propagation modes (such as ducting and tropospheric scatter) also play major roles in trans-horizon interference for a very small percent time. At low elevation angle, the atmospheric scintillation and multipath fading become significant. A microwave propagation scenario through the atmospheric medium is shown in Figure 1-1-1.

Atmospheric absorption, clouds, fog, precipitation, and scintillation incur losses in a transmitted signal. Previously, these losses were deemed negligible at the lower frequencies. As the frequency increases, this method is not acceptable. It is necessary to identify all the propagation mechanisms and estimate attenuation that might arise in the new frequency band.

JPL has expertise in the field of radio wave propagation through the earth atmospheric environment. In the last several years we have been developing non-ionized media propagation models for the International Telecommunication Union (ITU) and interference models for International Mobile Telecommunications (IMT)-2000. This is why we can accomplish this propagation channel study at a short period. We will continue to make our efforts until the sponsors are completely satisfied.

1.2 Objectives:

The SHF band in the frequency range of 3 to 30 GHz is an unidentified band for aeronautical telemetry operations. The objectives of this study are to identify all major propagation mechanisms and estimate attenuation that arises in the new frequency band. Changes in microwave power attenuation as frequency increases from the range of 1.4–2.4 GHz to the range of 3–30 GHz will be determined. Any new propagation anomalies that might arise at some frequencies in the range of investigation need to be reliably identified.

As final study results, a limited set of link scenarios to serve as useful benchmark comparison paths and of benchmark weather cases that will be applied to each scenario need to be established. Upper and lower bounds on systematic and random path attenuation components at 3, 6, 12, and 24 GHz will be estimated. In the SHF band, for the radio waves propagating through the atmospheric medium, the compensation factor to the Friis free space equation need to be conservatively estimated. This study must reliably estimate upper and lower bounds on the degree to which factors currently assumed negligible such as atmospheric absorption and weather will cause additional systematic and random losses at higher frequencies.

II. Analysis

2.1. General Propagation Theory

2.1.1 Free Space Loss

The Friis Equation is used to estimate distance related loss for free space or an atmospheric medium but at lower frequency (generally < 3 GHz).

$$P_r = \frac{P_t G_t}{4\pi d} A_r = P_t G_t G_r \left(\frac{\lambda}{4\pi d} \right)^2 = \frac{P_t G_t G_r}{L_{FS}}$$

where: P_r : power received; P_t : power transmitted

G_t : transmitter antenna gain; G_r : receiver antenna gain

A_r : effective area of receiver antenna ($\lambda^2 G_r / 4\pi$)

L_{FS} : free space loss ($4\pi d / \lambda$)²;

d : distance between transmitter and receiver

λ : wavelength of radio wave

When representing the Friis Equation in decibels (dB), we have

$$P_r = P_t + G_t + G_r - L_{FS} \quad \text{in dB}$$

or

$$P_r = EIRP + G_r - L_{FS} \quad \text{in dB}$$

where: $EIRP$ is effective isotropically radiated power in dBW;

and $L_{FS} = 92.45 + 20\log f + 20\log d \quad \text{in dB}$

where: frequency, f , in GHz,

distance, d , in km.

The free space losses as functions of frequency and distance are shown in Figures 2-1-1 and 2-1-2.

2.1.2. Modification of Friis Equation

For microwave signals in the SHF band passing through the atmospheric medium, the Friis Equation should be modified as

$$P_r = \frac{P_t G_t}{4\pi d L_a} A_r = \frac{P_t G_t G_r}{L_a} \left(\frac{\lambda}{4\pi d} \right)^2 = \frac{P_t G_t G_r}{L_{FS} L_a}$$

Expressed in Decibels (dB)

$$P_r = P_t + G_t + G_r - (L_a + L_{FS}) \quad \text{in dB}$$

or

$$P_r = EIRP + G_r - (L_a + L_{FS}) \quad \text{in dB}$$

where L_a is a very complicated loss term due to atmospheric gas absorption, rain, fog/cloud, scintillation/multipath, and other atmospheric effects. This term is usually negligible at lower frequency bands, but cannot be neglected at higher frequency bands. The term is dependent on weather condition (percentage of time) and radio wave frequencies (increases with increasing frequency)

In this study, we will concentrate on studying this term, which includes all contributions from atmospheric absorption, clouds, fog, precipitation, and scintillation, etc.

2.1.3. Elevation Angle Dependence

There are two types of problems that will restrict the direct application of all types of microwave propagation models into the military communication link scenario.

The first problem is that for most of time (98%) the military receivers work below elevation angles of 20°, and 85% of time they work below elevation angles of 5°, as shown in Figure 2-1-3.

The second problem is that most propagation models can only apply for satellite zenith link with a total atmospheric path, instead of a limited (or partial) atmospheric path linking between the aircraft and ground as shown in Figure 2-1-4.

To solve these problems, in this study we have developed a method of scaling the total atmospheric path loss into the partial oblique path loss as shown below.

We assume that all atmospheric propagation parameters have an exponential decrease with altitude and with a vertical scale height H , that is, $A = a_0 \cdot \exp(-z/H)$, where a_0 is a coefficient and z is the vertical distance. Thus, to calculate the total zenith losses through the entail atmosphere, we have

A vertical loss for a total atmospheric path:

$$L_{\infty}(90^\circ) = \int_0^{\infty} a_0 \cdot \exp(-z/H) dz = a_0 H$$

A vertical loss for a partial atmospheric path, h :

$$L_h(90^\circ) = \int_0^h a_0 \cdot \exp(-z/H) dz = a_0 H [1 - \exp(-h/H)]$$

The loss for a total oblique path:

$$L_{\infty}(\theta) = \int_0^{\infty} a_0 \cdot \exp(-z/H) ds = \int_0^{\infty} a_0 \cdot \exp(-z/H) dz / \sin \theta = a_0 H / \sin \theta$$

The loss for a partial oblique path (h, θ):

$$L_h(\theta) = a_0 H [1 - \exp(-h \sin \theta / H)] / \sin \theta$$

where $L_{\infty}(\theta) = L_{\infty}(90^\circ) / \sin \theta$ (dB) and $5^\circ \leq \theta \leq 90^\circ$

Thus, finally we have:

$$L_h(90^\circ) = L_{\infty}(90^\circ) [1 - \exp(-h/H)]$$

and

$$L_h(\theta) = L_{\infty}(\theta) [1 - \exp(-h \sin \theta / H)]$$

Using these equations, we can scale the total atmospheric path loss into the limited oblique path loss.

2.2. Microwave Propagation Models through the Atmospheric Medium

We first completed an extensive literature search on SHF band propagation studies. The literature includes two types of documents: One is in the experimental field on this frequency band, while another type is the theoretical and modeling studies.

We have studied the models of the atmospheric gaseous absorption and rain attenuation for various rainfall rates at 3–30 GHz. Atmospheric absorption and rain attenuation mainly occur at low altitudes, an area called as the troposphere. An atmospheric temperature profile below 70 km is shown in Figure 2-2-1.

There are several models for the atmospheric attenuation calculation. They are mostly regional dependence. We have found their similarities and differences between these models through a comparison study. In this study, we have mainly employed ITU (International Telecommunication Union) models for the estimate of microwave power margin losses in the SHF band (3–30 GHz).

2.2.1. Atmospheric Absorption:

The principal interaction mechanism between radio waves and gaseous constituents is molecular absorption from molecular oxygen and water vapor in the atmosphere. The oxygen volume ratio in the gases is quite stable, while the water vapor density varies a lot, with strong regional and seasonal dependence. Within the studied frequency band, there was an absorption line at 22.235 GHz (due to water vapor absorption). The following equations are used to plot the attenuation of oxygen and water vapor for the horizontal path, the vertical path, and different elevation angles over a specified frequency range.

For oxygen, specific attenuation in the horizontal dependence is given as:

$$\gamma_o = \left[7.19 \times 10^{-3} + \frac{6.09}{f^2 + 0.227} + \frac{4.81}{(f - 57)^2 + 1.50} \right] f^2 \times 10^{-3} \text{ dB/km}$$

where f is frequency in GHz.

For water vapor, specific attenuation in the horizontal dependence is given as:

$$\gamma_w = \left[0.067 + \frac{3}{(f - 22.3)^2 + 7.3} + \frac{9}{(f - 183.3)^2 + 6} + \frac{4.3}{(f - 323.8)^2 + 10} \right] f^2 \rho 10^{-4} \quad \text{dB}$$

in dB/km where f is frequency in GHz and ρ is the water vapor density in g/m^3 . In this study we have selected a maximum value of 12 g/m^3 and an average value of 7.5 g/m^3 .

$$\gamma_a = \gamma_o + \gamma_w \quad \text{dB/km}$$

The oxygen and water vapor equivalent heights are given as:

$$h_o = 6 \quad \text{km}$$

$$h_w = 2.2 + \frac{3}{(f - 22.3)^2 + 3} + \frac{1}{(f - 183.3)^2 + 1} + \frac{1}{(f - 323.8)^2 + 1} \quad \text{km}$$

The dependence on elevation angle is then taken into account.

$$A_a = \frac{h_o \gamma_o + h_w \gamma_w}{\sin \theta} \quad \text{dB}$$

Using the ITU gaseous absorption model, we have calculated attenuations due to both compositions along horizontal and vertical paths. Total zenith losses and its elevation angle dependence also are calculated and plotted. The losses at 3, 6, 12, and 24 GHz are estimated respectively.

Under clear weather, the dominant attenuations at SHF bands come from atmospheric absorption. These losses are negligible at the lower frequencies ($< 3 \text{ GHz}$). As the radio signal frequency increases, the absorption by atmospheric gases increases significantly.

Global maps of seasonal variations of water vapor density are analyzed. Based on these maps, we have calculated attenuations due to water vapor using two typical density values (7 and 12 g/m^3), which can be applied to the benchmark case study later. All plots for oxygen only and for water vapor only (two types of contents) and for both combination for a horizontal path are shown in Figures 2-2-2, 2-2-3, 2-2-4, and 2-2-5. For a vertical path, the zenith losses for a total path and for a partial vertical path are in

Figures 2-2-6, 2-2-7, 2-2-8, and 2-2-9. Elevation angle dependence for both water vapor contents are shown in Figures 2-2-10 and 2-2-11.

Points:

- Principal interaction mechanism between radio wave and gaseous constituents is molecular absorption from: Molecular Oxygen (O_2) – independent of weather; Water Vapor (H_2O) – dependent of weather/season
- Scale height for O_2 is about 6 km, while scale height for water vapor densities is about 2 km.
- Within studied frequency band, there is an absorption line at 22.235 GHz for water vapor. We advise avoiding use of telecommunication signal operation at this frequency and its neighborhood region.
- Atmospheric gas absorption occurs mainly at low altitudes

2.2.2. Attenuation by Rainfall

Rain and other hydrometeors, such as hail, ice, and snow, can cause severe attenuation for higher frequency signals. Water drops will absorb and scatter energy from incident waves. This absorption and scattering causes the attenuation to increase exponentially as the frequency increases. The attenuation coefficient is also strongly dependent on rainfall rate. ITU models on “Attenuation by Hydrometeors, in Particular Precipitation, and Other Atmospheric Particles” were used to plot the attenuation of rain different elevation angles and different rainfall rates over the specified frequency range.

We have performed a study for rain attenuation at SHF band. The severity of radio signal loss through the rain is strongly dependent on the local rainfall rates, rain cloud heights, and signal frequencies.

We have applied the ITU rain attenuation model to the studied frequency band (3–30 GHz) and have calculated attenuations along horizontal and vertical paths through the

rain region. This model shows that total specific attenuation rate, γ_R , is a function of rain fall rate, R , as

$$\gamma_R = kR^\alpha \quad \text{in } dB/km$$

where two coefficients α and k are functions of signal's frequency and elevation angle and have been experimentally determined in the model. Figures 2-2-12 and 2-2-13 show the attenuation rates for various rain fall rates for a horizontal and vertical paths, respectively.

The results show that for a rainfall rate of 50 mm/hour, rain attenuation at 30 GHz is about 10 dB/km, while it is only 1 dB/km at 9 GHz. Thus, the rain attenuation is the main problem at higher frequency for heavier rain.

Global maps which show 14 rain climatic zones worldwide with different precipitation characteristics are employed for this study (see figure A-7). At each zone, rainfall rate as a function of percent of time are formulated through long term statistics (see Figure A-8).

Points:

- Rain and other hydrometeors, such as hail, ice, snow etc., may cause severe attenuation for higher frequency signals
- Water droplets will absorb and scatter energy from incident waves
- Attenuation increases exponentially as the frequency increases
- Attenuation is highly dependent on rainfall rate which varies depends on weather, location, season
- Not highly correlated with elevation angle

2.2.3. Attenuation due to Clouds and Fog

Clouds and fog can be described as collections of smaller rain droplets. Different interactions from rain as the water droplet size in fog and clouds is smaller than the wavelength at 3–30 GHz. Attenuation is dependent on frequency, temperature (refractive

index), and elevation angle, and it can be expressed in terms of the total water content per unit volume based on Rayleigh Approximation:

$$\gamma_c = K_l M \quad \text{dB/km}$$

where:

γ_c : specific attenuation (dB/km) within the cloud

K_l : specific attenuation coefficient [(dB/km)/(g/m³)] as shown in Figure 2-2-14

M : liquid water density in the cloud or fog (g/m³)

To obtain the attenuation due to clouds for a given probability value, the statistics of the total columnar content of liquid water L (kg/m²), which is an integration of liquid water density, M , in kg/m³ along a column with a cross section of 1 m² from the surface to the top of clouds, or, equivalently, mm of precipitable water for a given site must be known yielding:

$$A = LK_l/\sin\theta \quad \text{dB} \quad \text{for } 90^\circ \geq \theta \geq 5^\circ$$

where θ is the elevation angle and K_l is read from Figure 2-2-14. Based on the L values from world maps shown in Figures A-9 and A-10, we have calculated attenuation values due to clouds for four benchmark case studies (See Tables 2, 3, 4, and 5).

Points:

- Not as severe as rain attenuation
- Typical value: 1.88 dB at 12.0 GHz for a 50-km path at East coast

2.2.4. Attenuation due to Scintillation/Multipaths at Low Elevation Angles

Scintillation is produced by turbulent air with variations in the refractive index. Attenuation due to scintillations rapidly increases with increasing frequency and decreasing elevation angle. These losses are strongly dependent on time percentage, elevation angle, and antenna size. The ITU scintillation model has been used for fading depth above 4° elevation angle. ITU scintillation/multipath models have been used to

study the shallow and deep fading depths between 5° and 0.5° elevation angles at different time percentages and elevation angles over the specified frequency range.

A 20% of time that a refractivity gradient in the lowest 100 m of the atmosphere is less than -100 N units/km value, as inputs, is applied to the scintillation fade depth calculation.

We have performed a study for amplitude scintillations at elevation angles greater than 5° at SHF bands. Attenuation significantly increases with increasing frequency and decreasing elevation angle. The attenuation is also characterized by percentage of time, based on long time statistics. Results as shown in Figures 2-2-15 and 2-2-16 provide the monthly and long-term statistics of the amplitude scintillation for elevation angles > 4 degrees.

At very low elevation angles, the fading comes from both atmospheric scintillation and multipath contribution as shown in Figure 2-2-17. Actually, losses caused by atmospheric scintillation and multipath are indistinguishable. We have performed shallow fading studies (scintillation/multipath) for paths with elevation angles less than 5° , because about 85% of time the receiver antenna works at elevation angle $< 5^\circ$. At very low elevation angles ($< 5^\circ$) for a very small percentage of time, for links over water or in coastal areas, the fading becomes very complicated and more severe due to both scintillation and multipath effects.

Figures 2-2-18 and 2-2-19 provide the fade depth statistics of the shallow part of the scintillation/multipath fading, for elevation angles < 5 degrees. For coastal and over water paths, and elevation angles overlapping between 4 and 5 degrees, both methods have been used, and the one giving the largest value of fade is considered to be the best estimate for the fading statistics.

Attenuations at low elevation angles have been calculated as functions of signal frequency, elevation angle, and percentage of time. The charts show that attenuations

linearly increase (from 5 to 50 dB) with increasing frequency (from 3 to 30 GHz) in a semi-log scale at a fixed elevation angle, but linearly decrease with increasing elevation angle (from 0.5° to 5°) in a semi-log scale at a fixed frequency. There is always higher attenuation corresponding to smaller percentage of time.

There is no model available for the scintillation fading below the 0.5° elevation angle. We are currently working with ITU study group 3 to develop the model.

Most scintillation models only apply to a satellite zenith link with a total atmospheric path, instead of a limited atmospheric path linking between the aircraft and ground. For this study we have scaled the total atmospheric path loss into the limited oblique path loss.

Points:

- Produced by the turbulent air with variations in refractive index
- Attenuation increases with increasing frequency
- Can cause rapid fluctuation of signals in amplitude and phase, affecting high-resolution data transmission.
- Attenuation depends elevation angle and antenna size, typically characterized by percentage time
- General model valid for elevation angle of 5 degrees and above
- Fadings caused by scintillation and multipath are indistinguishable below the 5° .

2.2.5. Anomalous Propagation Modes

In addition to the line of sight propagation, the radio wave can propagate transhorizontally through several anomalous models (see Figure 2-2-20). Anomalous modes propagation mechanisms depend on climate, radio frequency, time percentage of interest, distance, and path topography. At any one time a single mechanism (or more than one) may be present. The principal propagation mechanisms are as follows:

- *Line-of-sight*: The most straightforward interference propagation situation is when a line-of-sight transmission path exists under normal (i.e., well-mixed) atmospheric conditions. However, on all but the shortest paths (i.e., paths longer than about 5 km) signal levels can often be significantly enhanced for short periods of time by multipath and focusing effects resulting from atmospheric stratification.
- *Diffraction*: Beyond line-of-sight and under normal conditions, diffraction effects generally dominate wherever significant signal levels are to be found. For services where anomalous short-term problems are not important, the accuracy to which diffraction can be modelled generally determines the density of systems that can be achieved.
- *Tropospheric scatter*: This mechanism defines the “background” interference level for longer paths (e.g., more than 100–150 km) where the diffraction field becomes very weak. However, except for a few special cases involving sensitive earth stations or very high power interferers (e.g., radar systems), interference via troposcatter will be at too low a level to be significant.
- *Surface ducting*: This is the most important short-term interference mechanism over water and in flat coastal land areas, and it can give rise to high signal levels over long distances (more than 500 km over the sea). Such signals can exceed the equivalent “free-space” level under certain conditions.
- *Elevated layer reflection and refraction*: The treatment of reflection and/or refraction from layers at heights up to a few hundred meters is of major importance as these mechanisms enable signals to overcome the diffraction loss of the terrain very effectively under favorable path geometry situations. Again the impact can be significant over quite long distances.

Several anomalous propagation modes listed above can be used for transhorizon telecommunication, even they are very unstable and only work at a small percentage of time. We have performed studies of three anomalous propagation modes at SHF range: Terrain diffraction, tropospheric scattering, and ducting. Radio signals with the three

modes can propagate trans-horizontally along the great circle. These modes usually do not have impact on normal telecommunications except generating interference.

Terrain diffraction: Radio signals can be diffracted by hilltops or rounded obstacles and propagate beyond the line of sight. Diffraction effects generally dominate a surrounding area (with a radius < 200 km) and define the long-signal levels. Diffraction losses increase with increasing signal frequency and obstacle's sharpness, but have a weak dependence on the percentage of time. Diffraction loss over a hill can be calculated using a knife-edge model (as shown in Figure 2-2-21). Loss magnitude is dependent on the parameter, v , as shown in Figure 2-2-22.

Tropospheric scatter: Radio signals can be scattered by the tropospheric particles or turbulence to propagate forward into a large distance beyond the line of sight.

Tropospheric scatter losses as functions of distance, frequency, and percentage of time are calculated using ITU model at SHF range. For example, at 3.0 GHz, over a 300-km path, at 1% of time, tropospheric loss is 201 dB, while it is 216 dB at 12.0 GHz. Losses due to the troposcatter for various signal frequencies are shown in Figure 2-2-23, 2-2-24, and 2-2-25.

Ducting (surface and elevated): Due to the surface heating and radiative cooling, inversion temperature layers often are generated on the ocean or flat coastal surface. Radio signals can be trapped within this reflection layer at heights up to a few hundred meters and propagates over a long distance (>500 km over the sea). Surface and elevated duct parameters are described in Figure 2-2-26. Global occurrence maps for both surface and elevated ducts are shown in Figures A-11 and A-12. Such signals can even exceed the equivalent "free space" level. For example, at 12.0 GHz for a 200-km path, at 0.01% of time, ducting propagation loss is 154.0 dB, while the free space propagation loss is 159.5 dB. Ducting losses as functions of distance, frequency, and percentage of time are calculated using the ITU model at SHF band and also shown in Figures 2-2-27, 2-2-28, and 2-2-29.

For short transmission paths extending only slightly beyond the horizon, terrain diffraction is the dominant mechanism in most cases. Conversely, for longer paths (more than 100 km), scattering and ducting mechanisms need to be taken into account if there is no large mountain in between.

Points :

- At least three anomalous modes can propagate transhorizontally in the SHF band
 - Terrain diffraction: Generally dominates < 100km
 - Tropospheric scatter: Gives the “background” interference level for >100 km
 - Ducting (surface and elevated): Propagates over a long distance (>500km over the sea) along an inversion layer, and can exceed the equivalent “free space” level.

III. Benchmark Case Study

3.1. Benchmark Case Scenarios

We have contacted the Advanced Range Telemetry (ARTM) staff about available link scenarios. Bob Jefferis kindly provided us four benchmark link scenarios for case study: Patuxent River, Maryland; San Nicholas Island, California; Laguna Peak, California; and Edwards Air Force Base, California.

For the first important candidate, the Naval test range at Patuxent River, MD (commonly referred to as "PAX River" or simply PAX), the primary receiving antennas are 8 foot diameter (operating 1.4–2.4 GHz) just off the Chesapeake bay, slightly inland. The antennas are approximately 80–100 feet above ground level, which is not far above sea level. The coordinates of the receiving station is:

$38^{\circ}18'00''\text{N}$, $76^{\circ}24'00''\text{W}$, antenna elevation 30.5 m

An important worst case flight profile has a jet aircraft take off and fly out to sea at altitudes that can range from 1000 to 50,000 ft and go out as far as the radio horizon.

The second benchmark location is the Navy Weapons center. at Pt. Mugu, CA. Operations at this West Coast site often experience fog and ducting phenomena. There are two receiving antenna sites in the center. The first is on a low mountain called Laguna Peak. Antenna coordinates to use are:

$34^{\circ}6'25.79''\text{N}$, $119^{\circ}3'56.72''\text{W}$, elevation 416.7m

The second antenna location is on San Nicholas Island:

$33^{\circ}15'4.50''\text{N}$, $119^{\circ}31'14.10''\text{W}$, elevation 277.06m

They receive signals from all over the airspaces designated in FAA aviation sectional charts as R-2519 and W-289. In addition, they track high-flying vehicles (missile launches) originating from Vandenberg AFB from the point at which they can first see them to the point they lose signal far out over the Pacific.

The third and final location for a case study is Edwards AFB. The main receive site is located:

34 ° 53' 36.71"N, 118 ° 0' 40.39"W, elevation of antenna #1 is 899.2m.

Operations concentrate on the air spaces defined in FAA aviation sectional charts as R2508 and farther North in the "MOA" flight zones. Looking Eastward, it is not uncommon for signals to be tracked slightly beyond the Colorado river when vehicles are flying at the 20,000-foot pressure altitude and higher.

3.2. Terrain Profile Analysis

To calculate the link budget between the stations and the neighborhood areas, we need to perform a terrain profiles analysis first. Radio waves are bent when they propagate through atmospheric gases that decrease in density with altitude. The waves can therefore reach locations beyond the line of sight. The severity of the bending is determined by the gradient of the refractive index near the earth's surface. It is convenient to represent the radio ray as a straight line for the sake of analysis. For this reason an "Effective Earth Radius", a_e , is defined that in effect stretches the Earth radius by a factor depending on the refractivity gradient, ΔN . In this study a 4/3 earth radius has been used to modifying all terrain profiles.

Using the effective Earth radius, we can modify the elevation of terrain profile using the following equation.

$$y_i = h_i - x_i^2 / 2a_e$$

where y_i is modified elevation, h_i is terrain elevation above sea level, while x_i is distance from the receiver. The modified terrain profiles shown in Figures 3-1-2, 3-1-4, 3-1-5, 3-1-6, 3-1-7,

and 3-1-8 using the median effective Earth radius. All distances and heights are referenced to these modified plots.

To construct these plots, elevations h_i of the terrain are read from topographic maps versus their distance x_i from the receiving antenna. The terrain profiles, including terrain elevations and the sea level, have been adjusted according to the average curvature of the radio ray path. The solid curve near the bottom of the figure indicates the shape of the sea level of constant elevation ($h = 0$) for all plots. The receiving station is put at left corner, while the transmitting aircraft from the right side. The vertical scales of the figure are exaggerated in order to provide a sufficiently detailed representation of terrain irregularities.

The elevation angles θ_{er} relative to receiver may be computed using the following equations:

$$\theta_{er} = \frac{h_{Lr} - h_{rs}}{d_{Lr}} - \frac{d_{Lr}}{2a_e}$$

where h_{Lr} is the elevation of horizon obstacle and h_{rs} is elevation of receiving antennas, respectively, all above the average mean sea level (AMSL). The d_{Lr} is sea level arc distance from receiving antenna to its radio horizon obstacle. The a_e is the median effective earth radius.

3.3. Radio Parameters and Calculation

We have applied the above method to path profile analysis for all of these four receiving stations. The map of Patuxent River and adjacent coastal areas is shown in Figure 3-1-1. Modified terrain profile along a 300-km path north from San Nicholas Island is shown in Figure 3-1-2. Assuming an aircraft is at an altitude of 4000 m, several paths with various elevation angles and lengths linking the receiving stations and the aircraft are drawn and analyzed later. The west coastal area around Pt. Mugu and inland area around Edwards AFB are shown in Figure 3-1-3. Figure 3-1-4 shows a westward 300-km path relative to San Nicholas Island receiver. Figure 3-1-5 shows a terrain profile between San Nicholas Island and Vandenberg AFB, while Figure 3-1-6 shows a terrain profile between Laguna

Peak and Vandenberg AFB. Figure 3-1-7 shows a westward 300-km path from Laguna Peak receiver. An east 400-km path from the Edwards AFB is also shown in Figure 3-1-8.

In order to perform the loss calculations for all types of attenuation for these locations, we need first to collect all radio climatologic parameters from these areas. We have listed all parameters in Table 1 for the four benchmark cases. We have used the following maps to make these parameters available. They are:

- Figure A-1: World map of refractive index, N , in February,
- Figure A-2: World map of refractive index, N , in August.
- Figure A-3: World map of vertical gradients of the radio refractive index, ΔN , in February
- Figure A-4: World map of vertical gradients of the radio refractive index, ΔN , in August
- Figure A-5: World map of surface water vapor density, ρ , in a unit of g/m^3 in winter
- Figure A-6: World map of surface water vapor density, ρ , in a unit of g/m^3 in summer.
- Figure A-7: Northern America rain zone map.
- Figure A-8: Rain fall rates (mm/h) for various rain zones as a function of percentage of time exceeded.
- Figure A-9: World map of normalized total columnar content of cloud liquid water (kg/m^2) exceeded for 1% of the year
- Figure A-10: World map of normalized total columnar content of cloud liquid water (kg/m^2) exceeded for 10% of the year
- Figure A-11: World map of surface duct occurrence rates (%) for an average year.
- Figure A-12: World map of elevated duct occurrence rates (%) for an average year.

These parameters are very important in accurately calculating propagation losses. All calculation results are shown in Tables 2, 3, 4, and 5 for the four benchmark cases.

By applying attenuation charts and a scaling method into Patuxent River Case Study, we find that for a 50-km path with elevation angle of 6.2 degrees, the total atmospheric loss at 12.0 GHz at 1.0% of time exceeded 8.3 dB; at 24 GHz it is 34.3 dB. For a 200-km path with an elevation angle of 0.2°, the total atmospheric loss at 12.0 GHz at 1.0% of the time is 36.1 dB. For 24 GHz, the loss is 139.5 dB.

There are occurrence rates of 50% for elevated ducting and of 15% for surface ducting, respectively, for San Nicholas Island and Laguna Peak, while both occurrence rates at Edwards AFB and Patuxent River are around 10%. This is because there are more elevated inversion layers formed over west coastal areas than over the east.

The layer height of elevated ducts at San Nicholas Island and at Laguna Peak is in an altitude range from 800 m to 1000 m, while the surface duct layer can extend up to 300 m altitude. As a comparison, Edwards AFB area has smaller duct thickness.

The receiver at San Nicholas Island has a lowest elevation angle of -0.44° and a maximum line of sight range of 65 km over the ocean. In the direction of Vandenberg, the elevation angle is -0.24° . For the receiver at Laguna Peak, the lowest elevation angle is -0.54° , and the line of sight range is 80 km over the ocean. In the direction of Vandenberg, the elevation angle is -0.16° . However, beyond these ranges, radio signals still can propagate transhorizontally up to ~ 1000 km through the anomalous ducting mode along the ocean surface.

At San Nicholas Island, total propagation losses due to gaseous absorption, rain attenuation, cloud attenuation and scintillation/multipaths (except the free space loss) for a 100-km path with 3.1° elevation angle are 12.8 dB for 12 GHz, and 49.2 dB for 24 GHz, respectively. The corresponding losses at Edwards AFB are 11.0 dB and 39.2 dB,

respectively. This is because the west coastal area has less rain and cloud coverage when comparing with Patuxent River region (17.4 dB and 67.6 dB respectively).

Table 1. Radio Parameters at Four Case Study Area

Radio Parameters		Patuxent River	Laguna Peak	San Nicholas Island	Edwards AFB
Refractive Index	February	310 N-units	330 N-units	330 N-units	320 N-units
	August	360 N-units	345 N-units	350 N-units	330 N-units
Refractivity Gradient	February	40 N-units	45 N-units	45 N-units	40 N-units
	August	50 N-units	55 N-units	60 N-units	45 N-units
Water Vapor Content	February	5 g/m ³	7.0 g/m ³	7.5 g/m ³	5.5 g/m ³
	August	12 g/m ³	12 g/m ³	13 g/m ³	10 g/m ³
Rainfall Zone and Rainfall Rate	Zone	K	E	E	E
	0.1% of Time	12 mm/h	6.2 mm/h	6.2 mm/h	6.2 mm/h
	1.0% of Time	2.5 mm/h	1.8 mm/h	1.8 mm/h	1.8 mm/h
Cloud Liquid Water Columnar Content	1.0% of Time	1.2 kg/m ²	0.5 kg/m ²	0.5 kg/m ²	0.4 kg/m ²
	10% of Time	0.4 kg/m ²	0.2 kg/m ²	0.2 kg/m ²	0.2 kg/m ²
Radio Climatic Zone	Inland, Coastal or Sea	A1	A1	B	A2
Ducting	Surface Duct	10%	15%	15%	10%
	Elevated Duct	10%	50%	50%	10%

Table 2. Total Propagation Losses for Typical Paths around Patuxent River

Distance (km)		Elevation Angle (degree)	Free Space Loss (dB)	Gaseous Absorption (H ₂ O with 12 g/m ³)	Rain Attenuation at 1.0% of Time	Cloud Attenuation at 1.0% of Time	Scintillation /Multipath at 1.0% of Time	Total Atmospheric Attenuation (dB)	Total Attenuation (dB)
For 12.0 GHz	10	23.6	134.1	0.2	0.6	0.5	0.2	1.5	135.6
	50	6.2	148.1	2.0	3.0	1.9	1.4	8.3	156.3
	100	3.1	154.1	4.0	6.0	3.8	3.6	17.4	171.5
	200	0.2	160.1	8.0	12.0	7.50	8.6	36.1	196.2
For 24.0 GHz	10	23.6	140.1	1.6	3.2	1.0	0.4	6.2	146.3
	50	6.2	154.1	9.0	17.5	5.0	2.8	34.3	188.4
	100	3.1	160.1	18.0	35.0	10.0	4.6	67.6	227.3
	200	0.2	166.1	36.0	70.0	20.0	13.5	139.5	305.6

Table 3. Total Propagation Losses for Typical Paths around San Nicholas Island

Distance (km)		Elevation Angle (degree)	Free Space Loss (dB)	Gaseous Absorption (H ₂ O with 13 g/m ³)	Rain Attenuation at 1.0% of Time	Cloud Attenuation at 1.0% of Time	Scintillation /Multipath at 1.0% of Time	Total Atmospheric Attenuation (dB)	Total Attenuation (dB)
For 12.0 GHz	10	23.6	134.1	0.2	0.4	0.2	0.2	1.0	135.1
	50	6.2	148.1	2.2	1.6	0.8	1.4	6.0	154.1
	100	3.1	154.1	4.4	3.2	1.6	3.6	12.8	166.9
	200	0.2	160.1	8.8	6.4	3.1	8.6	26.9	187.0
For 24.0 GHz	10	23.6	140.1	1.9	1.8	0.4	0.4	4.5	144.6
	50	6.2	154.1	10.7	9.2	2.1	2.8	24.8	178.9
	100	3.1	160.1	21.4	19.0	4.2	4.6	49.2	209.3
	200	0.2	166.1	42.7	38.0	8.3	13.5	102.5	268.6

Table 4. Total Propagation Losses for Typical Paths around Laguna Peak

Distance (km)		Elevation Angle (degree)	Free Space Loss (dB)	Gaseous Absorption (H ₂ O with 12 g/m ³)	Rain Attenuation at 1.0% of Time	Cloud Attenuation at 1.0% of Time	Scintillation /Multipath at 1.0% of Time	Total Atmospheric Attenuation (dB)	Total Attenuation (dB)
For 12.0 GHz	10	23.6	134.1	0.2	0.4	0.2	0.2	1.0	135.1
	50	6.2	148.1	2.0	1.6	0.8	1.4	5.8	153.9
	100	3.1	154.1	4.0	3.2	1.6	3.6	12.4	166.5
	200	0.2	160.1	8.0	6.4	3.1	8.6	26.1	186.2
For 24.0 GHz	10	23.6	140.1	1.6	1.8	0.4	0.4	4.2	144.3
	50	6.2	154.1	9.0	9.2	2.1	2.8	23.1	177.2
	100	3.1	160.1	18.0	19.0	4.2	4.6	45.8	205.9
	200	0.2	166.1	36.0	38.0	8.3	13.5	95.8	261.9

Table 5. Total Propagation Losses for Typical Paths around Edwards AFB

Distance (km)		Elevation Angle (degree)	Free Space Loss (dB)	Gaseous Absorption (H ₂ O with 10 g/m ³)	Rain Attenuation at 1.0% of Time	Cloud Attenuation at 1.0% of Time	Scintillation /Multipath at 1.0% of Time	Total Atmospheric Attenuation (dB)	Total Attenuation (dB)
For 12.0 GHz	10	23.6	134.1	0.2	0.3	0.2	0.2	0.9	135.0
	50	6.2	148.1	1.6	1.4	0.6	1.4	5.0	153.1
	100	3.1	154.1	3.3	2.8	1.3	3.6	11.0	165.5
	200	0.2	160.1	6.9	6.0	2.5	8.6	24.0	184.1
For 24.0 GHz	10	23.6	140.1	1.2	1.7	0.3	0.4	3.6	143.7
	50	6.2	154.1	6.8	8.8	1.7	2.8	20.1	174.2
	100	3.1	160.1	13.5	17.8	3.3	4.6	39.2	199.3
	200	0.2	166.1	27.0	35.0	6.7	13.5	82.2	248.3

IV. Summary of Study Results

The Advanced Range Telemetry Project was tasked by the Department of Defense, Director Operational Test & Evaluation Central Test & Evaluation Investment Program and Test & Evaluation / Science and Technology Program, to study the technical and financial impact of moving some aeronautical telemetry (AT) operations to an unidentified band in the frequency range of 3 to 30 GHz. The present study has provided an impact assessment on microwave power link margin as operating frequency increases. Through this study we can obtain the following conclusions:

- There are four main types of atmospheric losses that need to be taken into account at new SHF band: Atmospheric gaseous absorption, rain attenuation, clouds attenuation, and scintillation.
- At high elevation angles, atmospheric gaseous absorption and rain attenuation are the two dominant factors at SHF band.
- While the atmospheric gaseous absorption plays a major role under a clear weather, heavy rainfalls can cause several tens of dB loss for a 100-km path through the rain.
- Attenuations due to rain, clouds, and scintillation have strong time percentage dependences, based on the long-term statistics
- At very low elevation angles ($< 5^\circ$), atmospheric scintillation/multipath fading becomes a very important factor.
- There are at least three anomalous propagation modes which can propagate trans-horizontally. These modes may be used for communication for a small percentage of time.
- There are occurrence rates of 50% for elevated ducting and of 15% for surface ducting at San Nicholas Island and Laguna Peak.
- Layer heights of elevated ducts at San Nicholas Island and Laguna Peak are in an altitude range from 800 m to 1000 m, while the surface duct layer can extend up to 300 m altitude.

- San Nicholas Island has a lowest elevation angle of -0.44° , while Laguna Peak has a lowest elevation angle of -0.54° over the ocean. However, radio signals can propagate transhorizontally up to ~ 1000 km through the anomalous ducting mode over the ocean.
- At San Nicholas Island, total atmospheric propagation losses (except free space loss) for a 100-km path are 12.8 dB at 12 GHz, and 49.2 dB at 24 GHz, respectively. The corresponding losses at Edwards AFB are 11.0 dB and 39.2 dB, respectively, while losses at Patuxent River region are 17.4 dB and 67.6 dB respectively.

V. Potential Follow-on Study

There are still some propagation issues remaining to be studied. These issues are very important for military communication systems. We are willing to attack these complicated issues for possible solutions within a period of a one-year study.

1. Dust (sand)storm effects on signal attenuation: In the Iraq War at the end of last March, there was about one week of heavy dust storm in the Mideast area. The dust storm limited the use of high tech weapons because the visibility was near zero. At the U.S. continental, Edwards AFB, and New Mexico White Sands region, there were also dust storm reports. As we known, dust storms have less effect on low frequency signals, which have lower resolution on remote sensing and lower bandwidth on transmission, while dust storms have large attenuation effects on high frequency, especially on SHF band or Ka band.

Sand or dust particles can cause attenuation of radio waves through the scattering and absorption by particles. When the particle size is smaller than the wavelength, Rayleigh scattering theory applies. When the particle size is larger than the wavelength, we should use Mie scattering theory to calculate effective refractive index.

For terrestrial sand or dust storms, the visibility is often used to describe the distance at which a mark disappears against the background. Storms usually have a visibility of 10 m or less, with a minimum of 3.8 m, and can reach a height of 1 km or more. Dust particles have an average size of 10 to 20 μm , with the largest in a range of 80–300 μm . For an extreme case, with a particle number density, N_T , of $10^8/\text{m}^3$, and mass density, ρ , $2.8 \times 10^6 \text{ g/m}^3$, mass loading can reach 40–60 g/m^3 . It is found that radio signal attenuations have strong dependence on the dust particles size and material properties. There are a few reports on dielectric constant, permittivity of dust, and their dependence on dust moisture,

JPL has done significant study on dust storm effects at high frequency, especially on Mars dust storm effects at frequencies from UHF to Ka band. We will review available

theoretical and experimental studies on radiowave attenuation passing through a dust storm region and expand these results into the SHF band.

2. Noise temperature due to clouds: Sky noise from clouds can be calculated based on the radiative transfer theory approximations. JPL performed the study of cloud noise on high sensitive DSN receivers since 1982 (Slobin's cloud model) using radiative transfer methods and a four layer cloud model. Slobin calculated the zenith sky noise temperature for several frequencies of interest. We will improve his cloud model based on new measurements and extend it into higher frequency.

3. Depolarization due to rain or ice at high frequency: The depolarization which generally becomes a problem at frequency above 3 GHz, is a change in the polarization characteristics of a transmitted radiowave induced by the earth's atmosphere. A knowledge of depolarization effects is important in the design and performance of frequency reuse communications systems. Depolarization due to differential attenuation and phase shift between polarized waves caused by non-spherical rain drops, or ice crystals, is usually determined by using the cross polarization discrimination, XPD, a ratio of the power received at desired polarization to the undesired polarization. We will work on a depolarization prediction model within the frequency ranging from 3 to 30 GHz to apply for a slant aircraft path relative to the ground station.

VI. Figure Captions and Plots

Figure 1-1-1. Microwave atmospheric propagation environment. Some typical radio paths linking aircraft to the ground and ground to ground are shown. There are mainly 4 types of attenuations at SHF band: Atmospheric gaseous attenuation from O₂ and condensed H₂O, rain attenuation, cloud and fog absorption and scintillation.

Figure 2-1-1. The SHF band microwave free space propagation losses calculated using Friis Equation for various frequencies. The losses are shown as a function of the distance from the transmitter.

Figure 2-1-2. Free space propagation losses at SHF band calculated using Friis Equation for various distances. The losses are shown as a function of the frequency for radio signals.

Figure 2-1-3. Military receiving antenna pointing angle distribution. Receivers mainly work at lower elevation angles with a range from -5° to 90°, but 98% of time they are below the 20° and 85% of time below the 5°.

Figure 2-1-4. Vertical atmospheric path vs. oblique atmospheric path and total atmospheric path vs. partial atmospheric path. Most microwave propagation models apply for the link between the satellite and ground, counting total atmospheric losses. For this present study, the link between an aircraft and the ground only takes a partial atmospheric path. An algorithm to convert the total atmospheric loss into the partial atmospheric loss needs to be developed.

Figure 2-2-1. The Earth's atmospheric vertical structure of temperature. Radio refractive index is governed by both temperature and pressure which decreases exponentially with altitude. The troposphere (below the 10 km altitude) has dominant effects on microwave attenuation.

Figure 2-2-2. Specific attenuation (dB/km) due to atmospheric gaseous absorption from

oxygen only for a horizontal path. Attenuation increases slowly with increasing frequency.

Figure 2-2-3. Specific attenuation (dB/km) due to atmospheric gaseous absorption from water vapor only for a horizontal path. Two curves in the plots show two types of water vapor densities: 7.5 g/m^3 and 12 g/m^3 , respectively. Attenuation increases rapidly with increasing frequency. At 22.3 GHz there is a strong absorption peak.

Figure 2-2-4. Atmospheric gaseous absorption from both oxygen and water vapor with a density of 7.5 g/m^3 for a horizontal path. The plot gives the total specific attenuation at a rate of dB per kilometer for a frequency range of 1–30 GHz.

Figure 2-2-5. Total atmospheric gaseous absorption from both oxygen and water vapor with a density of 12.0 g/m^3 for a horizontal path.

Figure 2-2-6. Total vertical attenuation (dB) due to oxygen absorption only for a zenith path. Attenuation is obtained through an integration along a vertical path from the ground to the infinite (∞) height. Attenuation for a 10 km vertical path also is shown using a green line. Scale height for O_2 is 6 km.

Figure 2-2-7. Total vertical attenuation (dB) due to atmospheric gaseous absorption from water vapor only for a zenith path. Two curves in the plots show two types of water vapor densities: 7.5 g/m^3 and 12 g/m^3 , respectively, for a infinite vertical path. Attenuation for a 5 km vertical path for 7.5 g/m^3 water vapor density also is shown using a green line. Scale height for water vapor densities is 2 km.

Figure 2-2-8. Total vertical attenuation (dB) from both oxygen and water vapor with a density of 7.5 g/m^3 for a zenith path.

Figure 2-2-9. Total atmospheric gaseous absorption from both oxygen and water vapor with a density of 12.0 g/m^3 along a vertical path.

Figure 2-2-10. Elevation angle dependence of atmospheric attenuation for a total oblique atmospheric path for several typical frequencies. Elevation angles are for those greater than 10° , while water vapor density is for 7.5 g/m^3 .

Figure 2-2-11. Elevation angle dependence of atmospheric attenuation for a total oblique atmospheric path for several typical frequencies for water vapor density of 12.0 g/m^3 .

Figure 2-2-12. Specific attenuation (dB/km) due to rain attenuation for various rainfall rates for a horizontal path (elevation angle = 0°).

Figure 2-2-13. Specific attenuation (dB/km) due to rain attenuation for various rainfall rates for a vertical path (elevation angle = 90°) near the ground. The attenuation rate is slightly smaller than the horizontal attenuation rate.

Figure 2-2-14. Specific attenuation coefficient, K_l , in a unit of $[(\text{dB/km})/(\text{g/m}^3)]$ for fog and cloud attenuation for various temperatures as a function of frequency. Attenuation rate significantly increases with increasing frequency. Lower temperature is related to higher coefficient.

Figure 2-2-15. Fading depth (dB) due to atmospheric scintillation as a function of signal frequency for a 10° elevation angle atmospheric path for 1%, 3%, and 5% of time exceeded, respectively. There is higher attenuation at lower percentage of time exceeded. Antenna diameter of 1.0 m has been used for the calculation.

Figure 2-2-16. Elevation angle (for $> 4^\circ$) dependence of fading depth due to atmospheric scintillation for various frequencies. Fading depths are calculated at 1% of time exceeded. Attenuation significantly decreases with increasing elevation angle and decreasing frequency.

Figure 2-2-17. A cartoon showing that low-elevation angle fading is a combination of

both atmospheric scintillation and ground multipaths. At very low elevation angle ($< 5^\circ$), attenuations caused by scintillation and multipath are indistinguishable. The inserted data plot is a real experimental data showing large fading effects on 2 GHz and 30 GHz at an elevation angle of 2.8° . Fading significantly increases with increasing signal frequency and decreasing elevation angles.

Figure 2-2-18. Frequency dependence of attenuation due to scintillation/multipath at 2° elevation angle for 1%, 3%, and 5% of time exceeded, respectively in average worst month.

Figure 2-2-19. Elevation angle dependence of scintillation/multipath losses for various frequencies at 1% of time exceeded. Multipath fading is included for the fading calculation at the very low elevation angle.

Figure 2-2-20. Anomalous mode propagation mechanisms and scenarios. Except the line of sight propagation, there are three special modes that can propagate transhorizontally: ducting (surface and elevated), terrain diffraction, and troposcatter. These modes can be used for an unstable telecommunication during a small percentage of the time and they may generate unwanted interference signals.

Figure 2-2-21. Terrain diffraction over a simplified single knife-edge. The loss is dependent on the distances from hill to both transmitter and receiver, wavelength and hill height as shown in the equations above.

Figure 2-2-22. Diffraction loss as a function of the diffraction parameter ν . The ν is calculated using the equation shown in previous plot.

Figure 2-2-23. Troposcatter propagation losses as a function of percentage of time exceeded for various distances at 3.0GHz.

Figure 2-2-24. Ducting propagation losses as a function of percentage of time exceeded

for various distances at 3.0GHz. The upper panel is for 6.0 GHz, while the lower panel is for 12.0 GHz.

Figure 2-2-25. Ducting propagation losses as a function of percentage of time exceeded for various distances at 3.0GHz. The upper panel is for 24.0 GHz, while the lower panel is for 30.0 GHz.

Figure 2-2-26. Altitude structures of surface duct and elevated duct. Surface ducts are characterized by their strength, S_s (M-units) or E_s (M-units), and their thickness, S_t (m) or E_t (m). Two additional parameters are used to characterize elevated ducts: namely, the base height of the duct E_b (m), and E_m (m), the height within the duct of maximum M.

Figure 2-2-27. Ducting propagation losses as a function of percentage of time exceeded for various distances at 3.0GHz.

Figure 2-2-28. Ducting propagation losses as a function of percentage of time exceeded for various distances. The upper panel is for 6.0 GHz, while the lower panel is for 12.0 GHz.

Figure 2-2-29. Ducting propagation losses as a function of percentage of time exceeded for various distances. The upper panel is for 24.0 GHz, while the lower panel is for 30.0 GHz.

Figure 3-1-1. Two maps show Patuxent River and adjacent east coastal area. Patuxent River Air Force base is marked with a star is at the center of each map.

Figure 3-1-2. A modified coastal terrain profile along a 300-km path north from the Patuxent River AFB. There is a minimum elevation angle of 0.2° relative to an airplane at 4000 m altitude and a maximum 200-km path of line of sight. The paths with 10-km, 50-km, and 100-km lengths at various elevation angles are also shown.

Figure 3-1-3. West coastal area map show Pt. Mugu (Laguna Peak and San Nicholas Island), Edwards AFB and adjacent areas. Arrow lines show the view directions of the receivers at concerned stations.

Figure 3-1-4. Terrain profile along a 300-km path west from San Nicholas Island. Relative to the receiver at San Nicholas Island, the minimum elevation angle for a line of sight in the west direction (270° azimuth) is -0.44° , corresponding to a maximum range of 65 km on the ocean surface. However, the radio signals from an aircraft can propagate beyond the horizon along a surface or elevated duct to the receiver.

Figure 3-1-5. Terrain profile between San Nicholas Island and Vandenberg AFB. Relative to a receiver at San Nicholas Island, the minimum elevation angle in the Vandenberg direction is -0.24° . The line of sight is blocked by Santa Rosa Island 95 km away. However, when an aircraft arises up to 2000 m above the Vandenberg AFB, there is a direct view from the San Nicholas Island receiver.

Figure 3-1-6. Terrain profile between Laguna Peak and Vandenberg AFB. The line of sight is blocked by Santa Ynez Mountains 110 km away, which has a -0.16° elevation angle relative to a receiver at Laguna Peak.

Figure 3-1-7. Terrain profile along a 300-km path west from Laguna Peak. Relative to the receiver at Laguna Peak, the minimum elevation angle for a line of sight in the west direction (270° azimuth) is -0.54° , corresponding to a maximum range of 80 km on the ocean surface. The plot shows that the radio signals from an aircraft can propagate transhorizontally along a surface or elevated duct to the receiver.

Figure 3-1-8. Terrain profile along a 400-km path east from Edwards AFB. Relative to the receiver at the base, the minimum elevation angle for a line of sight in the east direction (90° azimuth) is 0° due to a nearby hill.

Figure A-1. World map of radio refractive index, N , in February.

Figure A-2. World map of radio refractive index, N , in August.

Figure A-3. World map of vertical gradients of the radio refractive index, ΔN , at first 100 m altitude above the surface in February. The gradients will affect radio propagation, such as ray bending, ducting layer and diffraction, etc.

Figure A-4. World map of vertical gradients of the radio refractive index, ΔN , at first 100 m altitude above the surface in August.

Figure A-5. World map of surface water vapor density, ρ , in a unit of g/m^3 in winter.

Figure A-6. World map of surface water vapor density, ρ , in a unit of g/m^3 in summer.

Figure A-7. Northern America rain zone map. Most of southern California areas are in rain fall zone E.

Figure A-8. Rain fall rates (mm/h) for various rain zones as a function of percentage of time exceeded. Zones E, C and D have the same rain fall rates.

Figure A-9. World map of normalized total columnar content of cloud liquid water (kg/m^2) exceeded for 1% of the year, which is an integration of liquid water density, M , in kg/m^3 along a column with a cross section of 1 m^2 from the surface to the top of clouds.

Figure A-10. World map of normalized total columnar content of cloud liquid water (kg/m^2) exceeded for 10% of the year.

Figure A-11. World map of surface duct occurrence rates (%) for an average year.

Figure A-12. World map of elevated duct occurrence rates (%) for an average year.

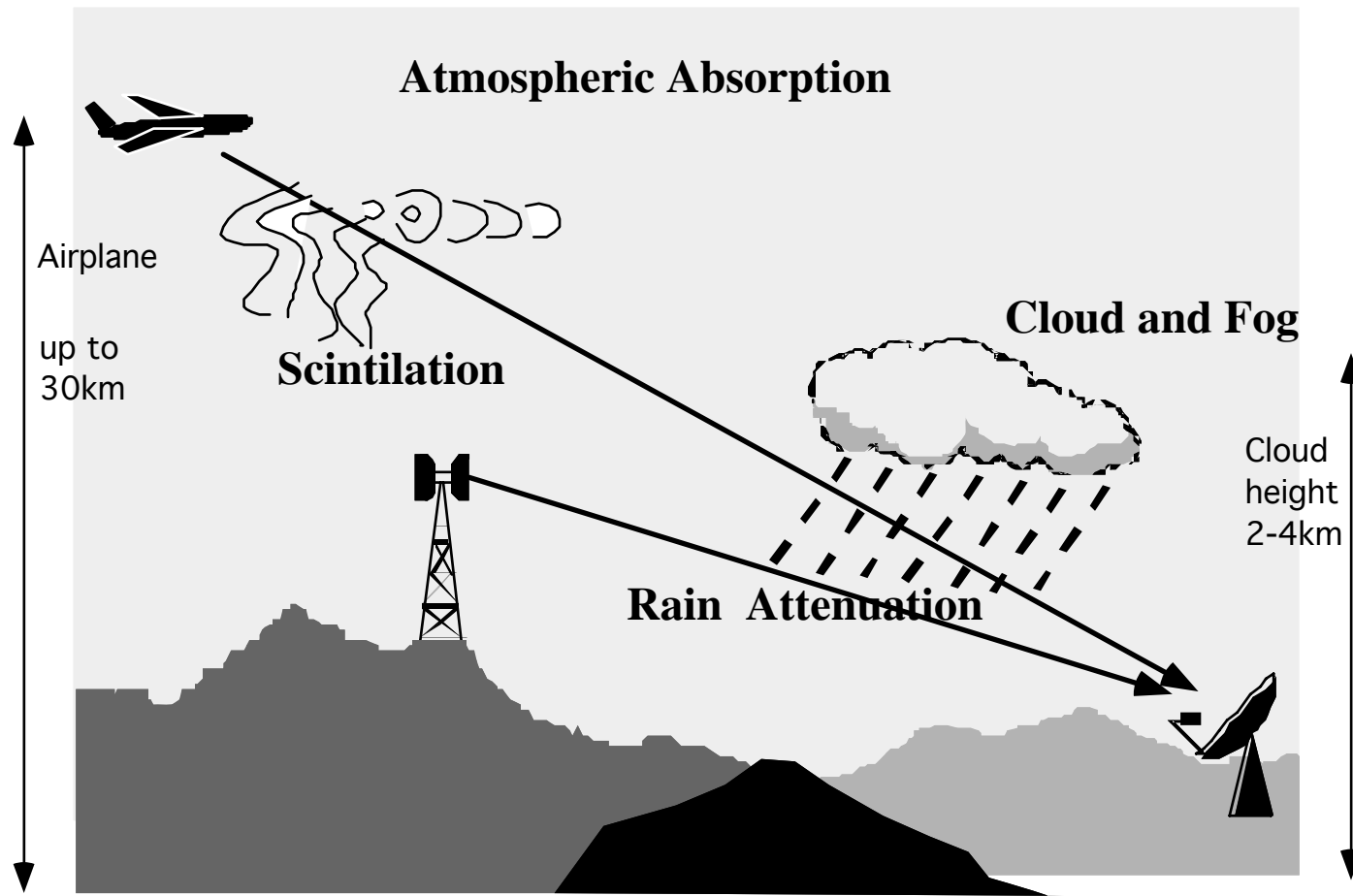


Figure 1-1-1

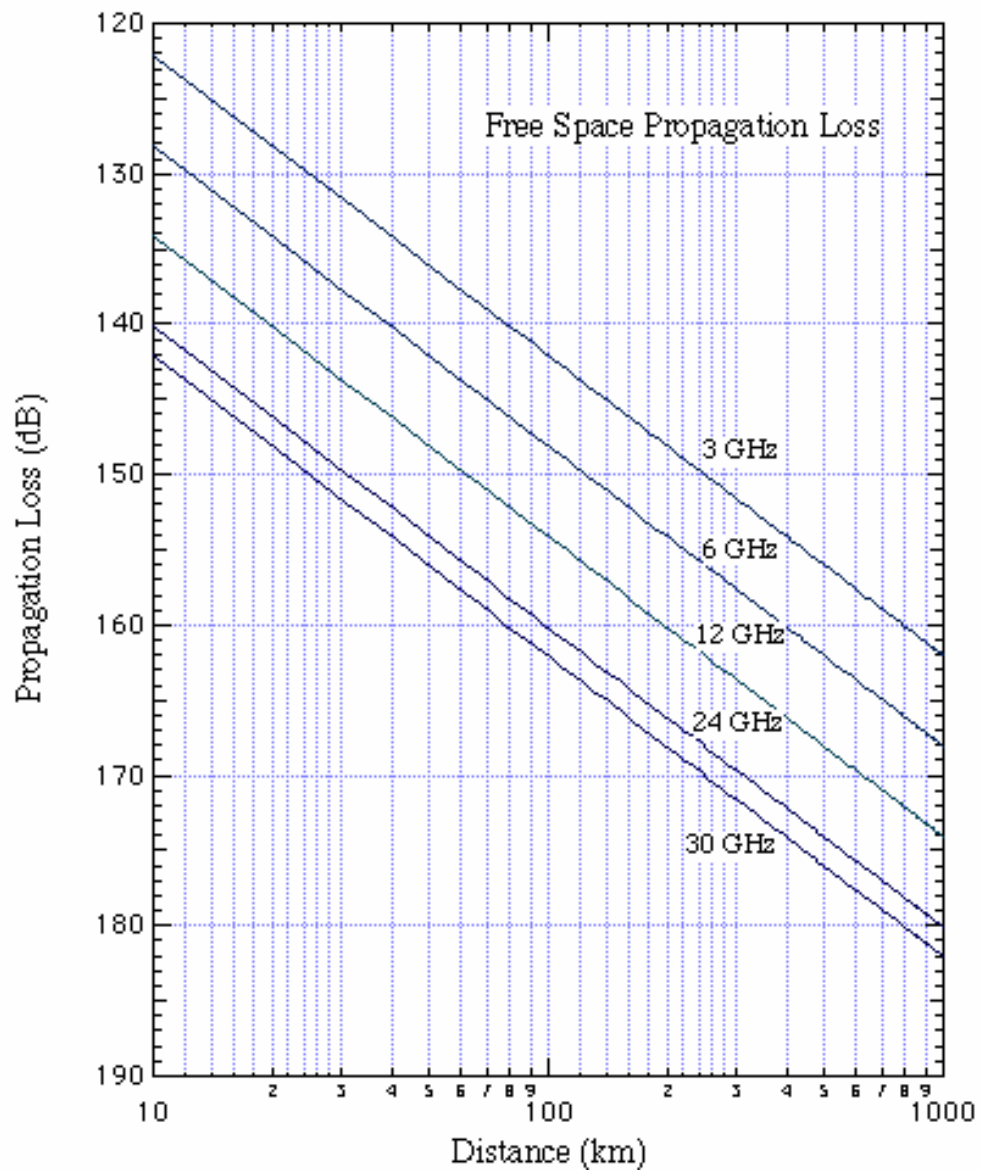


Figure 2-1-1

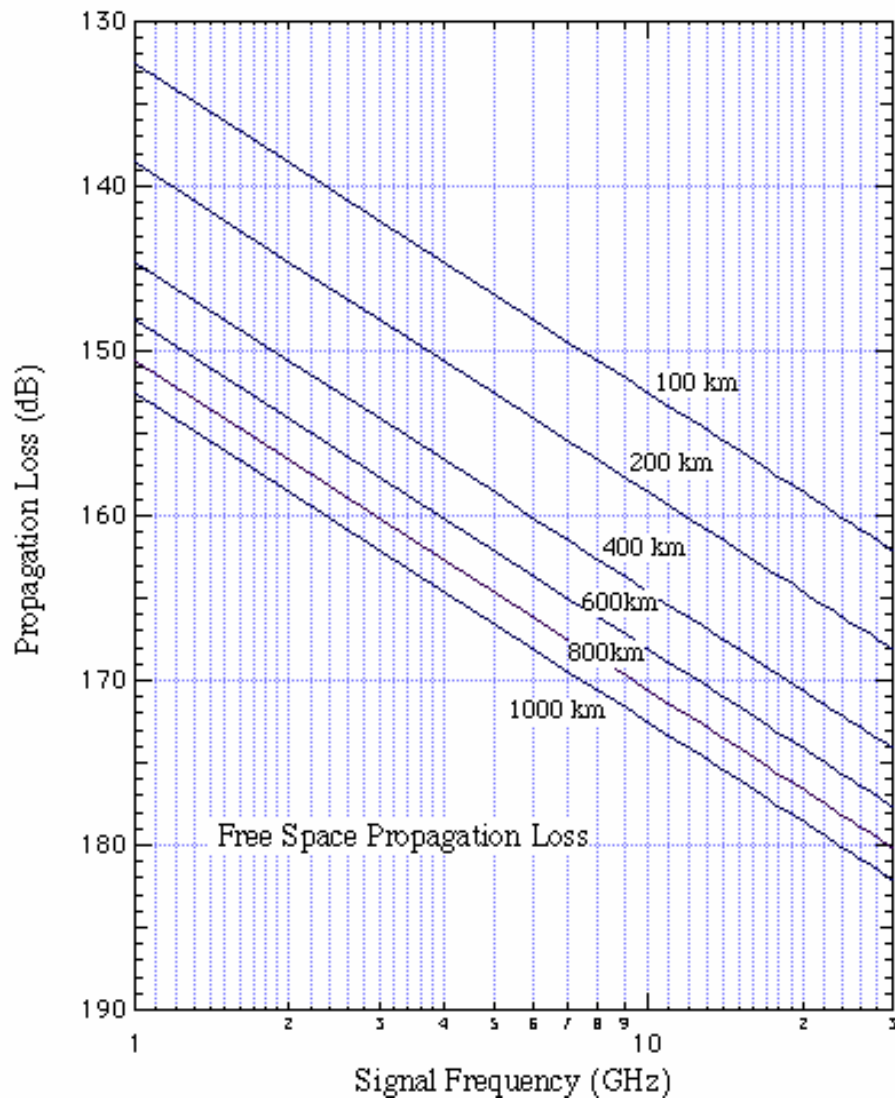


Figure 2-1-2

$$L_{\theta} = \frac{L_{90}(dB)}{\sin \theta} \quad 5^{\circ} \leq \theta \leq 90^{\circ}$$

where L_{90} : zenith Loss
under Clear Weather

Elevation range:

$$-5^{\circ} \leq \theta \leq 90^{\circ}$$

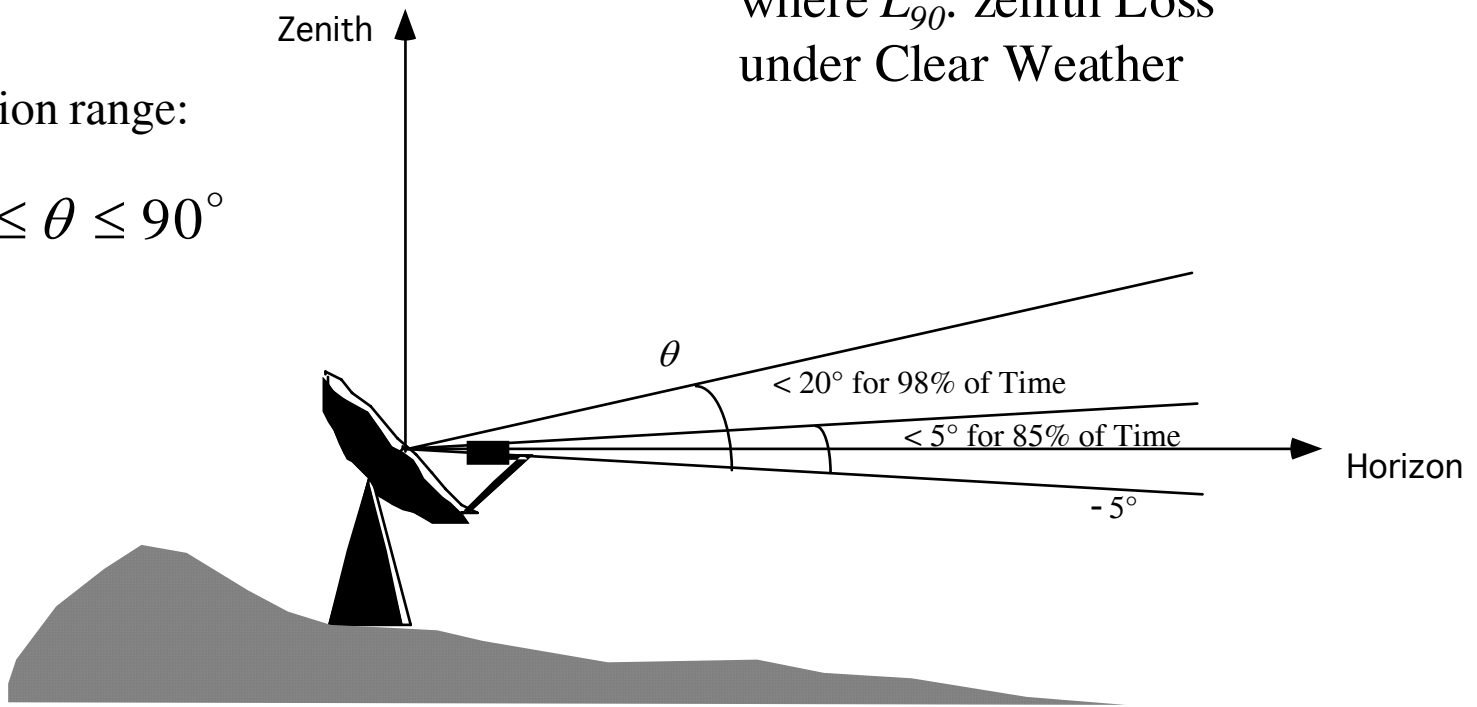


Figure 2-1-3

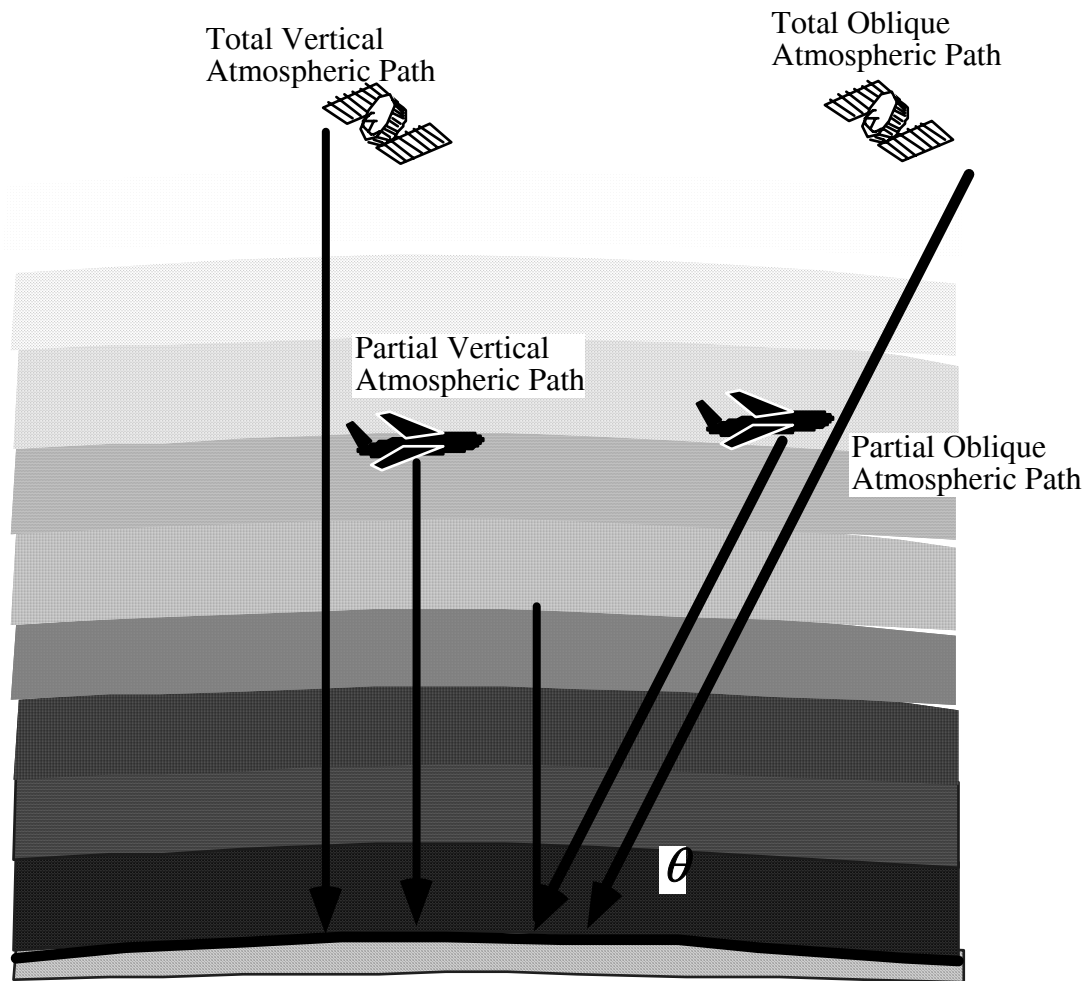


Figure 2-1-4

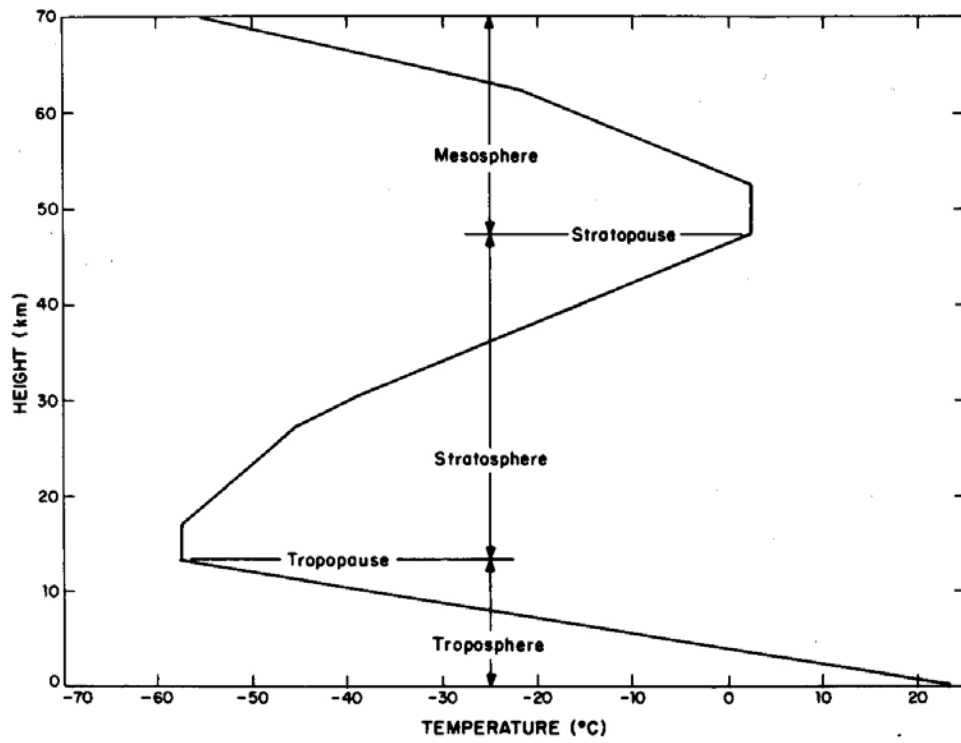


Figure 2-2-1

Specific Attenuation of Oxygen
for a Horizontal Path (1 - 30 GHz)

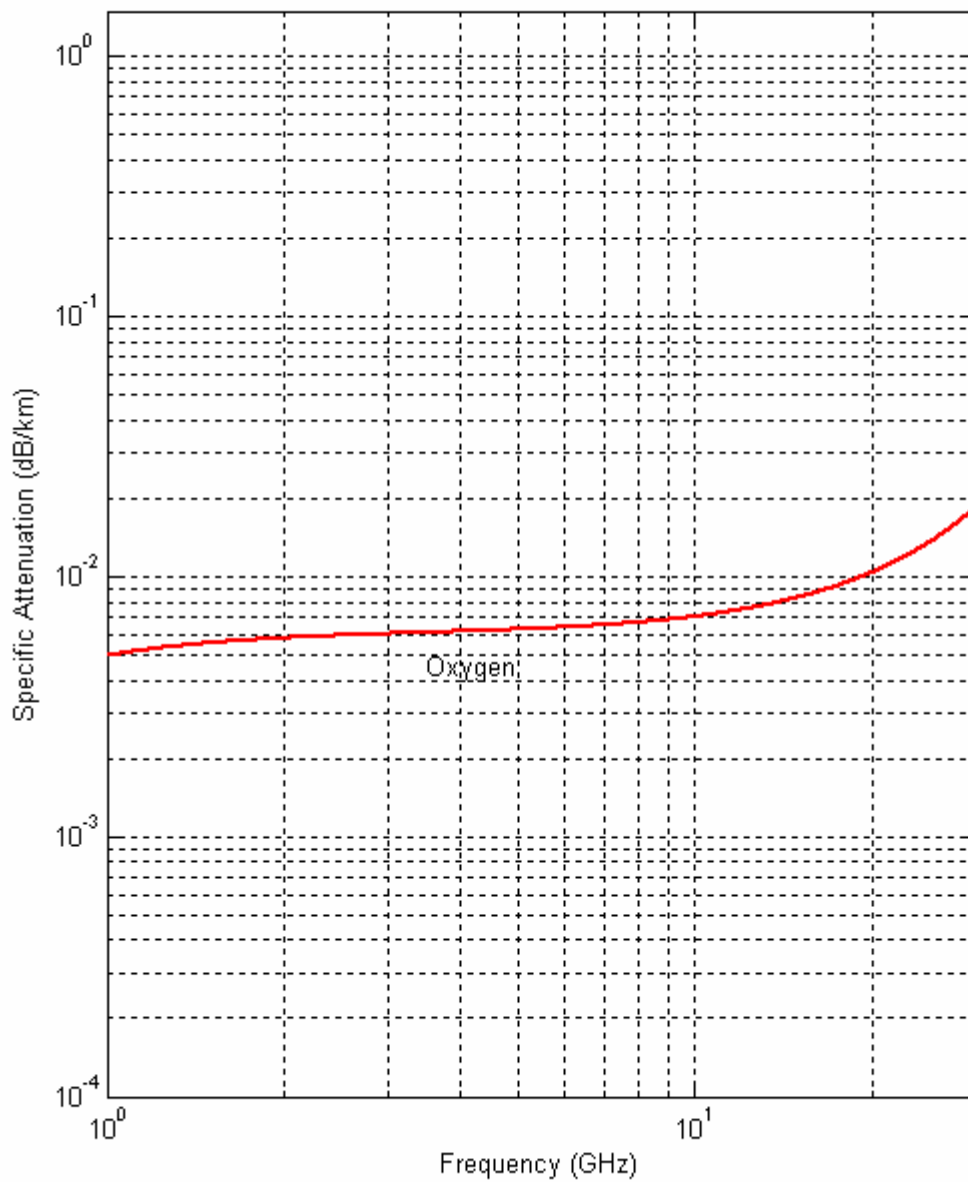


Figure 2-2-2

Specific Attenuation of Water Vapor (densities 7.5 and 12 g/m³)
for a Horizontal Path (1 - 30 GHz)

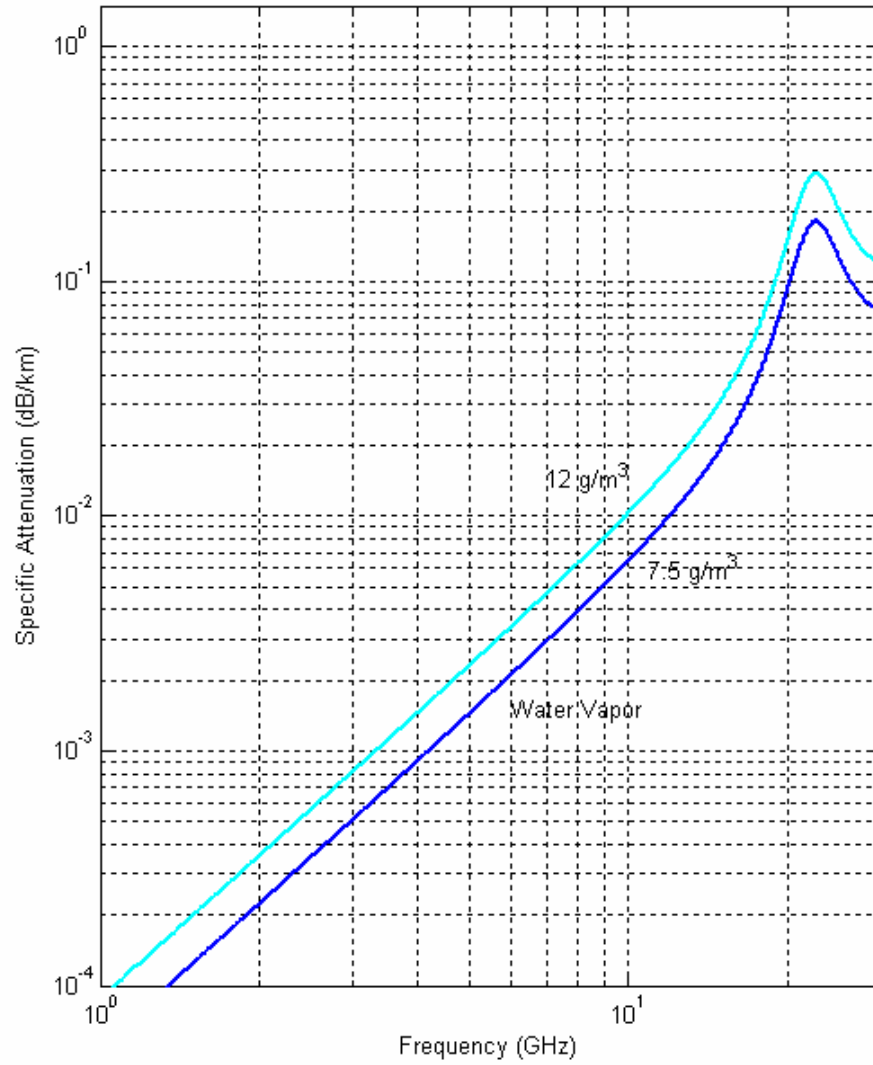


Figure 2-2-3

Attenuation of Oxygen and Water Vapor (density 7.5 g/m³)
for a Horizontal Path (1 - 30 GHz)

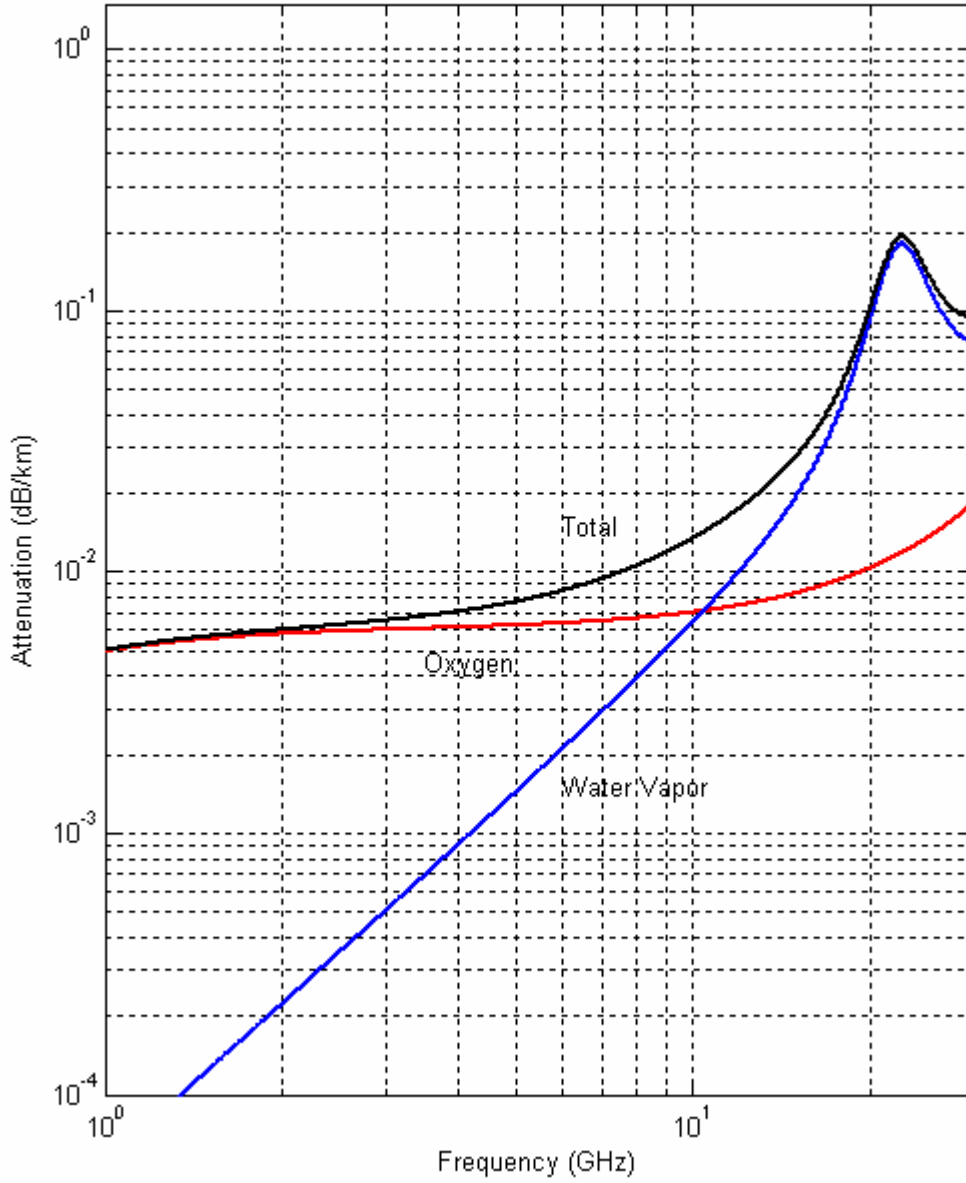


Figure 2-2-4

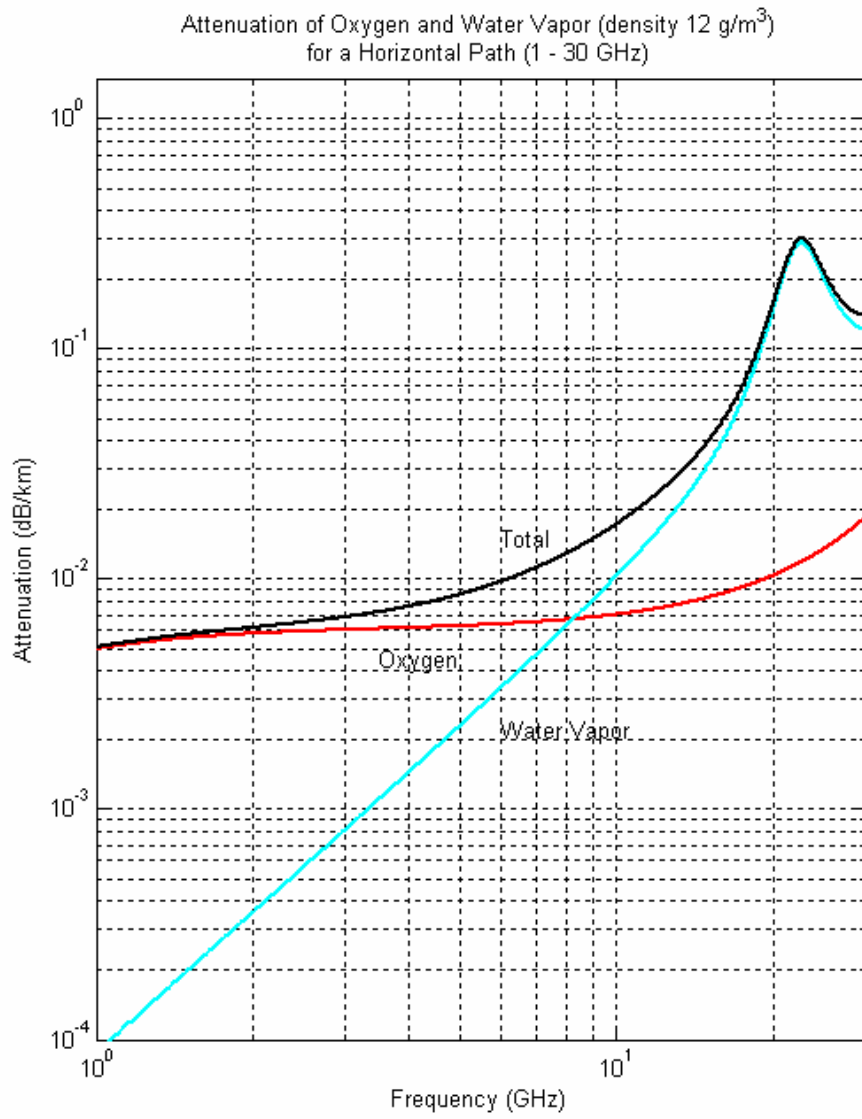


Figure 2-2-5

Zenith Attenuation of Oxygen
for a Vertical Path (1 - 30 GHz)

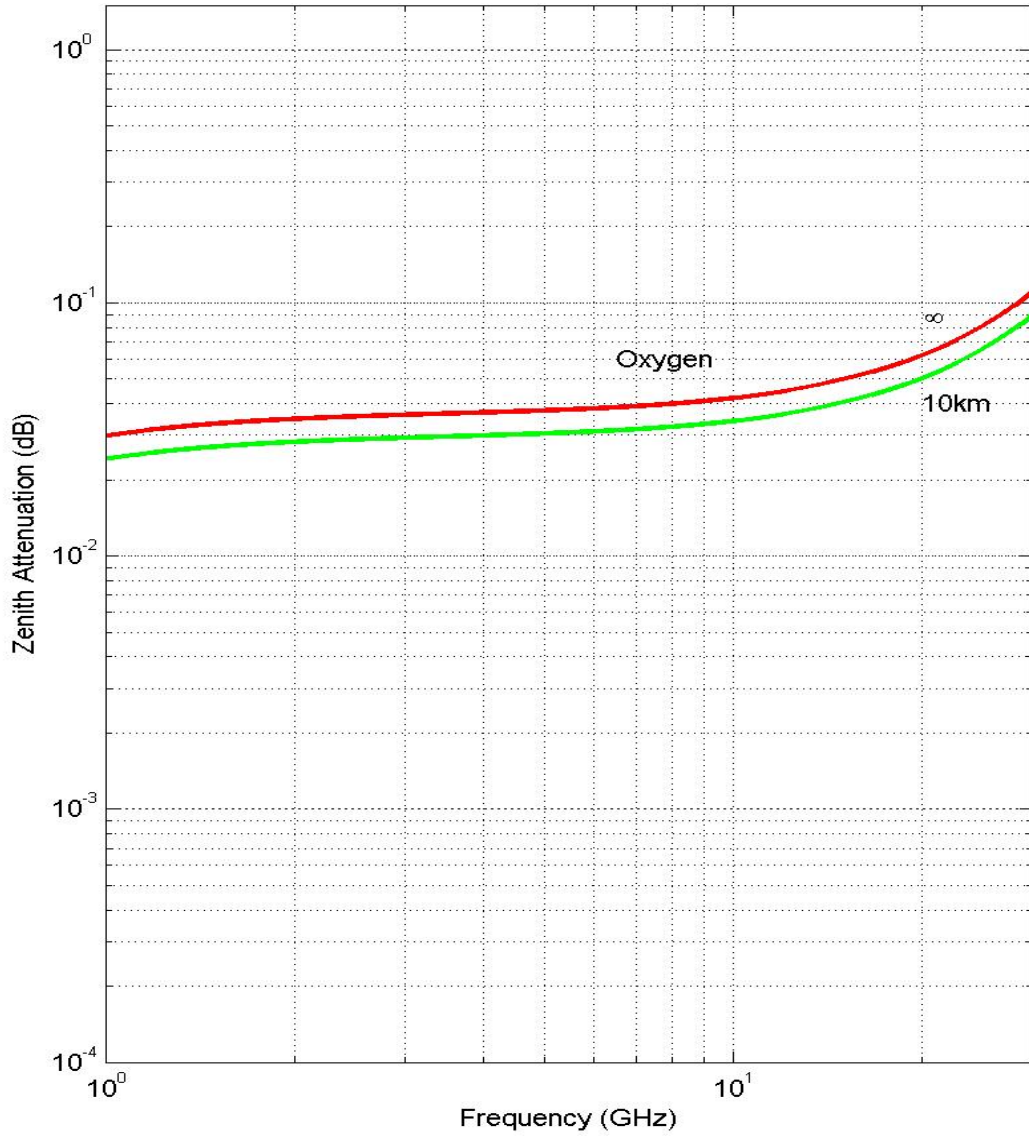


Figure 2-2-6

Zenith Attenuation of Water Vapor (densities 7.5 and 12 g/m³)
for a Vertical Path (1 - 30 GHz)

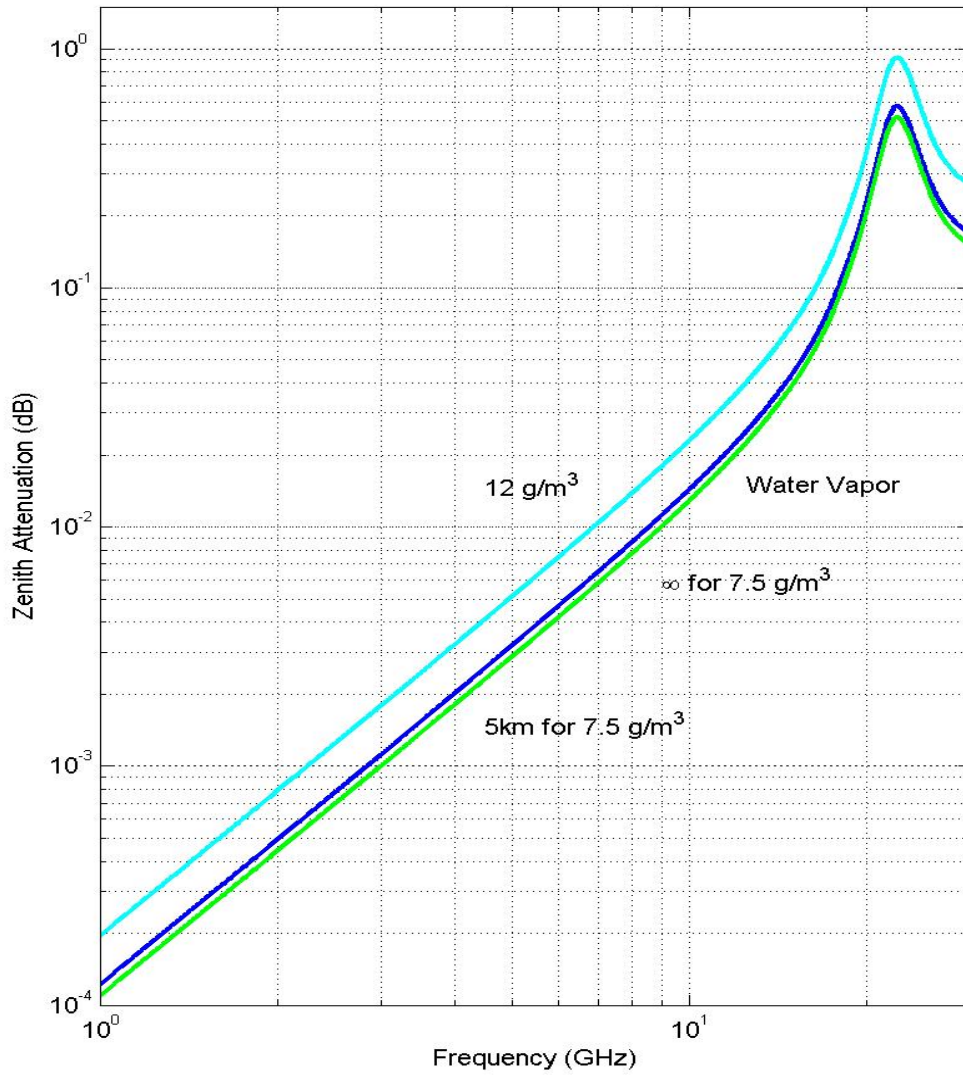


Figure 2-2-7

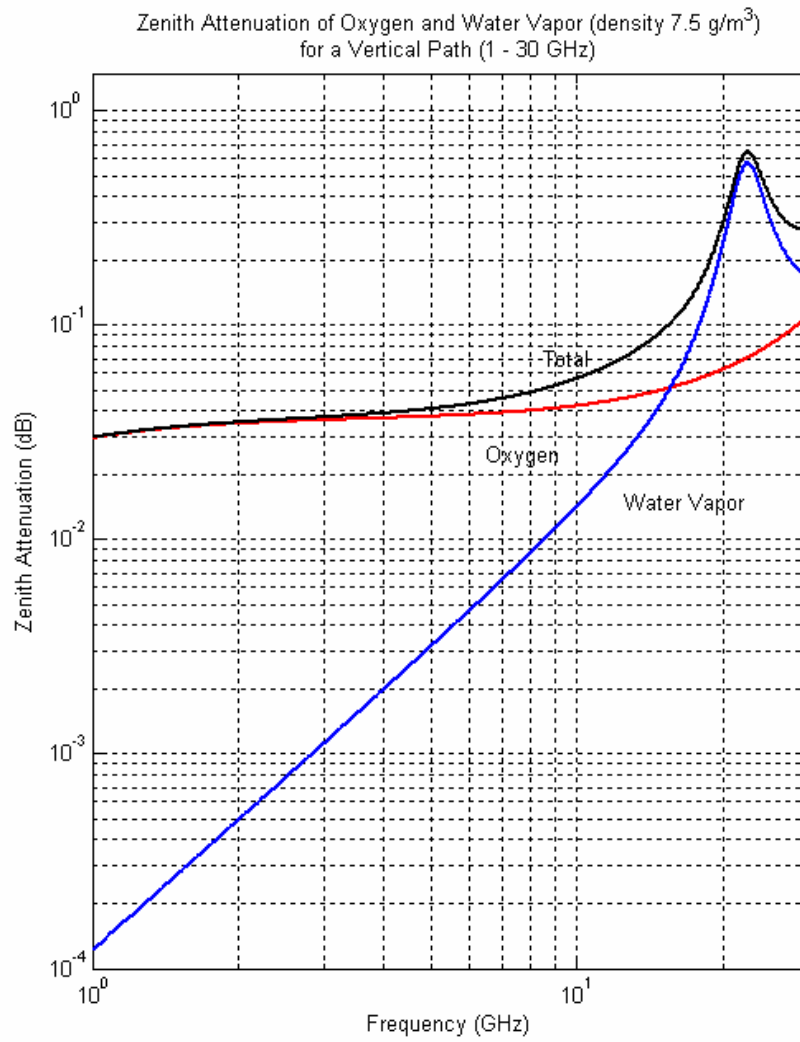


Figure 2-2-8

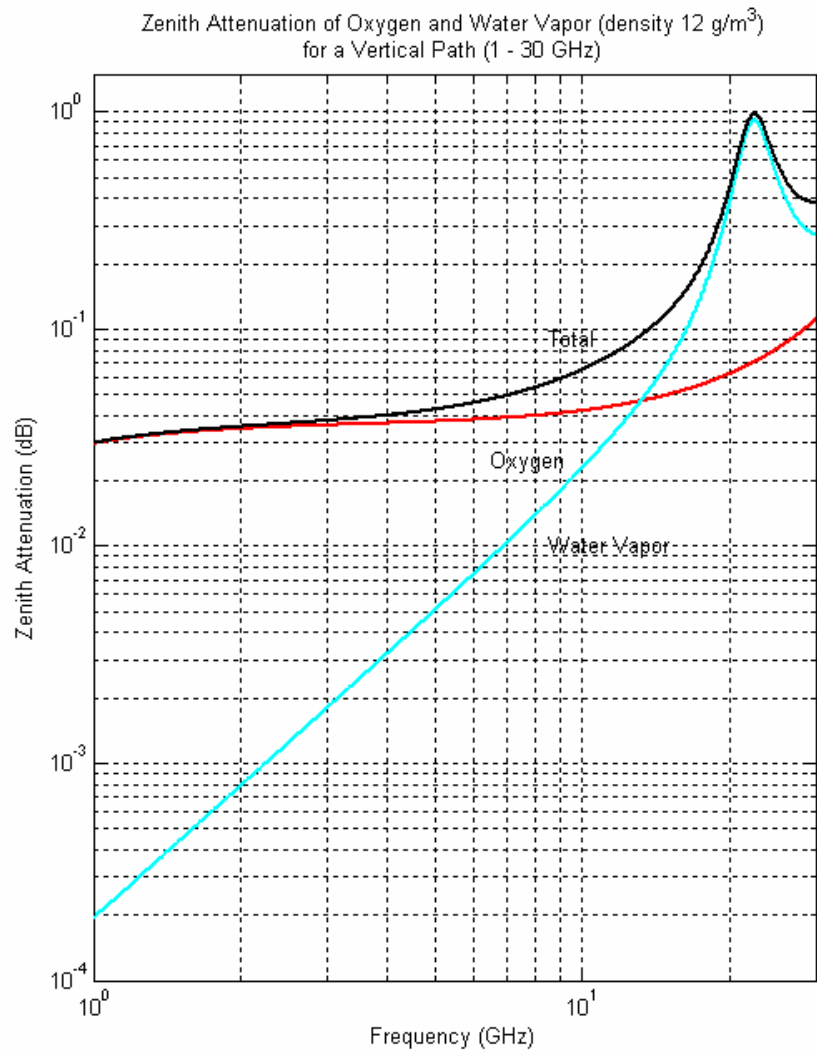


Figure 2-2-9

Elevation Angle Dependence of Atmospheric Attenuation
for 3, 6, 12, and 24 GHz (Water Vapor density 7.5 g/m³)

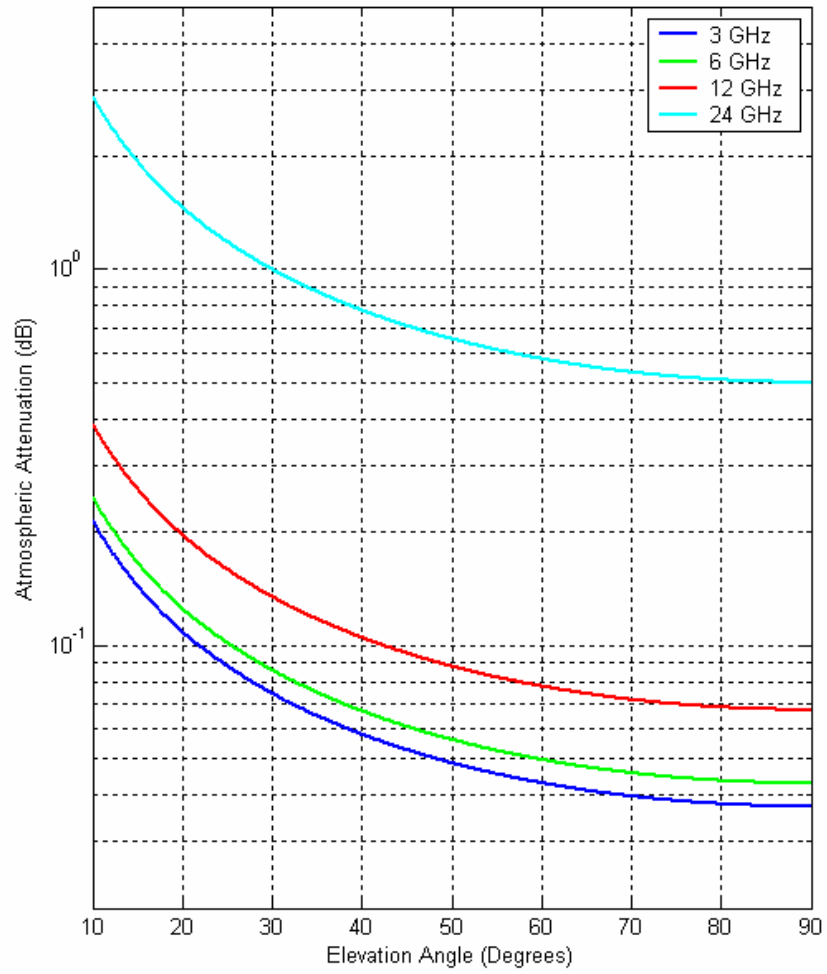


Figure 2-2-10

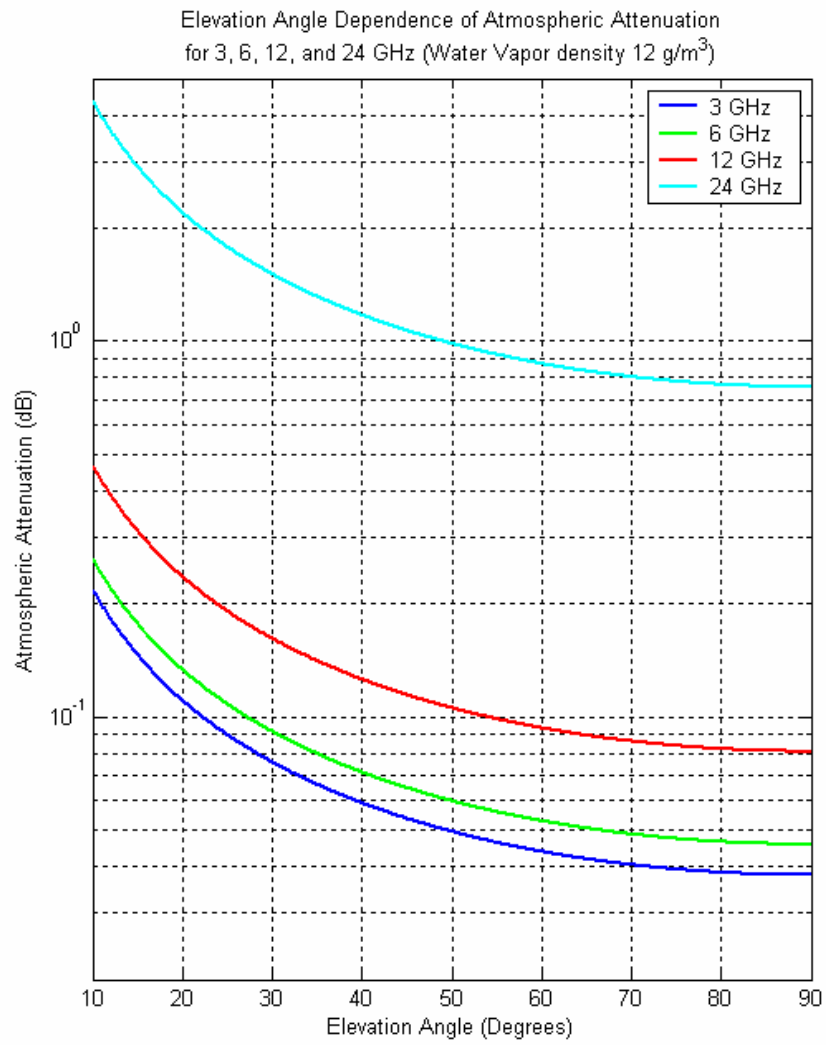


Figure 2-2-11

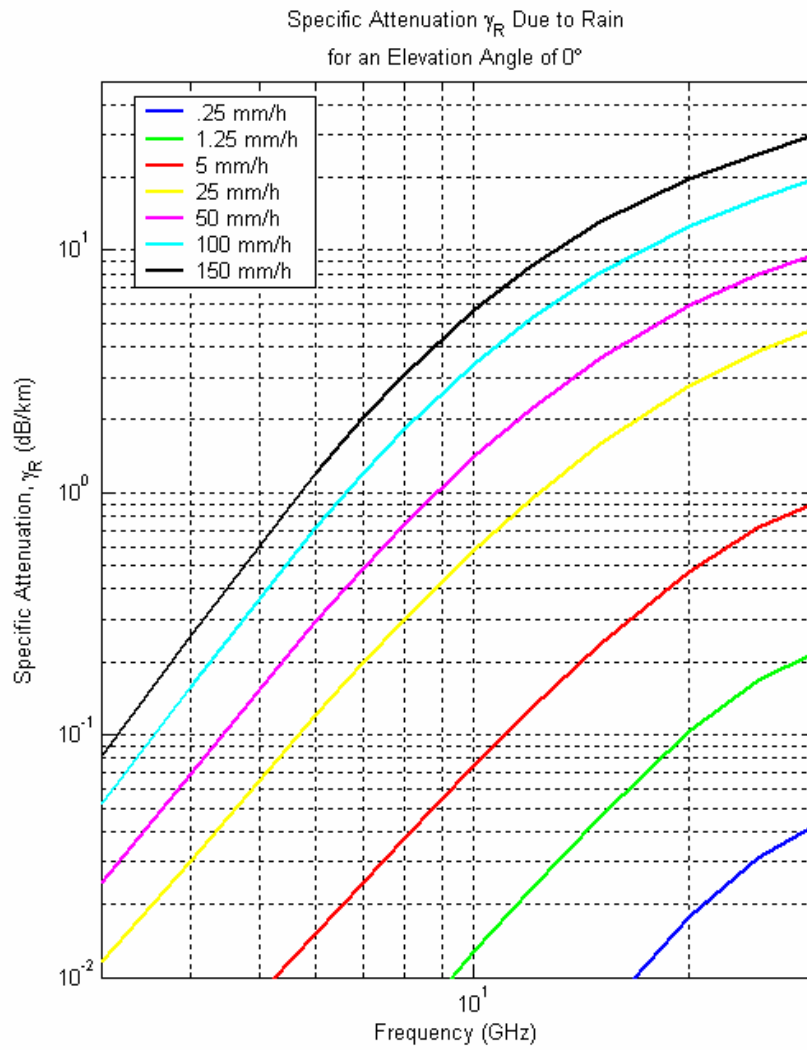


Figure 2-2-12

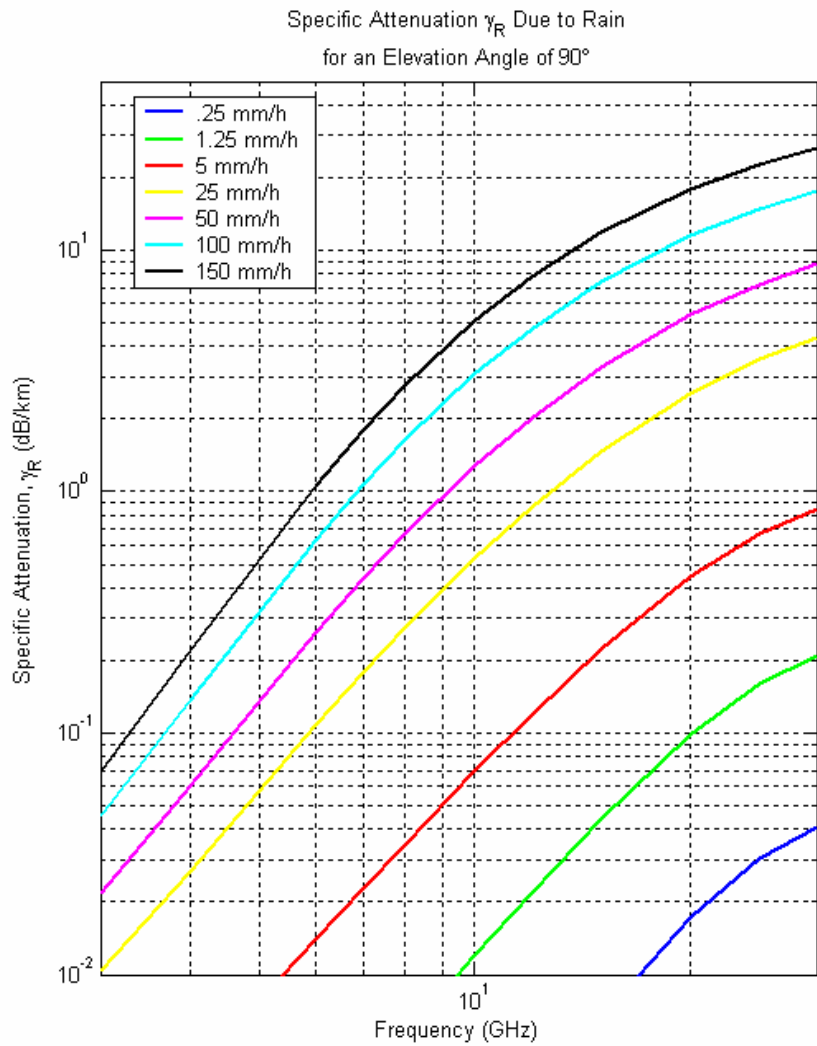


Figure 2-2-13

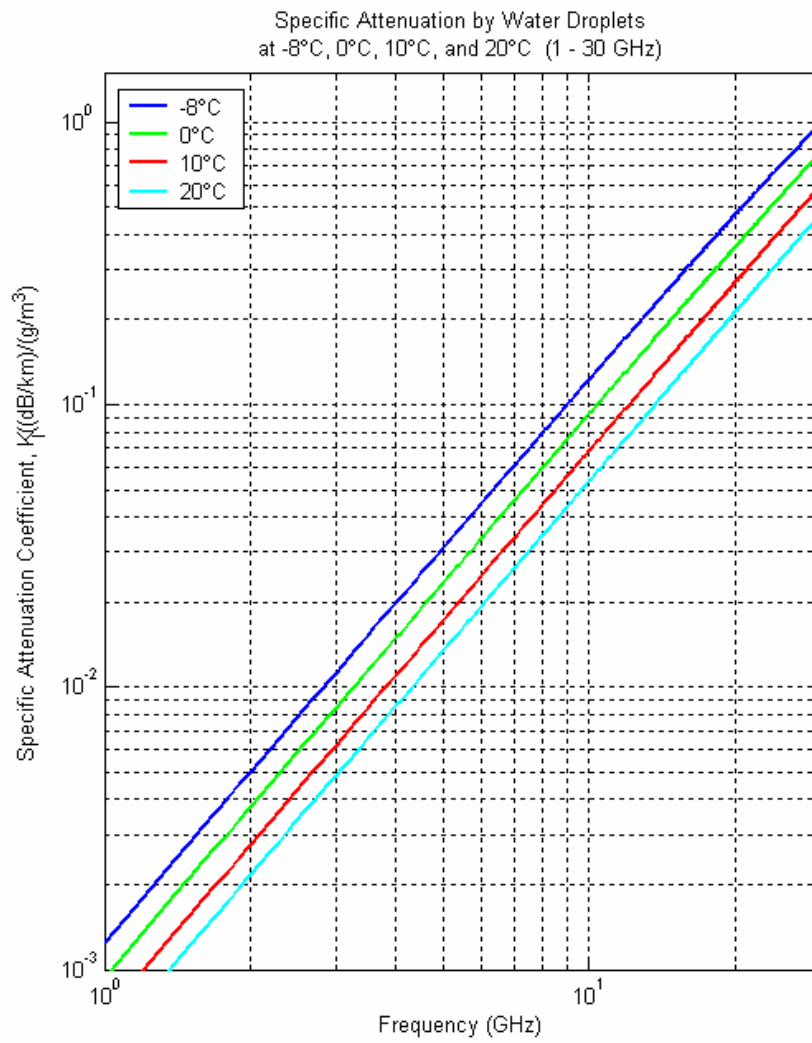


Figure 2-2-14

Frequency Dependence (10° Elevation Angle)
Scintillation Fade Depth 1%, 3%, 5% of Time Exceeded

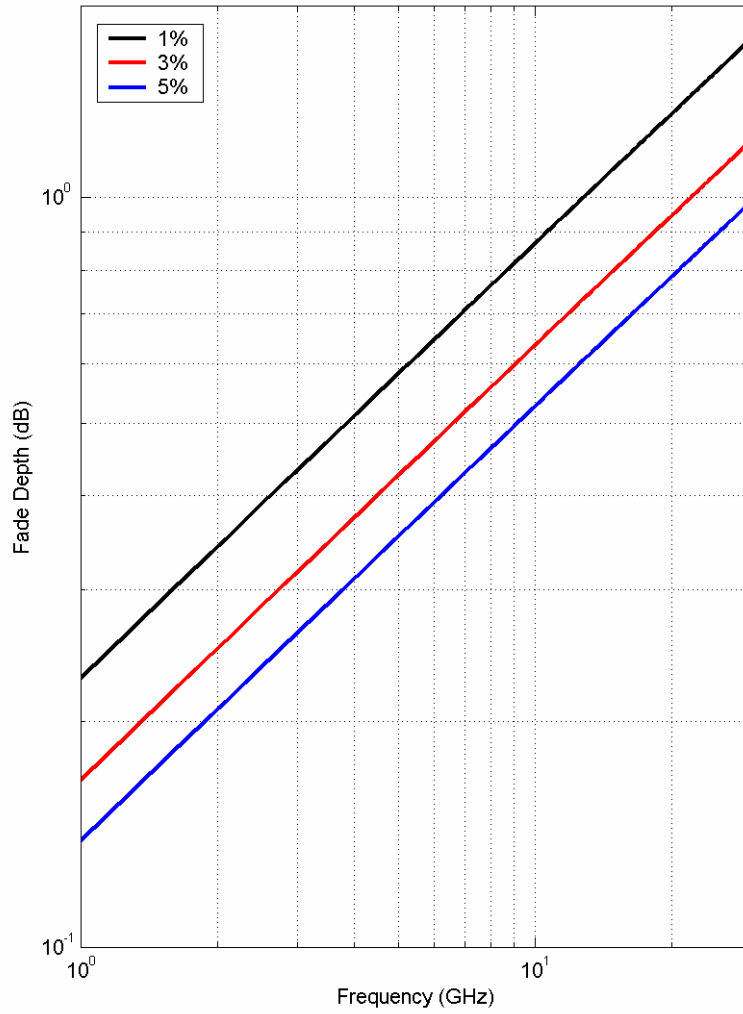


Figure 2-2-15

Elevation Angle Dependence (for Angle > 4°)
Scintillation Fade Depth 1% of Time Exceeded

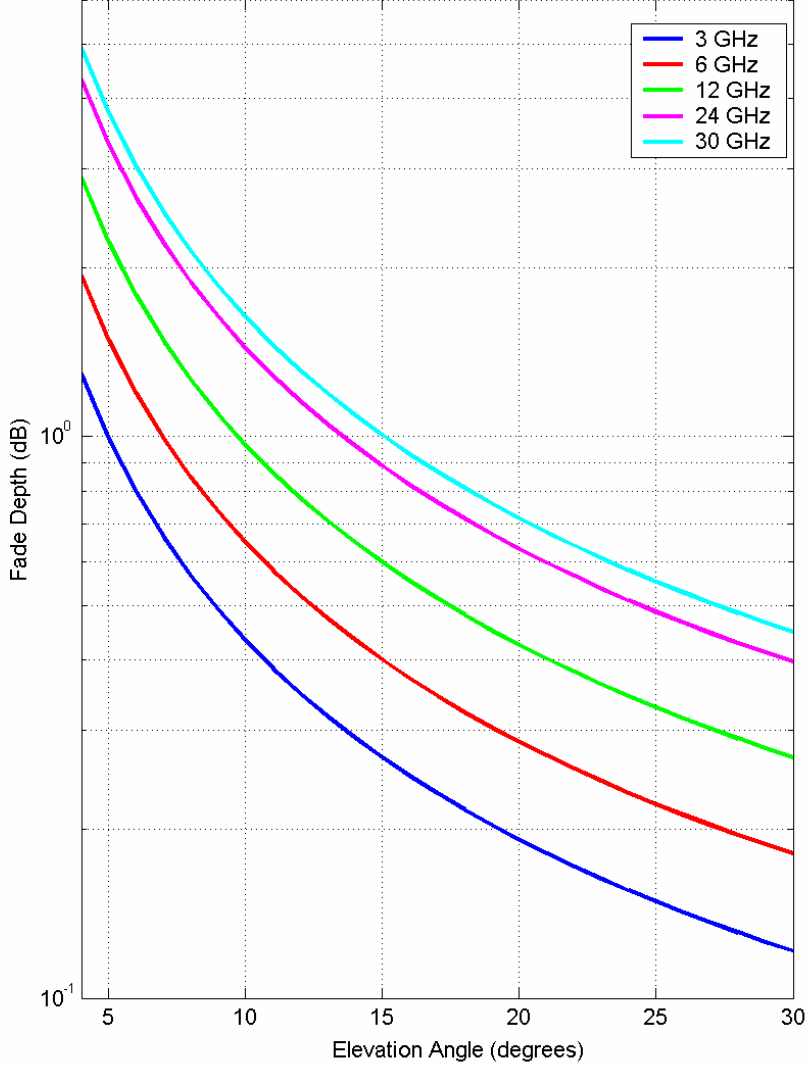


Figure 2-2-16

Low elevation Angle Fading is a Combination of Atmospheric Scintillation and Ground Multipaths

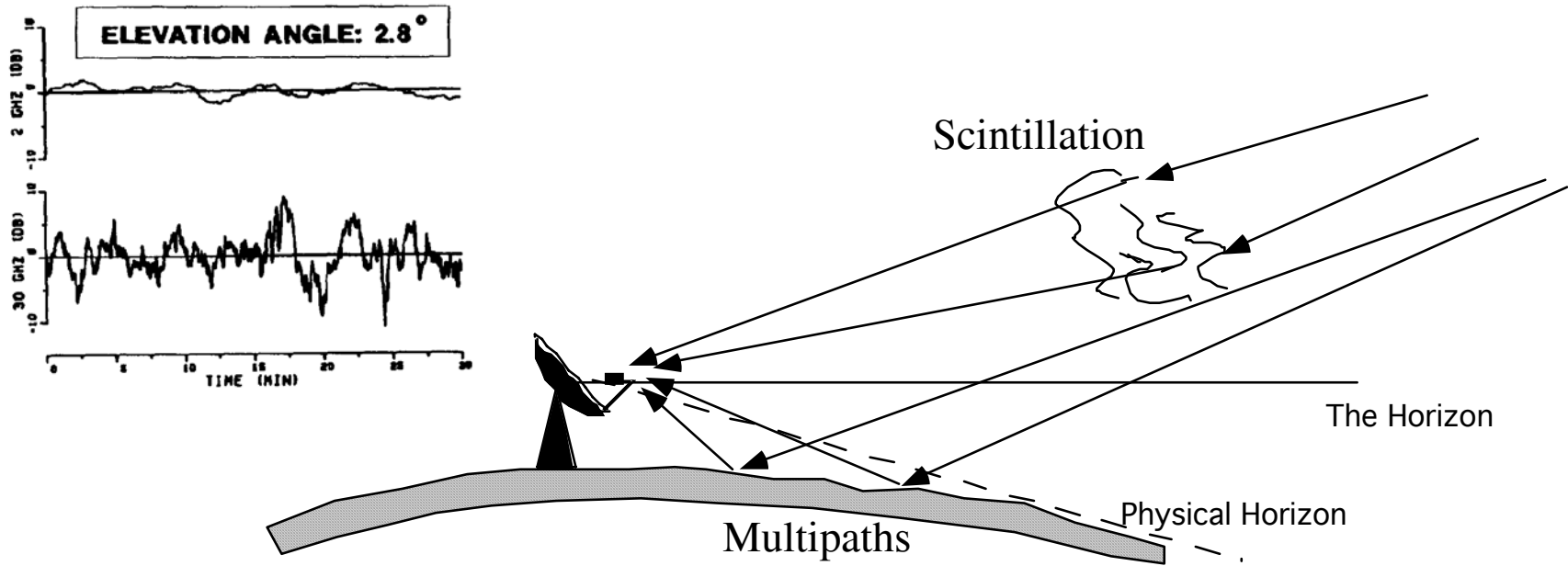


Figure 2-2-17

Frequency Dependence (2° Elevation Angle)
Deep Fading (Scintillation/Multipath) 1%, 3%, and 5% of Time Exceeded in Ave Worst Month
Percentage of Time Gradient ≤ -100 N-unit/km=20%

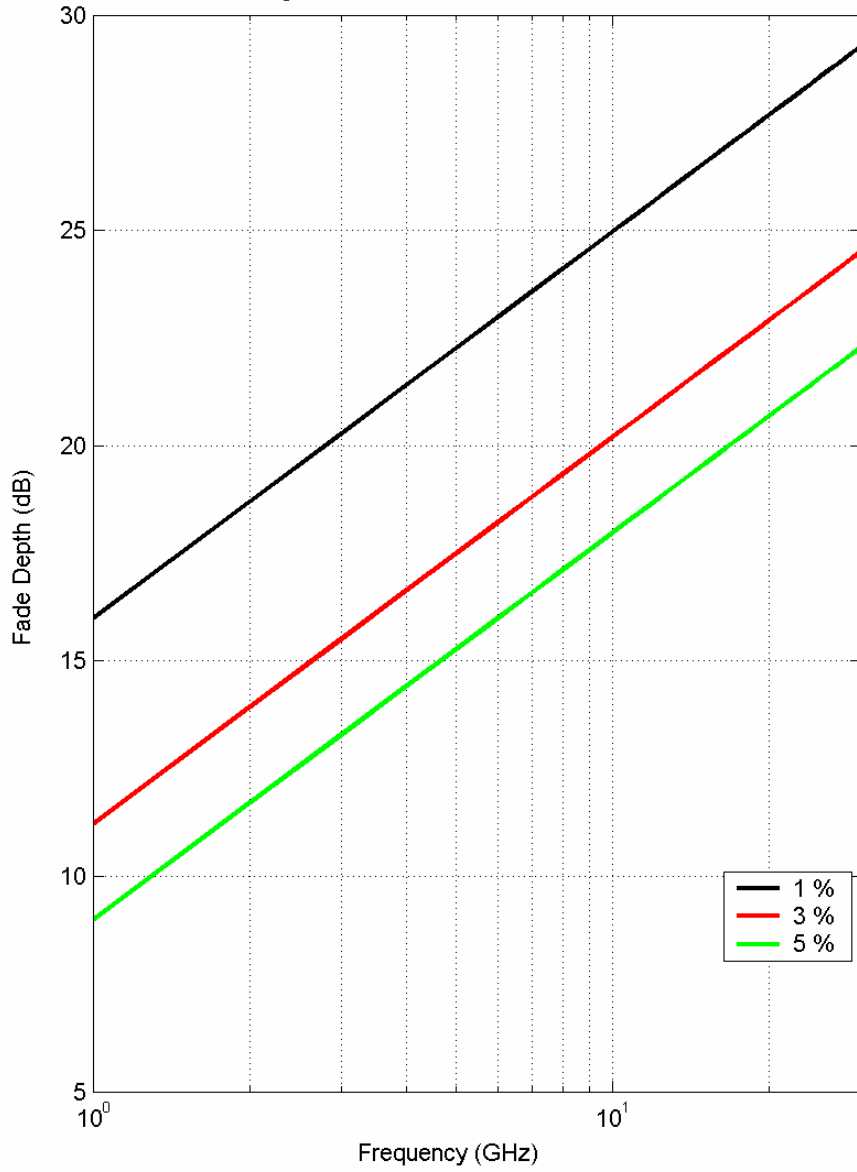


Figure 2-2-18

Elevation Angle Dependence (for Angle < 5°)
Deep Fading (Scintillation/Multipath) 1% of Time Exceeded in Average Worst Month
Percentage of Time Gradient <=-100 N-unit/km=20%

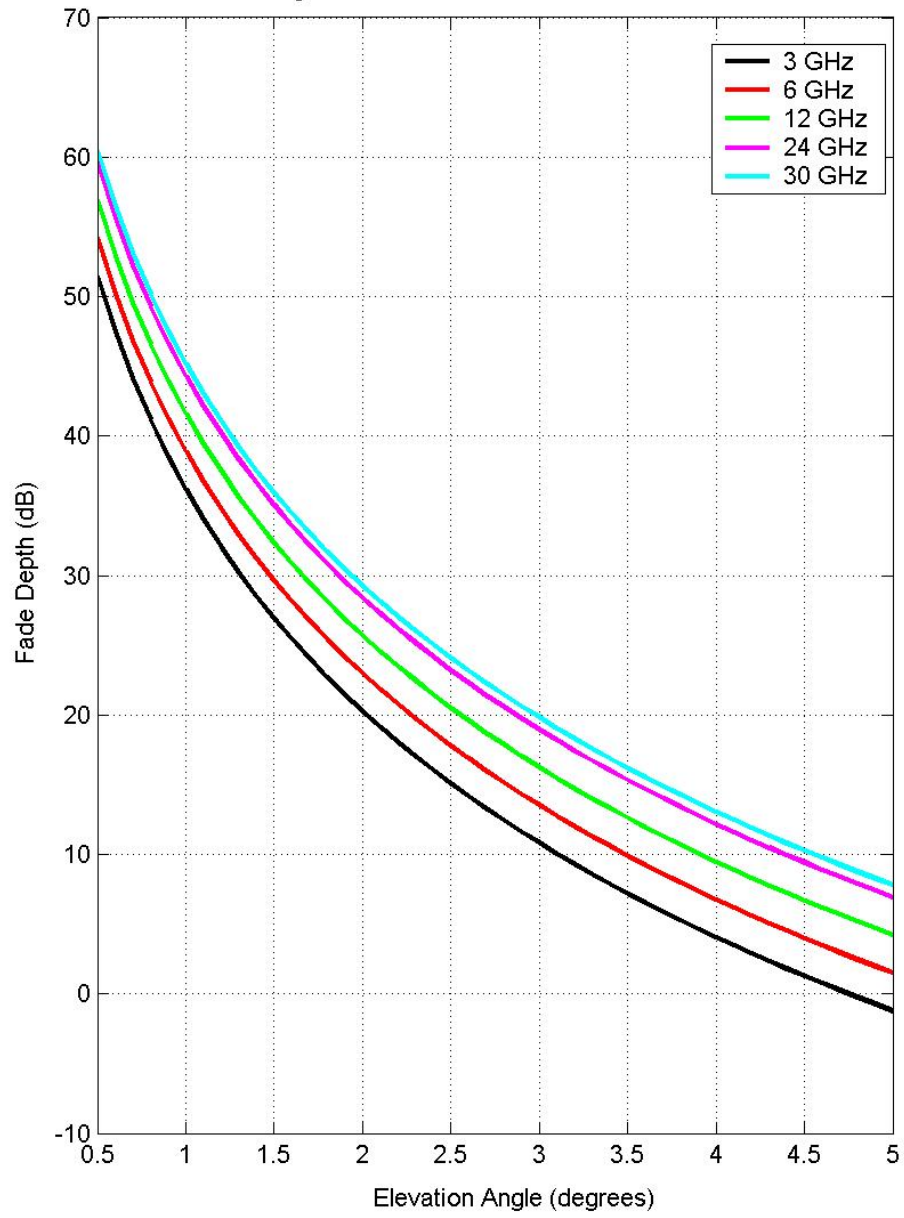


Figure 2-2-19

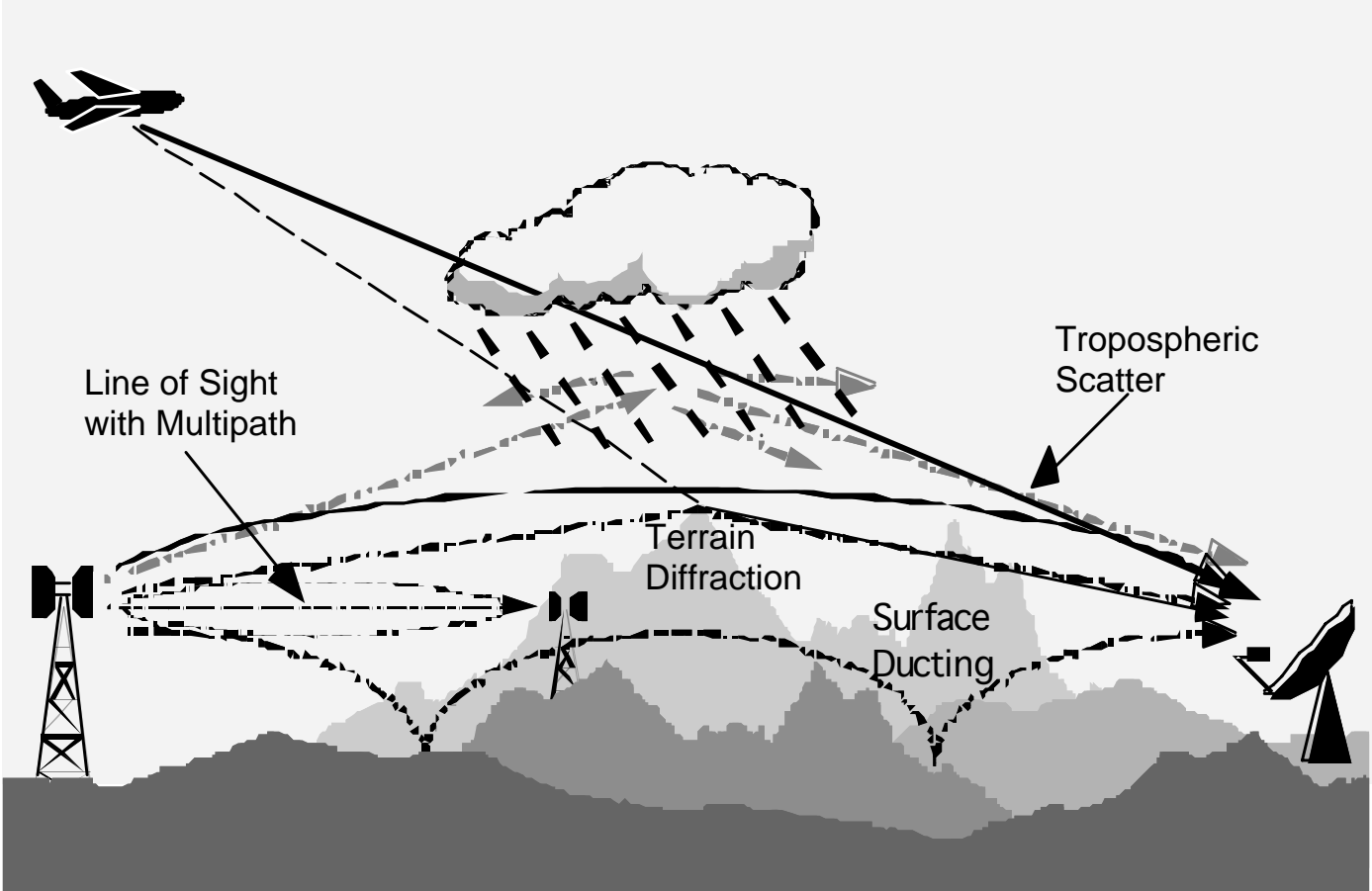


Figure 2-2-20

Terrain Diffraction Over a Single Knife-edge can be calculated Using the following equations:

$$v = h \sqrt{\frac{2}{\lambda} \left(\frac{1}{d_1} + \frac{1}{d_2} \right)}$$

$$J(v) = 6.9 + 20 \log \left(\sqrt{(v - 0.1)^2 + 1} + v - 0.1 \right) \quad \text{dB}$$

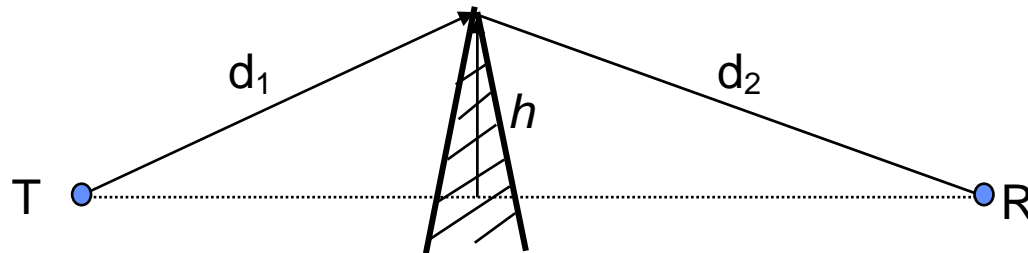
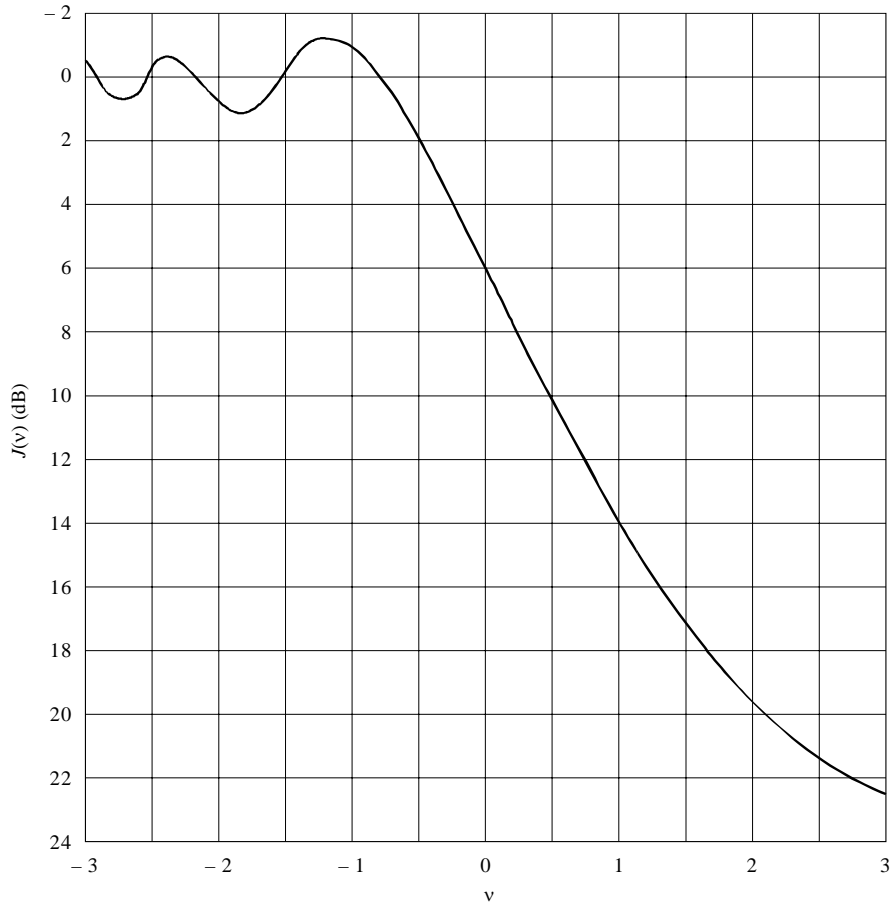


Figure 2-2-21

Knife-edge Diffraction Loss

FIGURE 7
Knife-edge diffraction loss



0526-07

Figure 2-2-22

Troposcatter Propagation Losses as Function of Percentage of Time and Distances

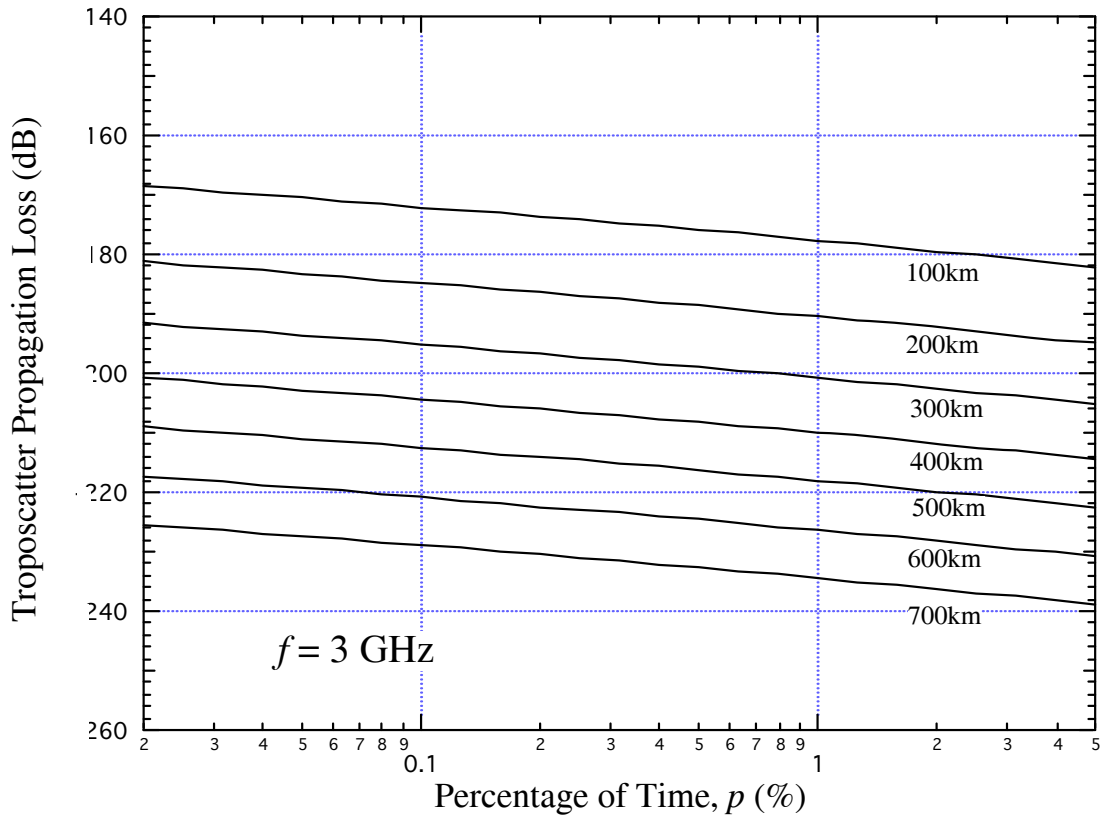


Figure 2-2-23

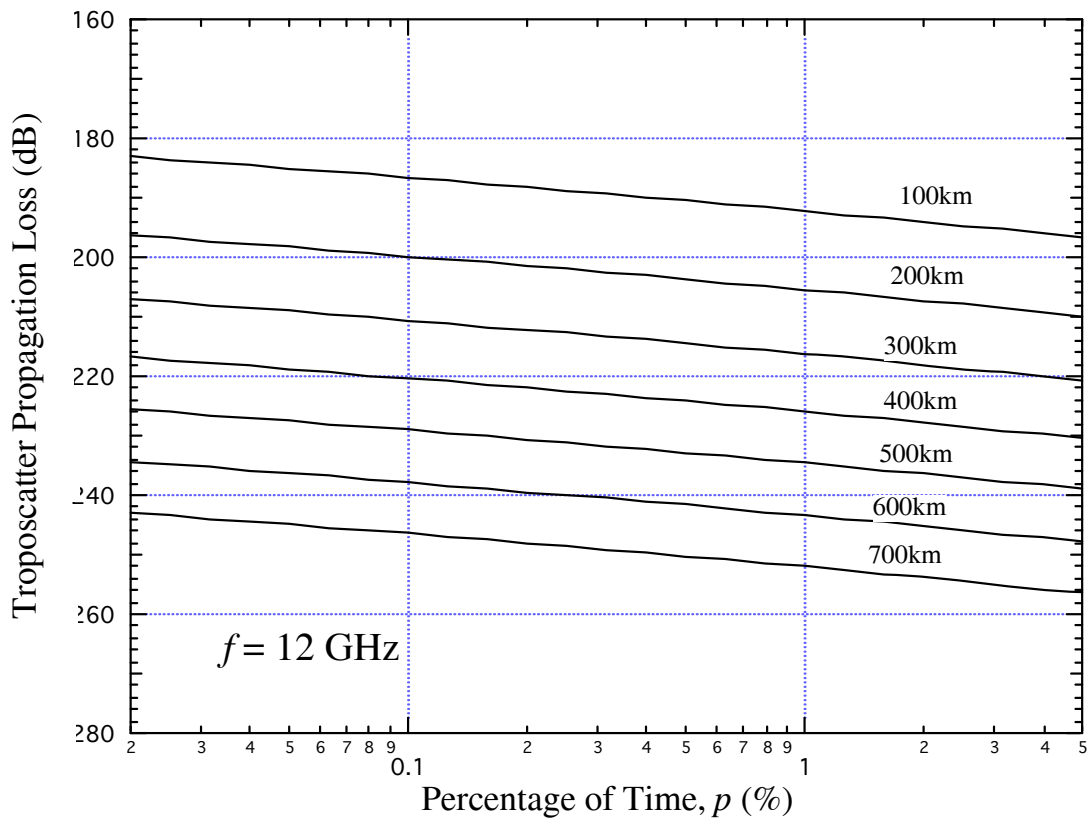
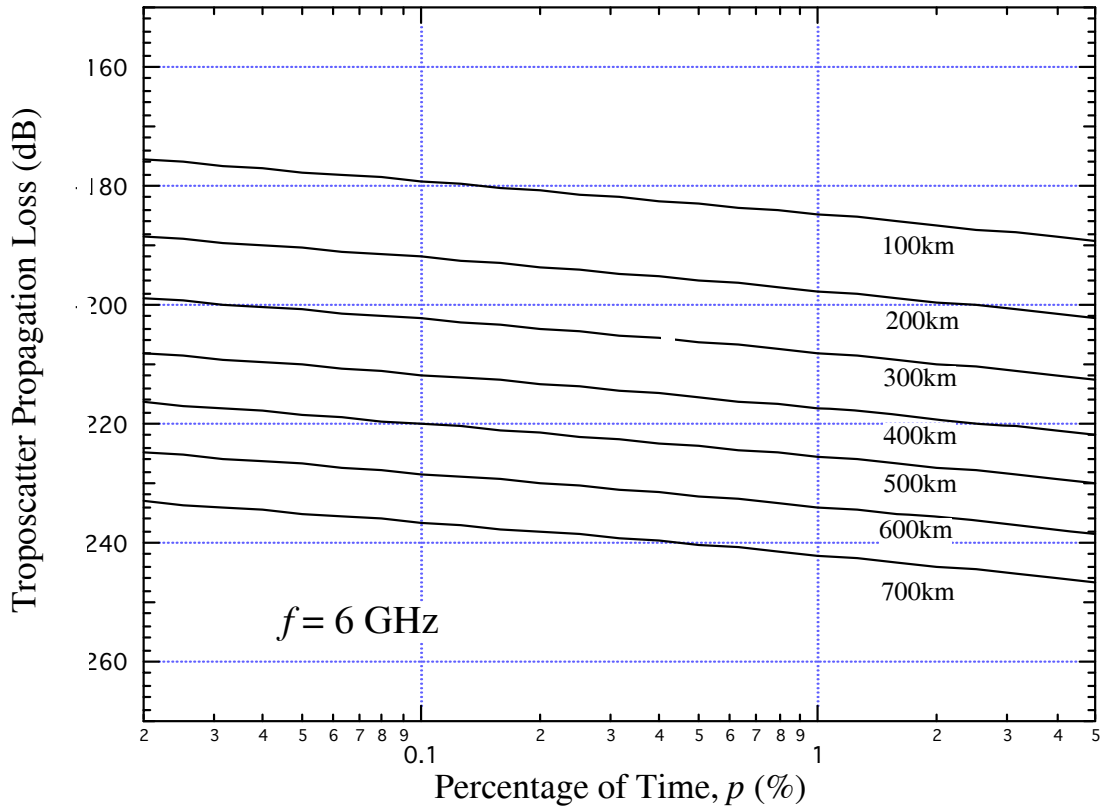


Figure 2-2-24

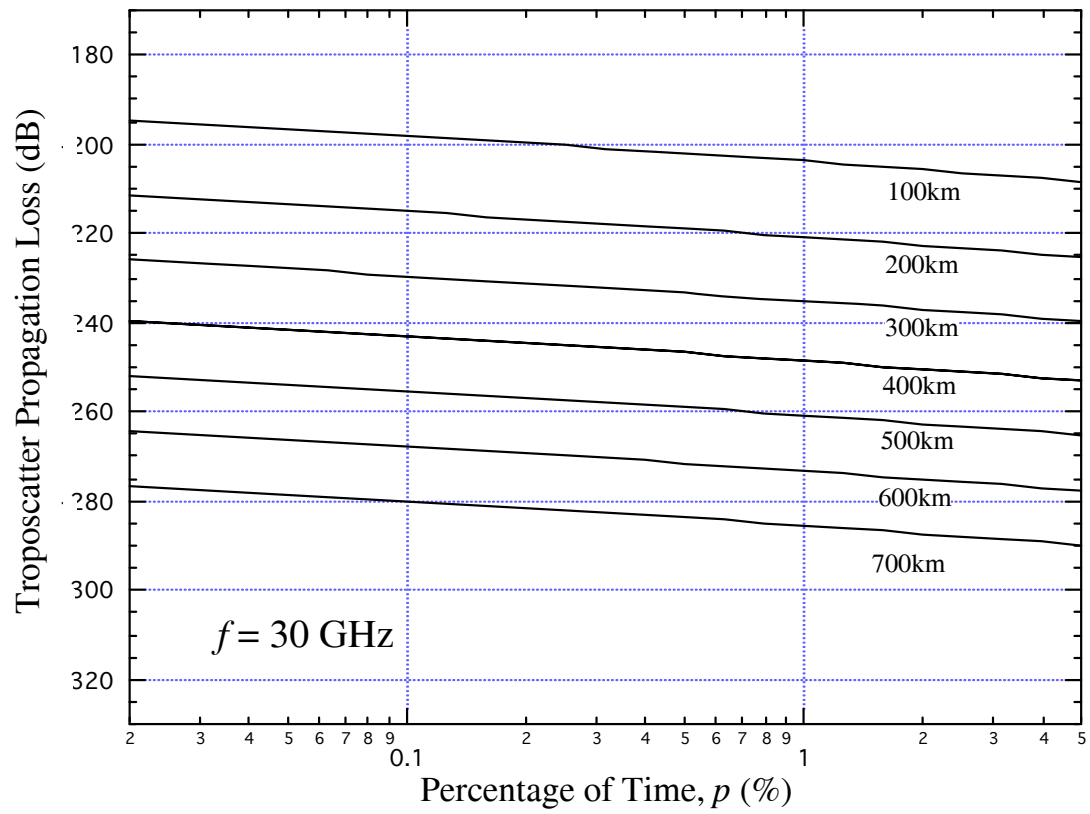
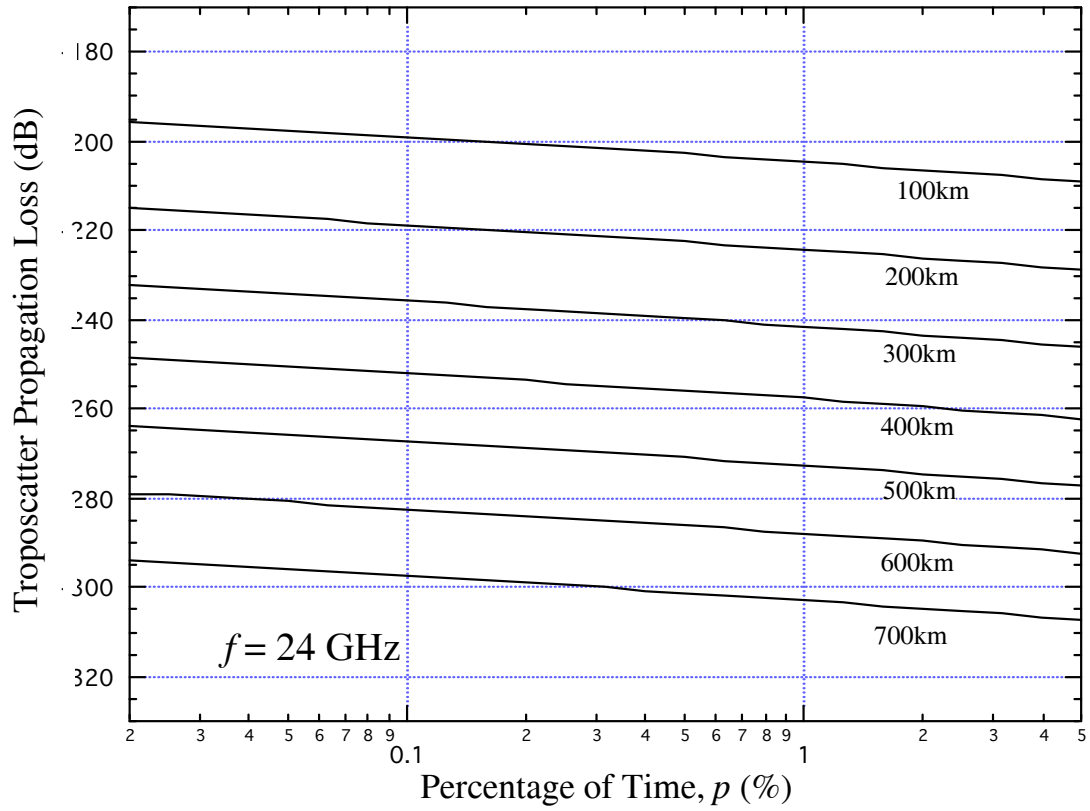
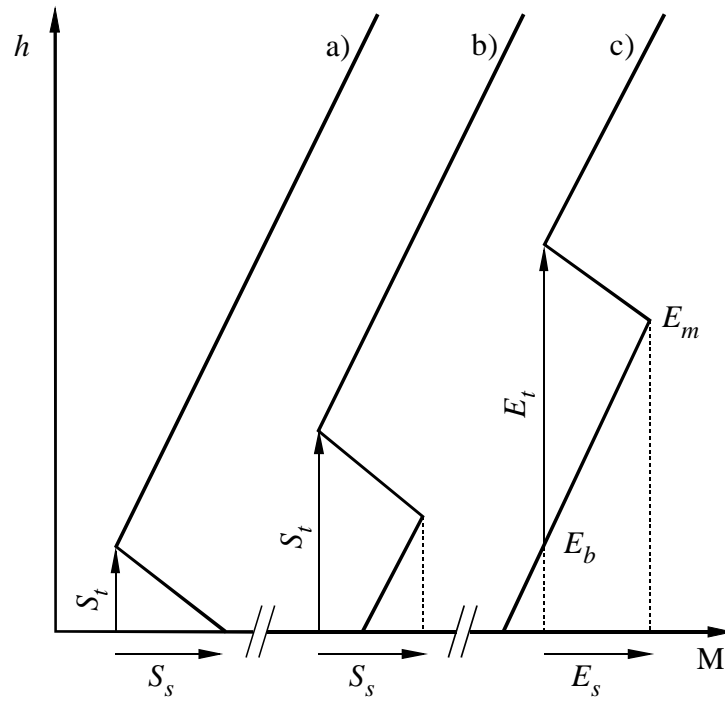


Figure 2-2-25

FIGURE 17

Definition of parameters describing a) surface, b) elevated surface and c) elevated ducts



0453-17

Figure 2-2-26

Ducting Propagation Losses as Function of Percentage of Time and Distances

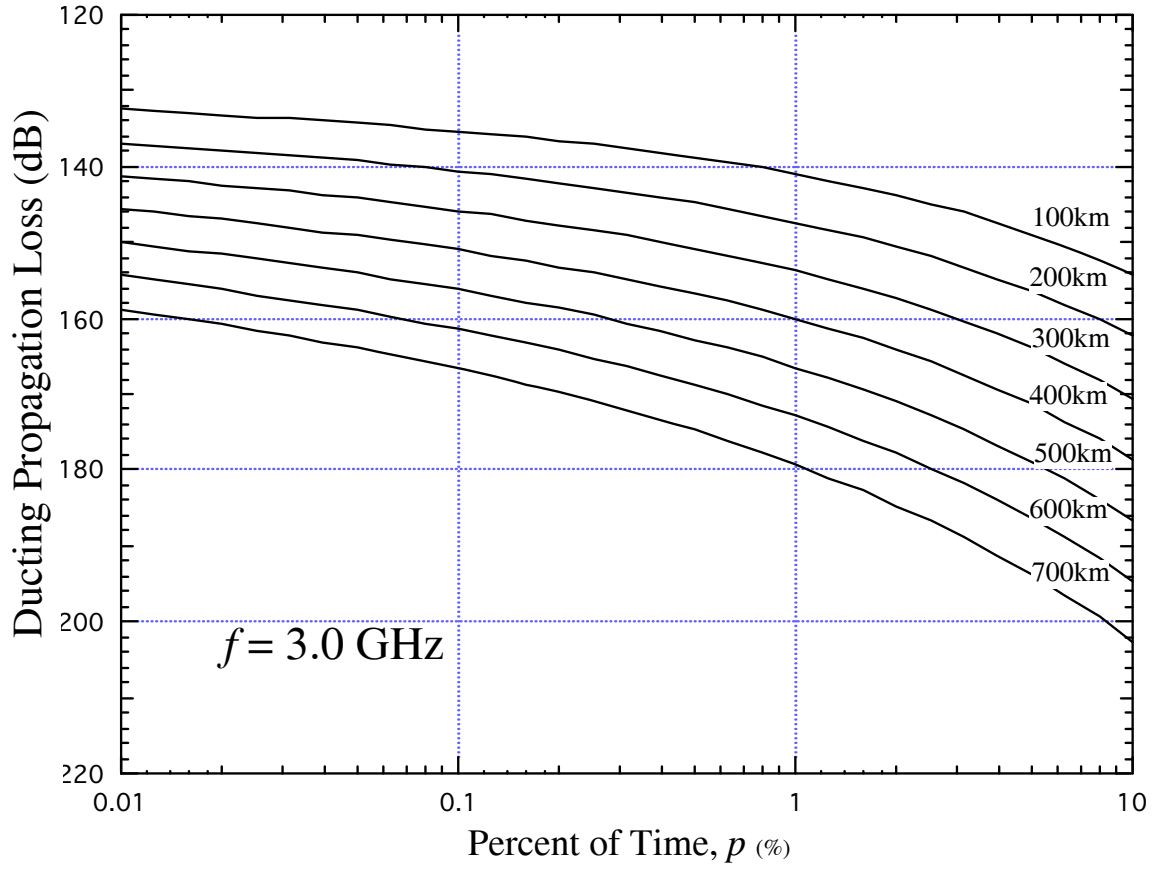


Figure 2-2-27

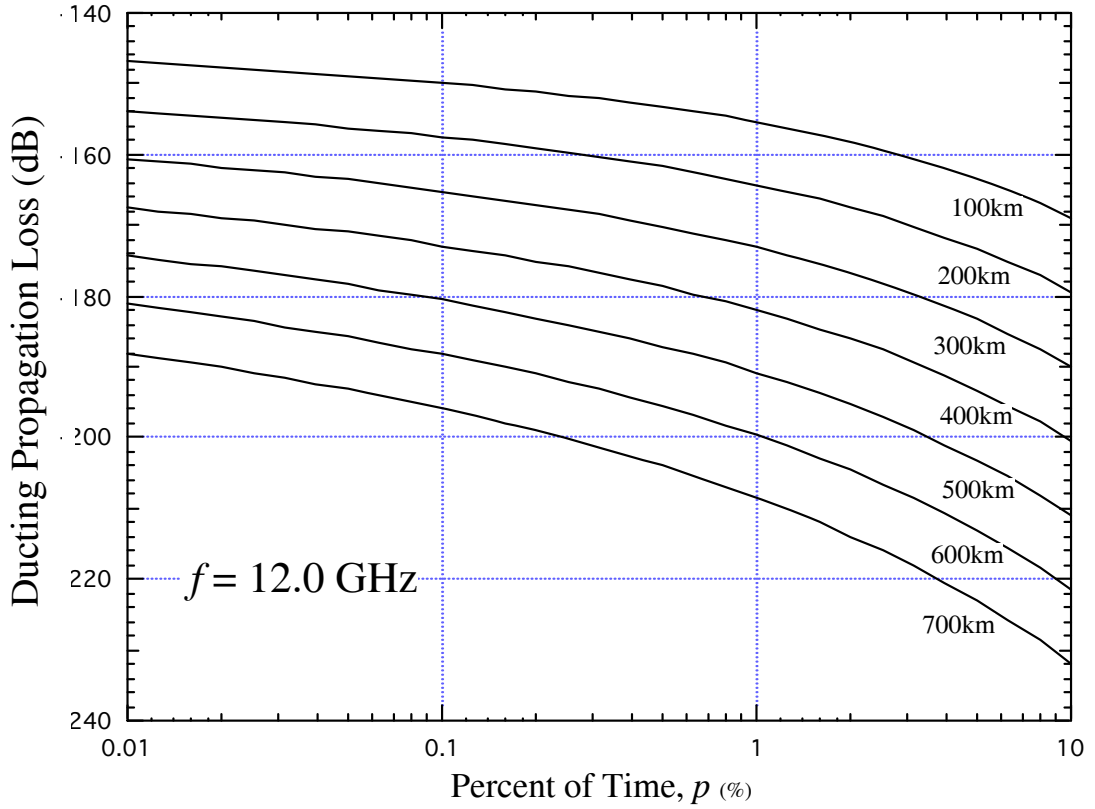
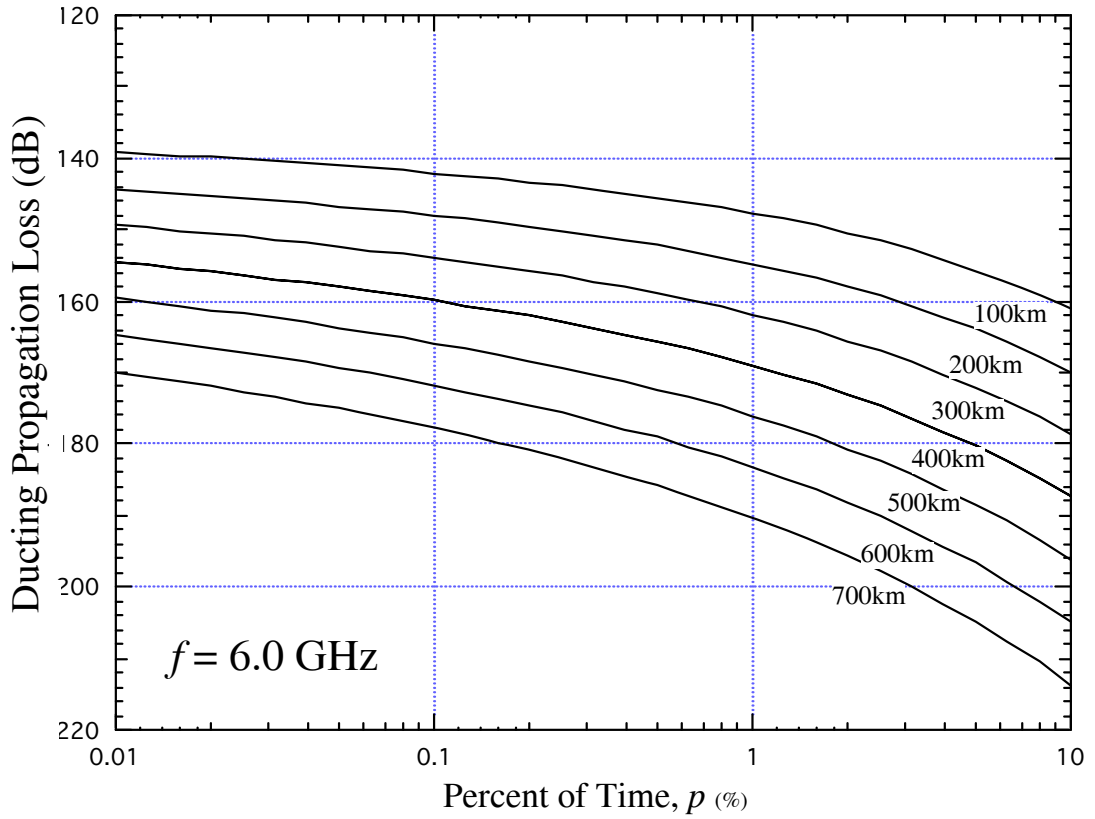


Figure 2-2-28

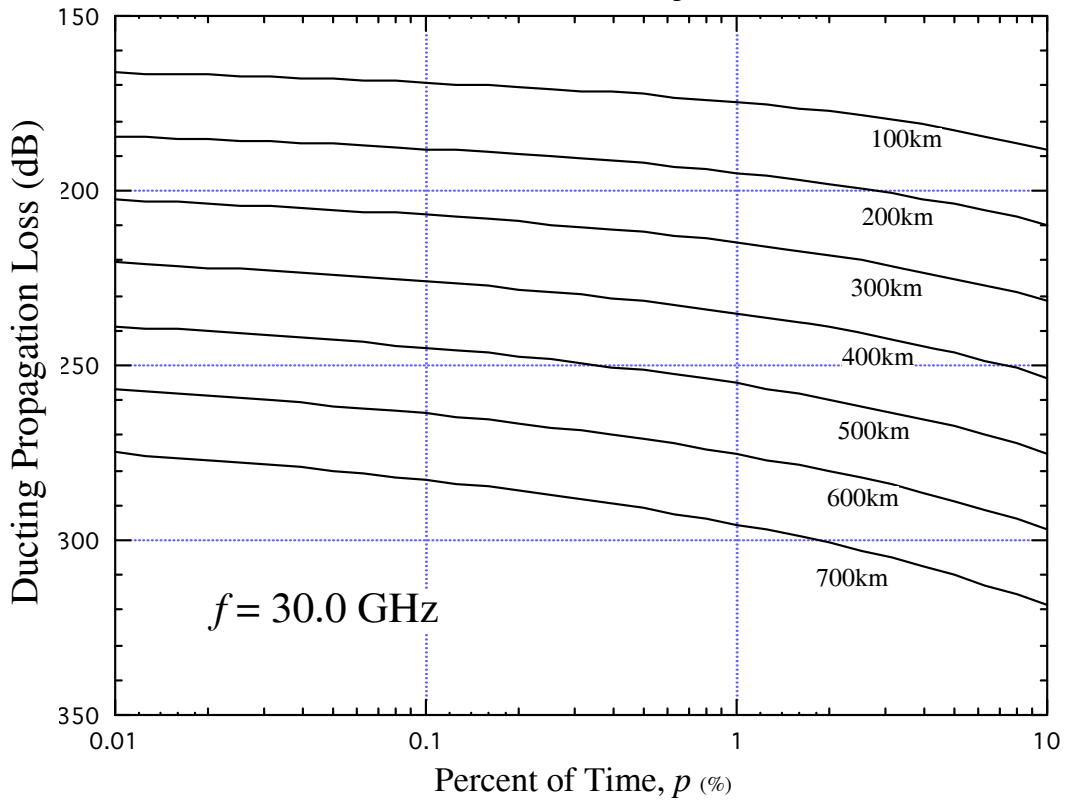
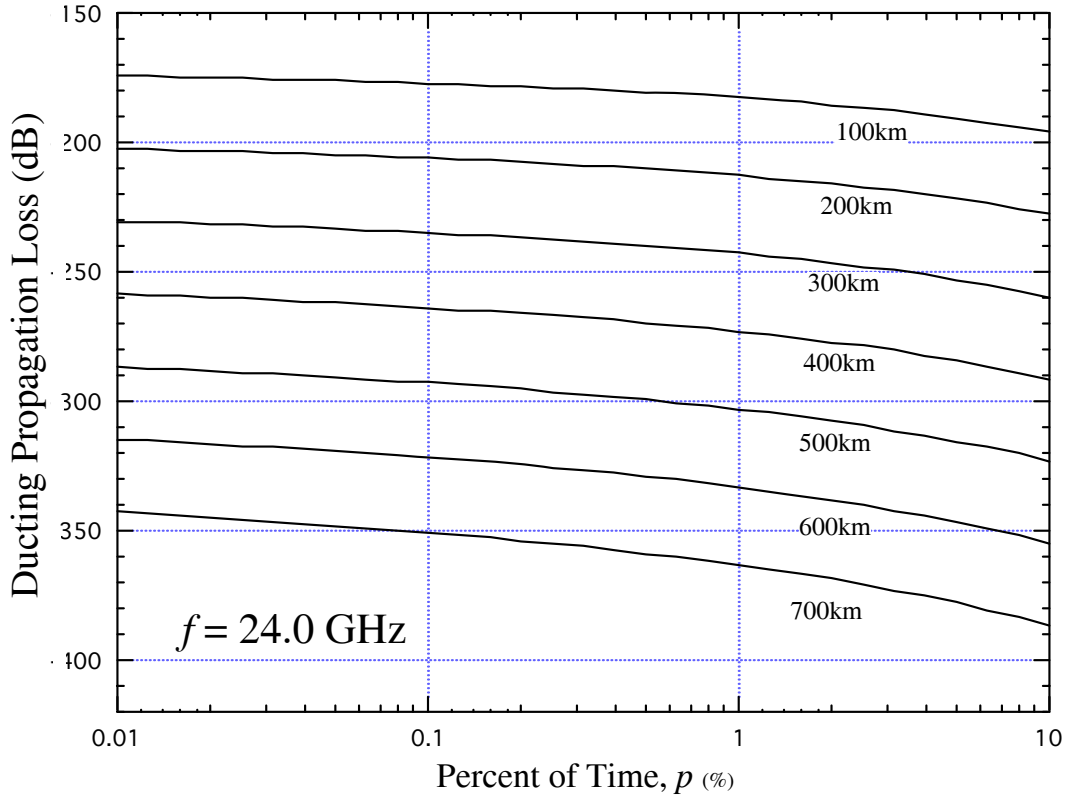


Figure 2-2-29

Patuxent River Base and Nearby Geographic Environment (38.3° N, 76.4° W)

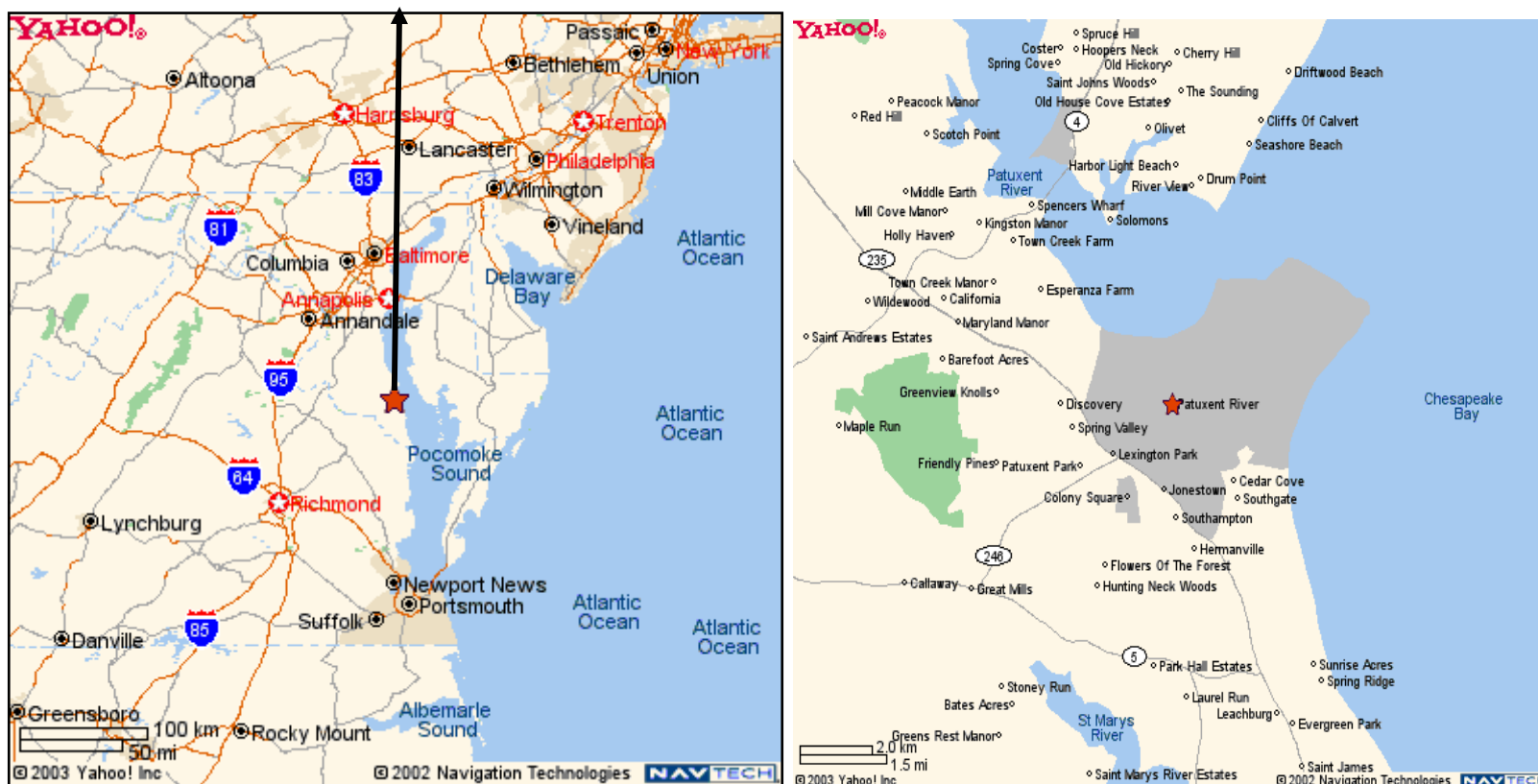


Figure 3-1-1

4/3 Earth
PR050Sep0803H.ques

Patuxent River -to- North 300km

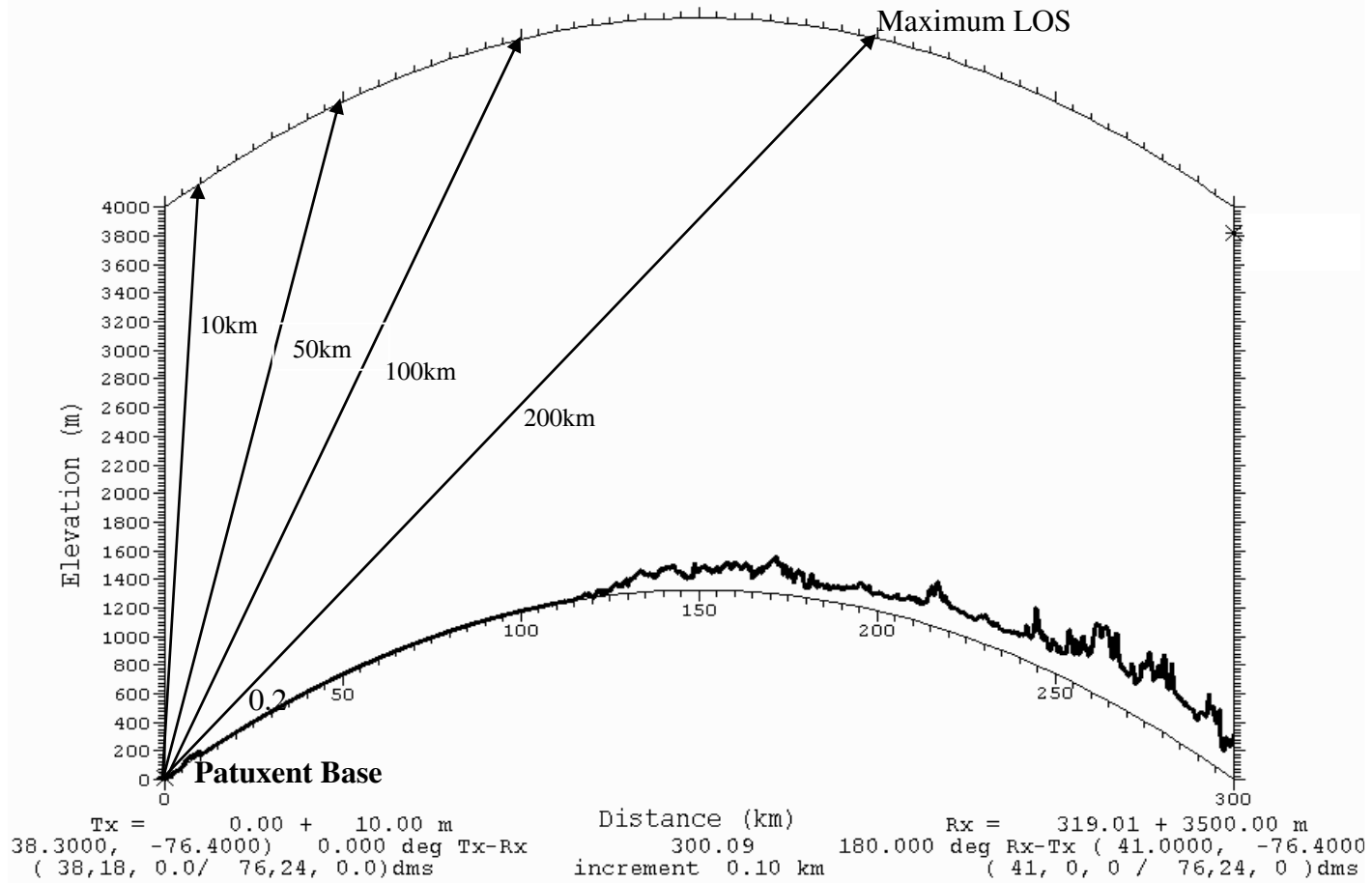


Figure 3-1-2



Figure 3-1-3

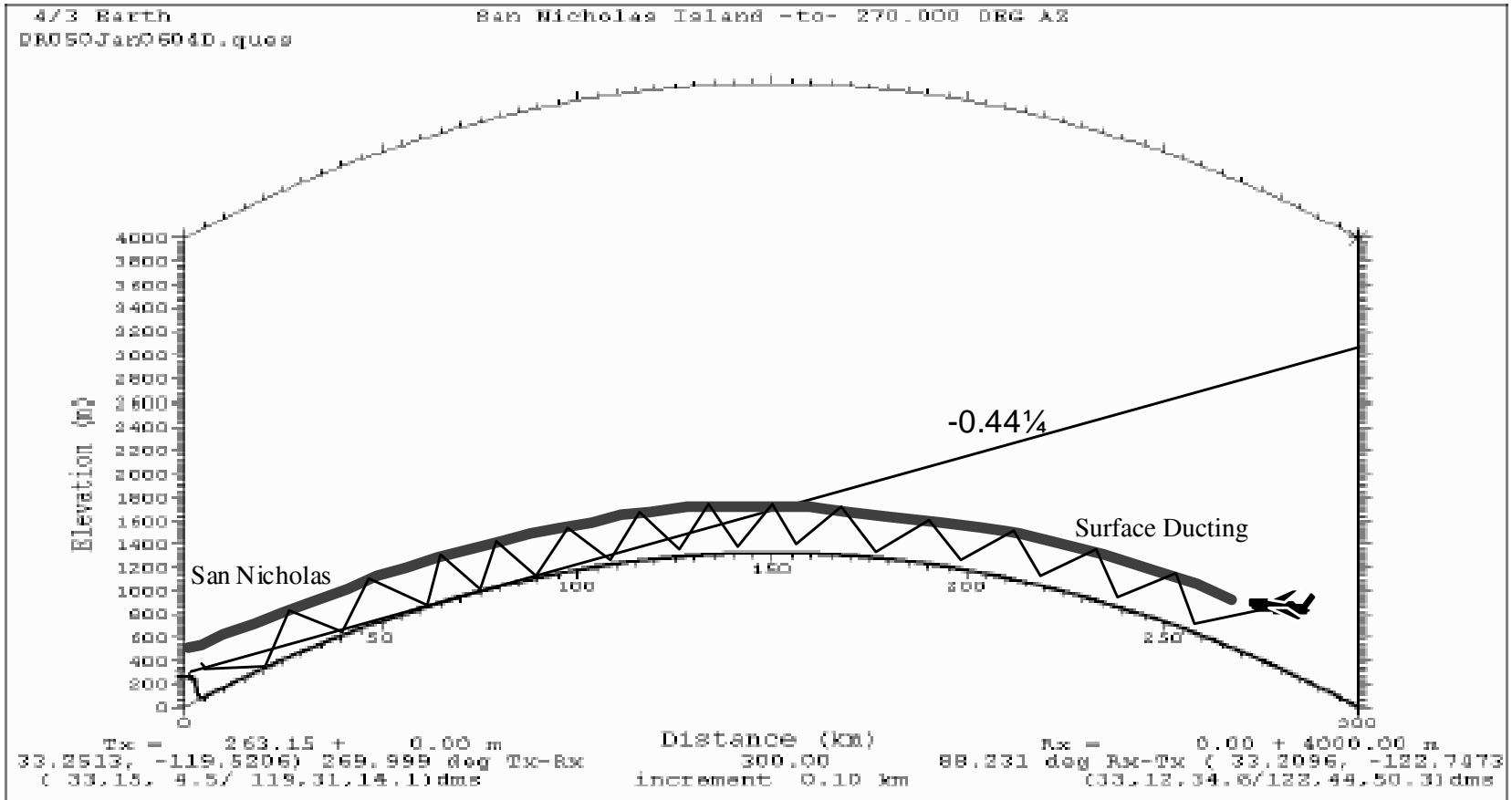


Figure 3-1-4

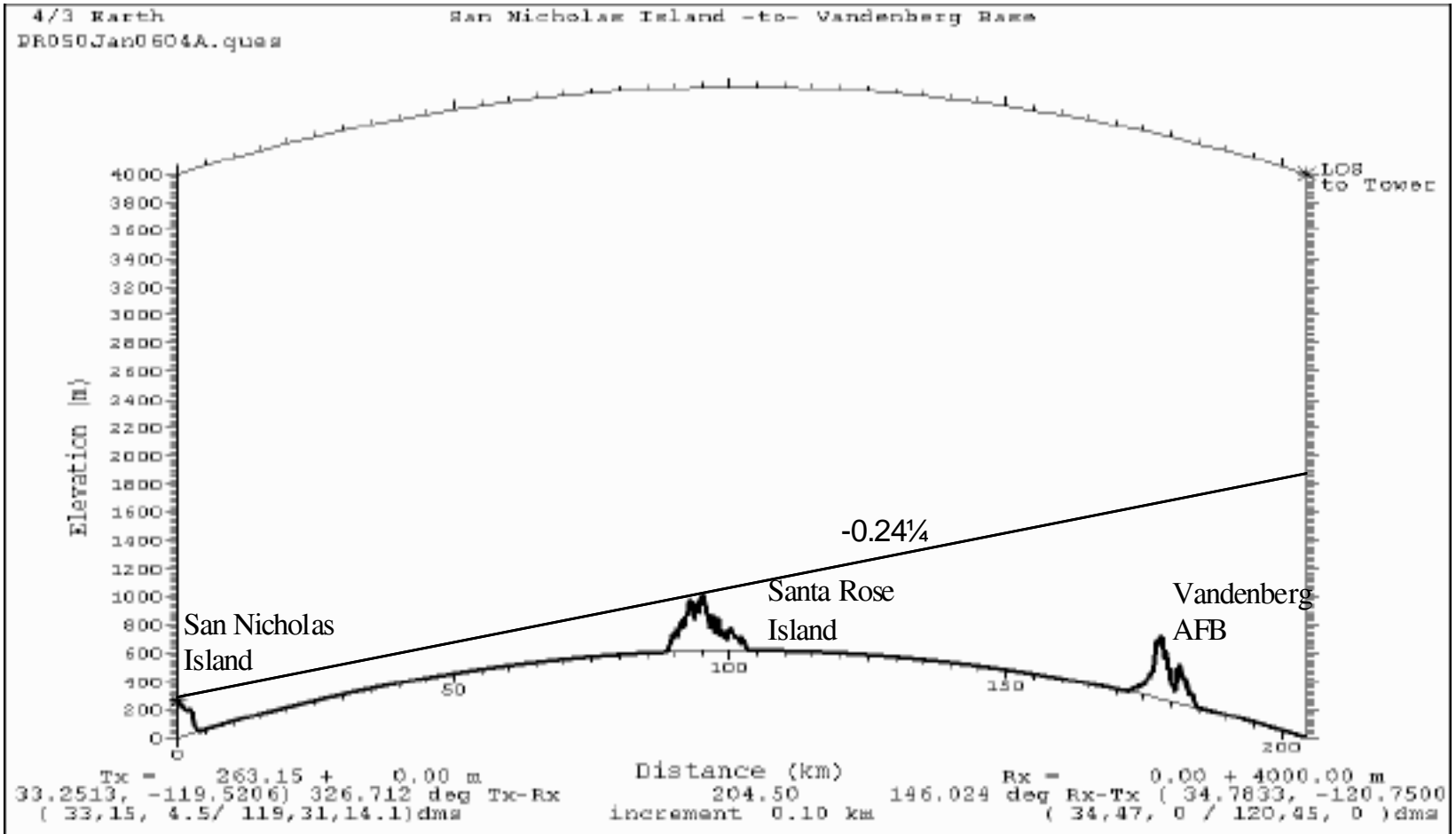


Figure 3-1-5

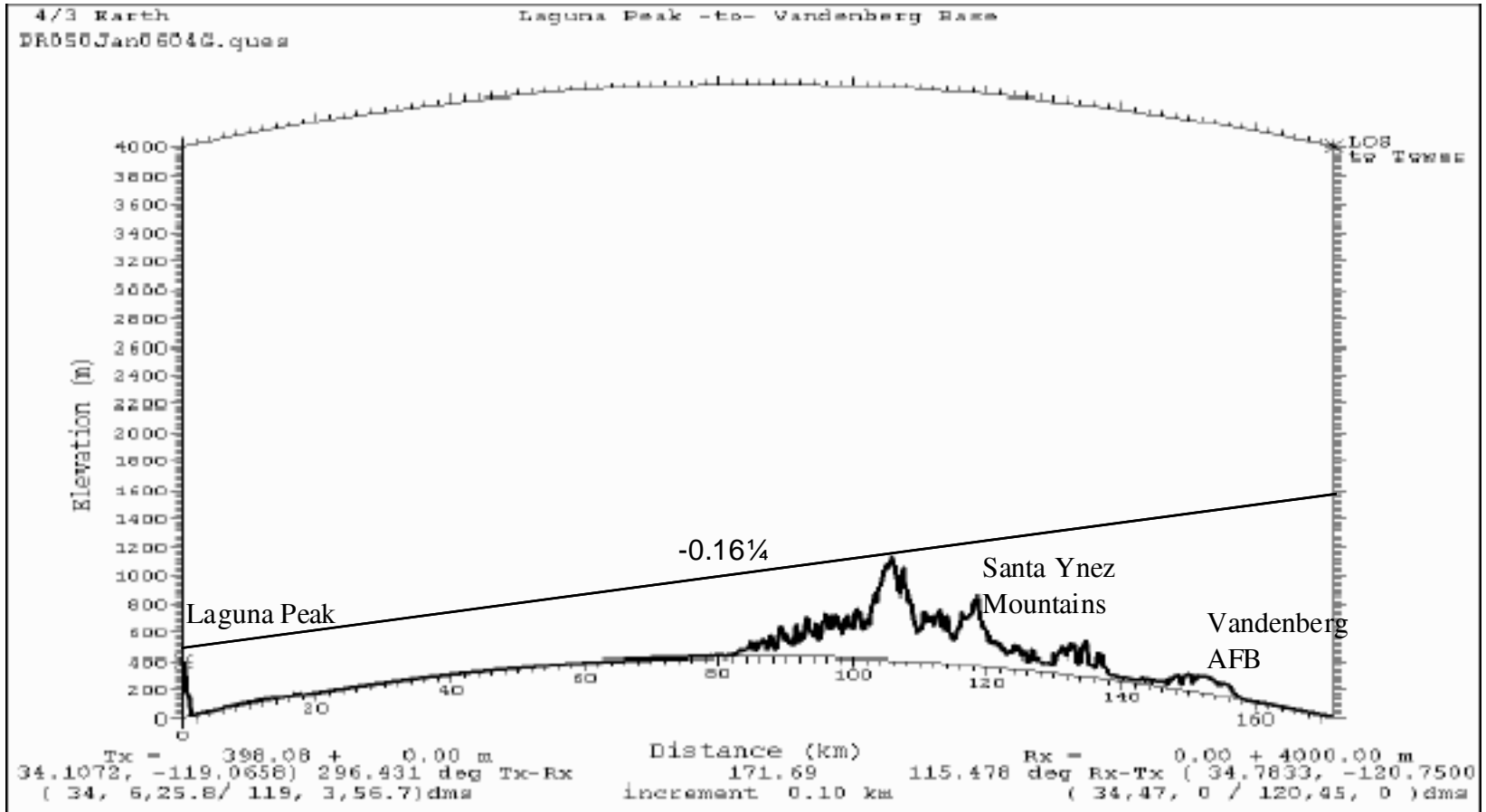


Figure 3-1-6

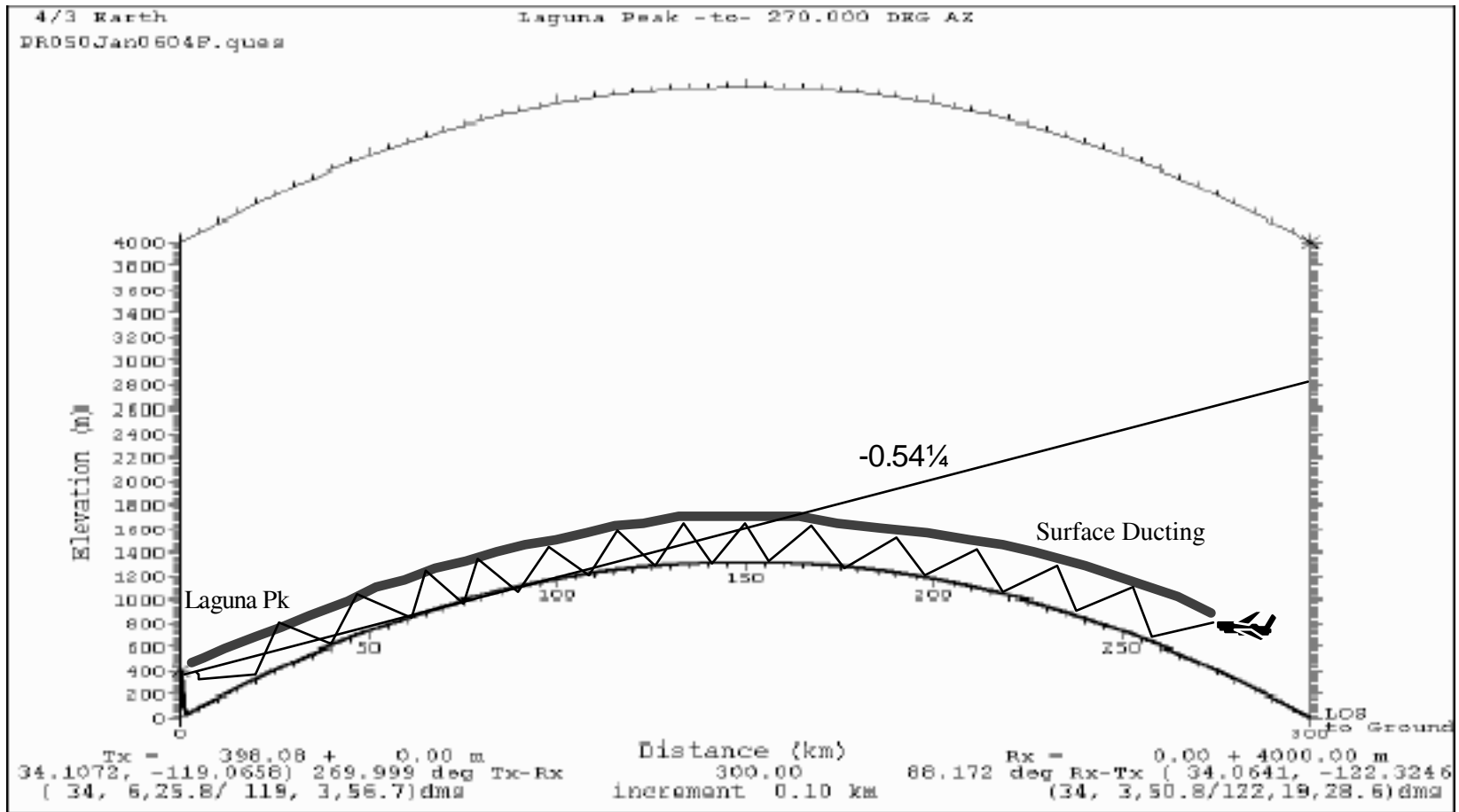


Figure 3-1-7

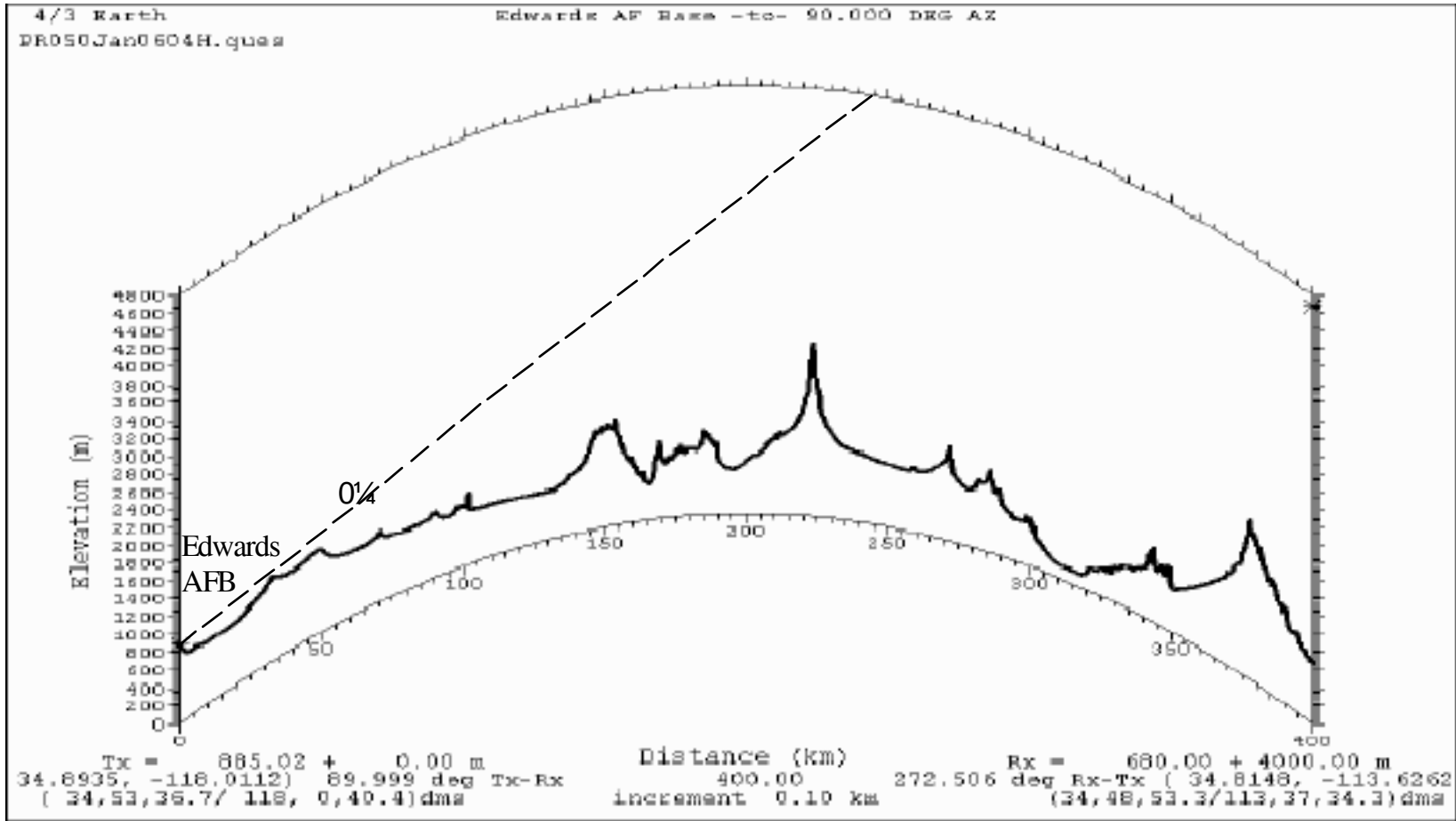
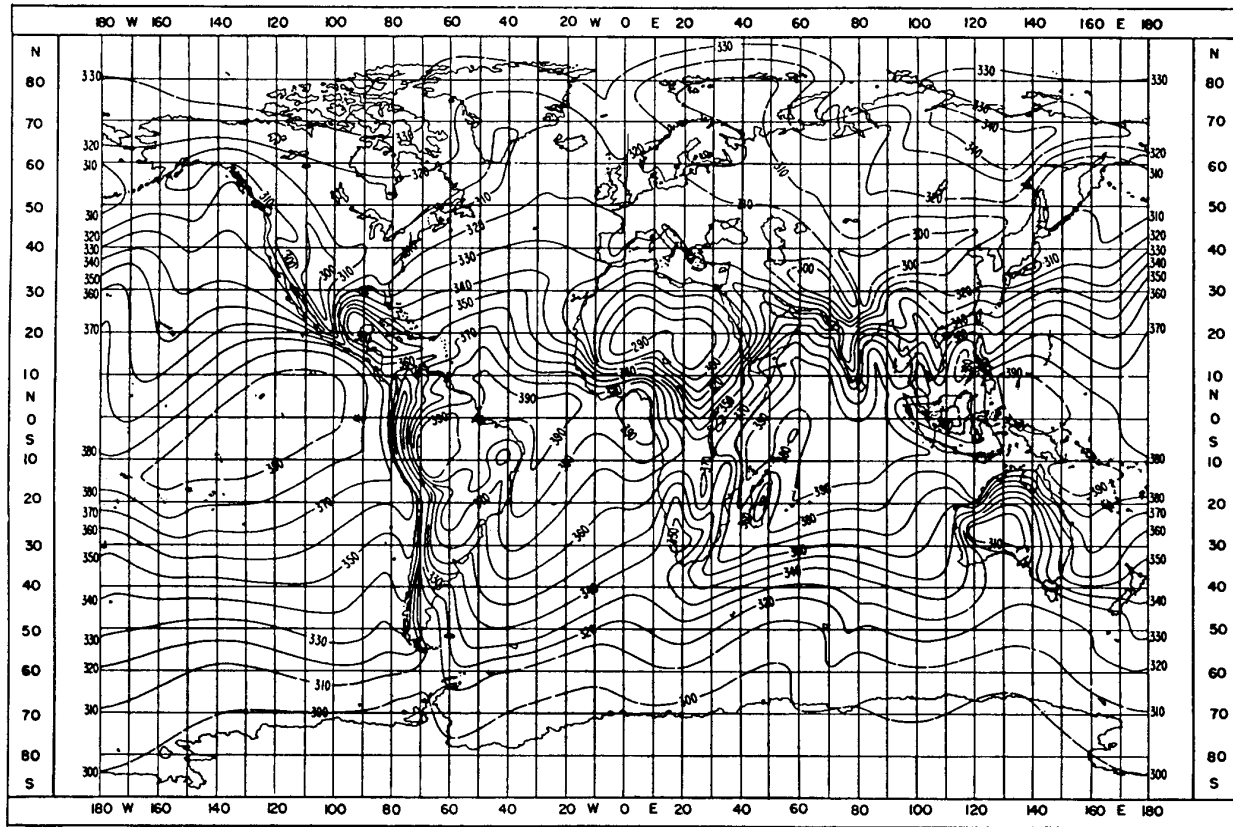


Figure 3-1-8

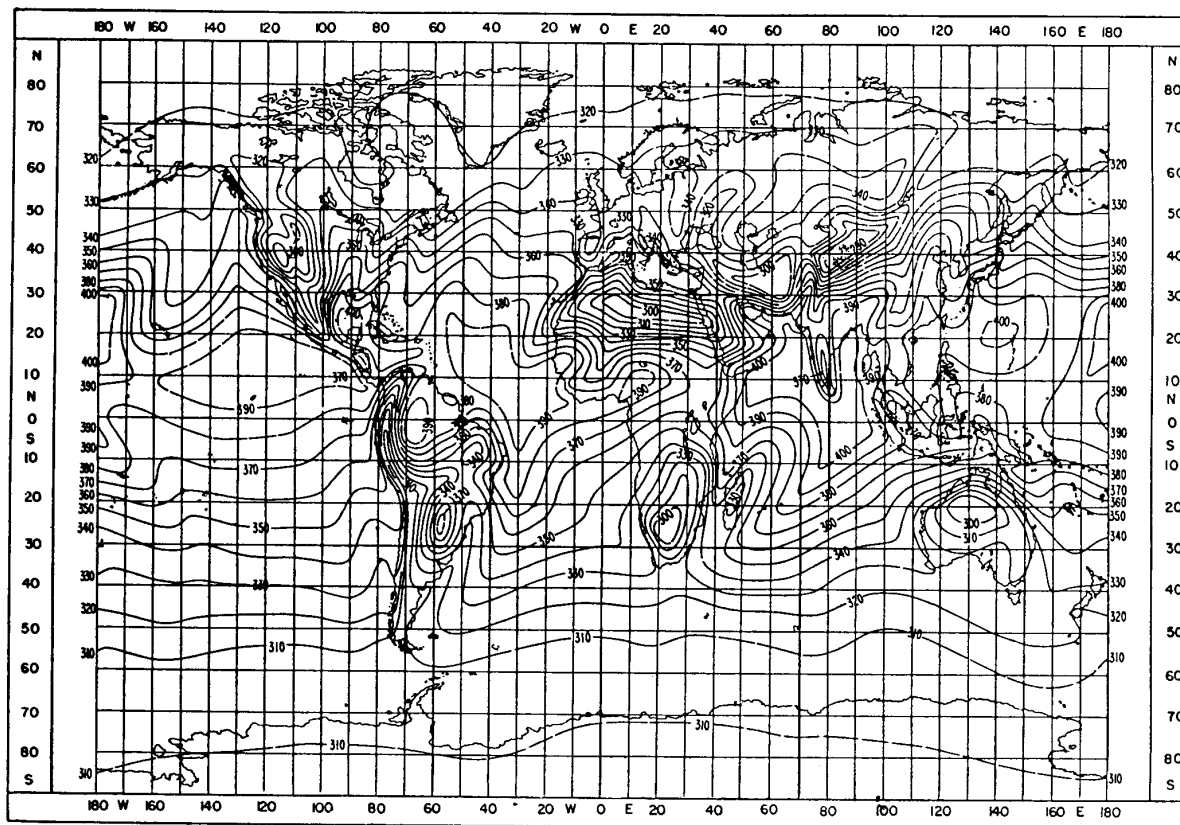
VII. Appendixes
Appendix I: Important Global Radio Climatologic Parameter Maps

FIGURE 1
Monthly mean values of N_0 : February



0453-01

FIGURE 2
Monthly mean values of N_0 : August



0453-02

Figure A-2

Monthly mean values of ΔN : February

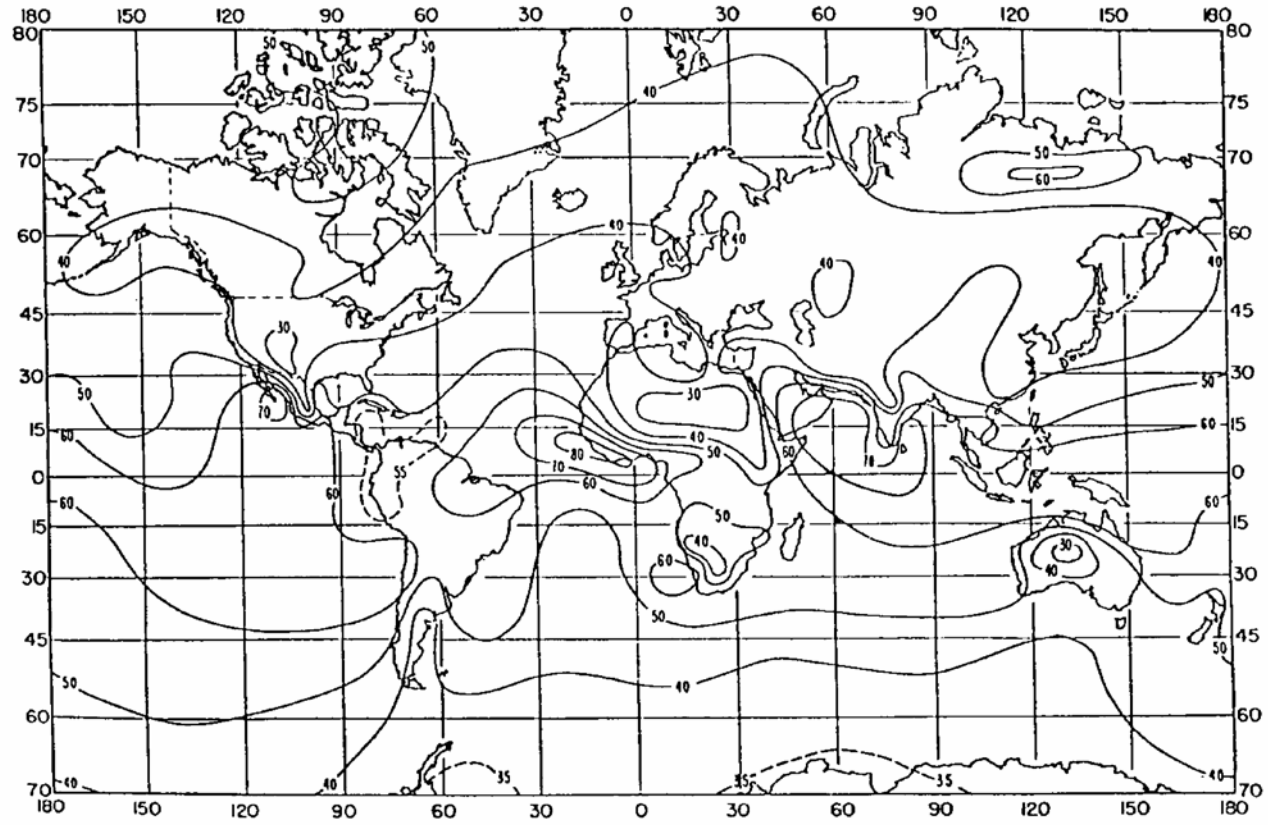


Figure A-3

Monthly mean values of ΔN : August

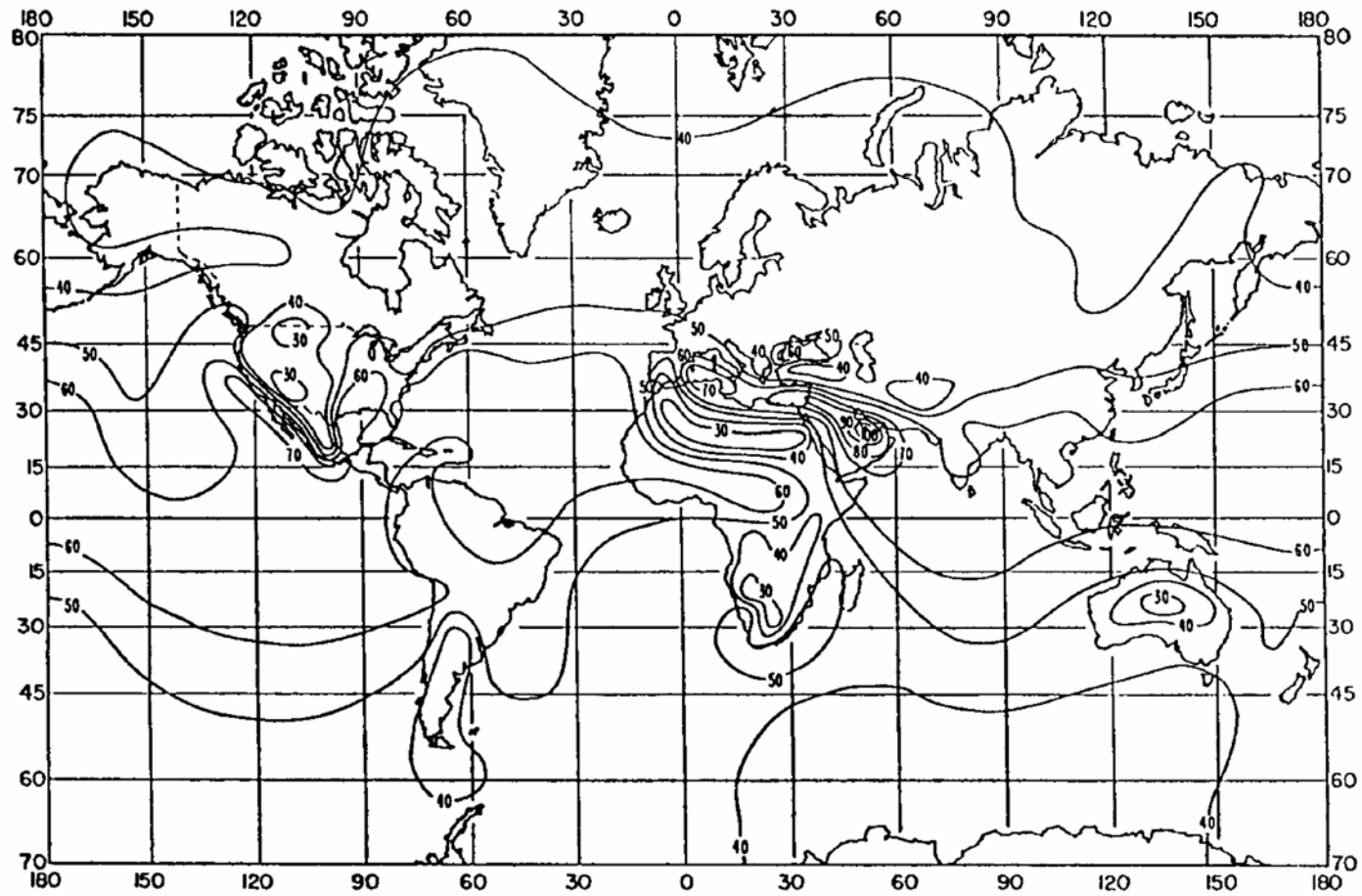


Figure A-4

FIGURE 2

December, January, February: surface water vapour density (g/m^3)

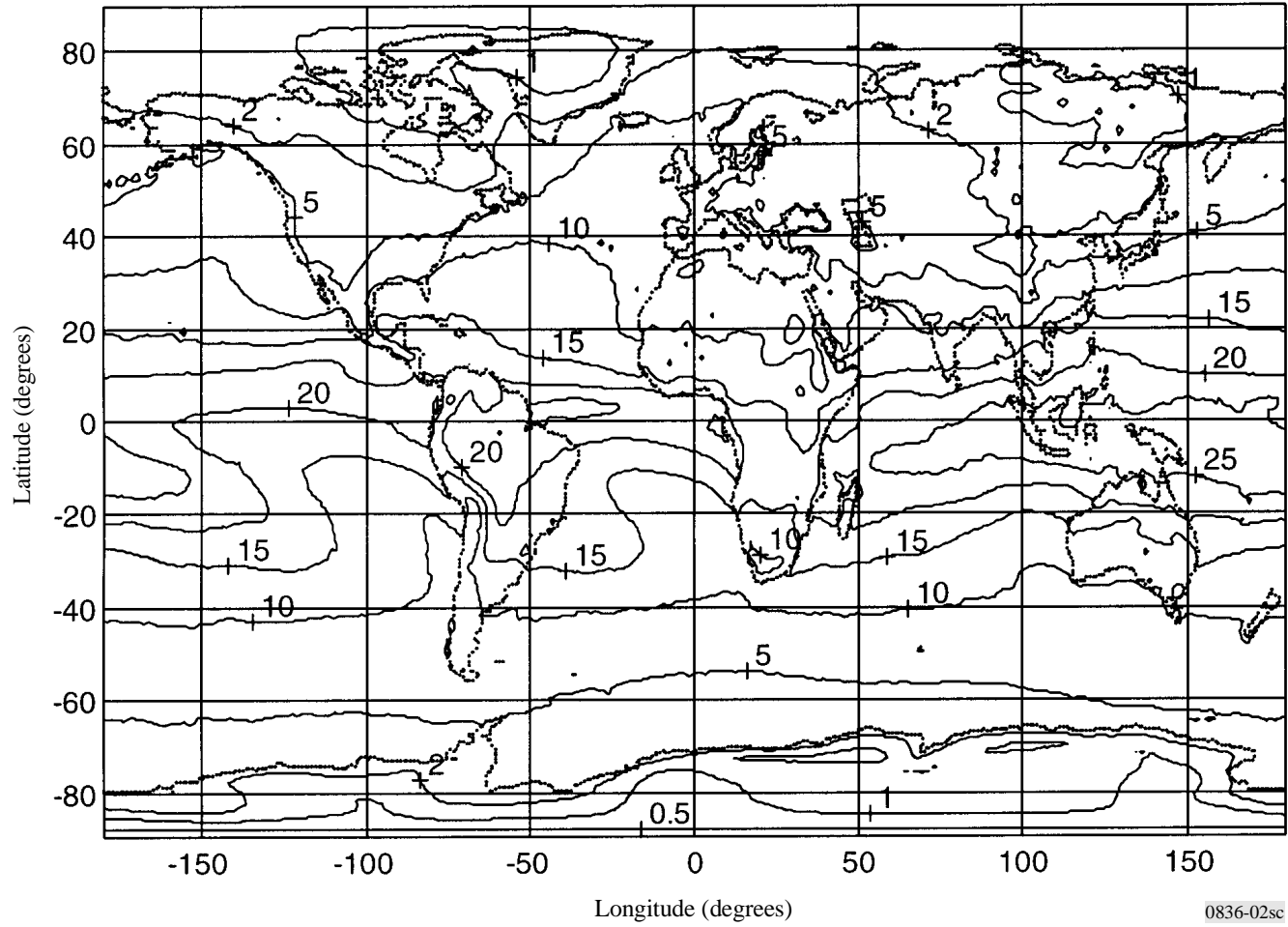


Figure A-5

FIGURE 4

June, July, August: surface water vapour density (g/m^3)

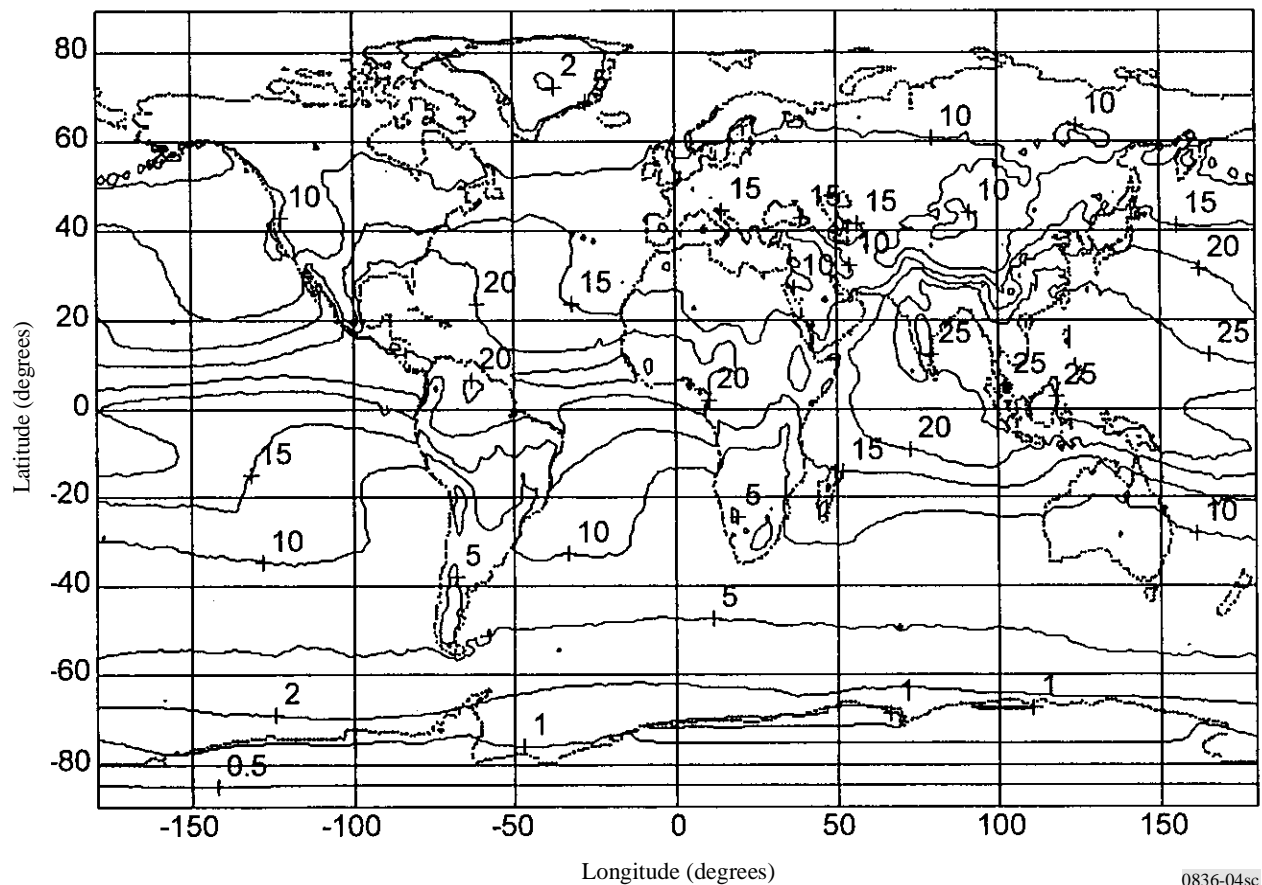
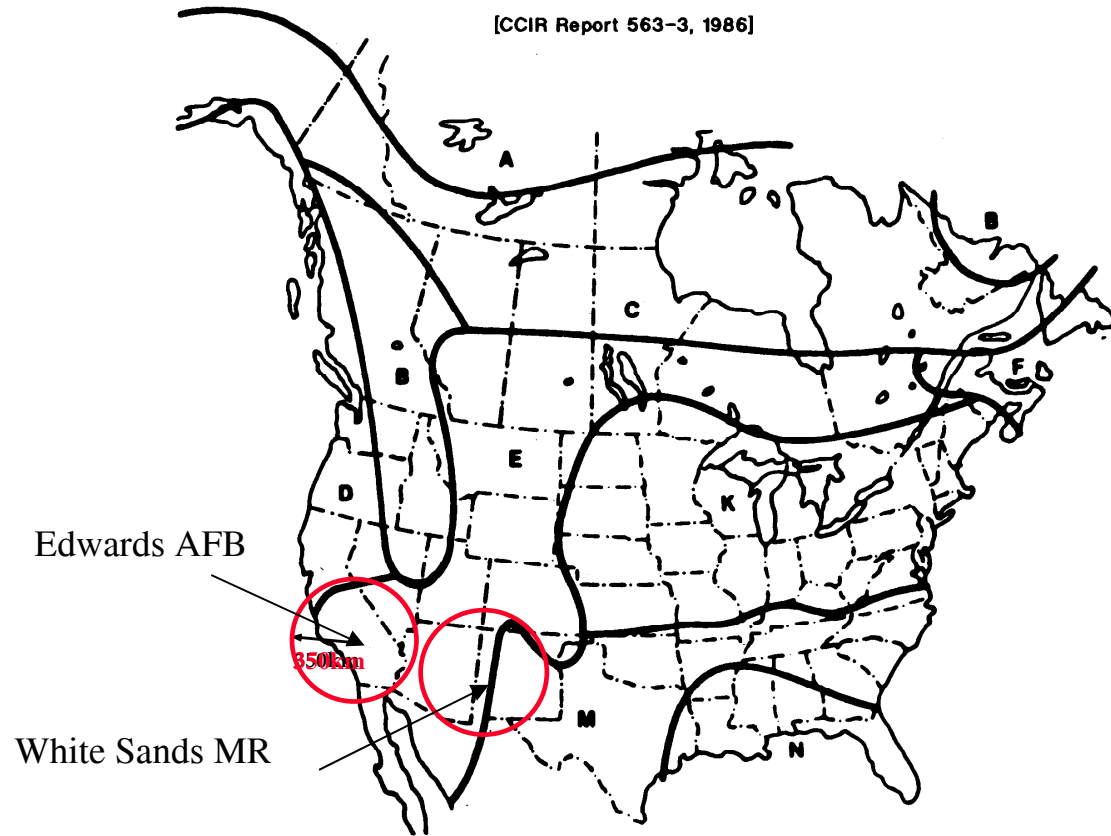


Figure A-6

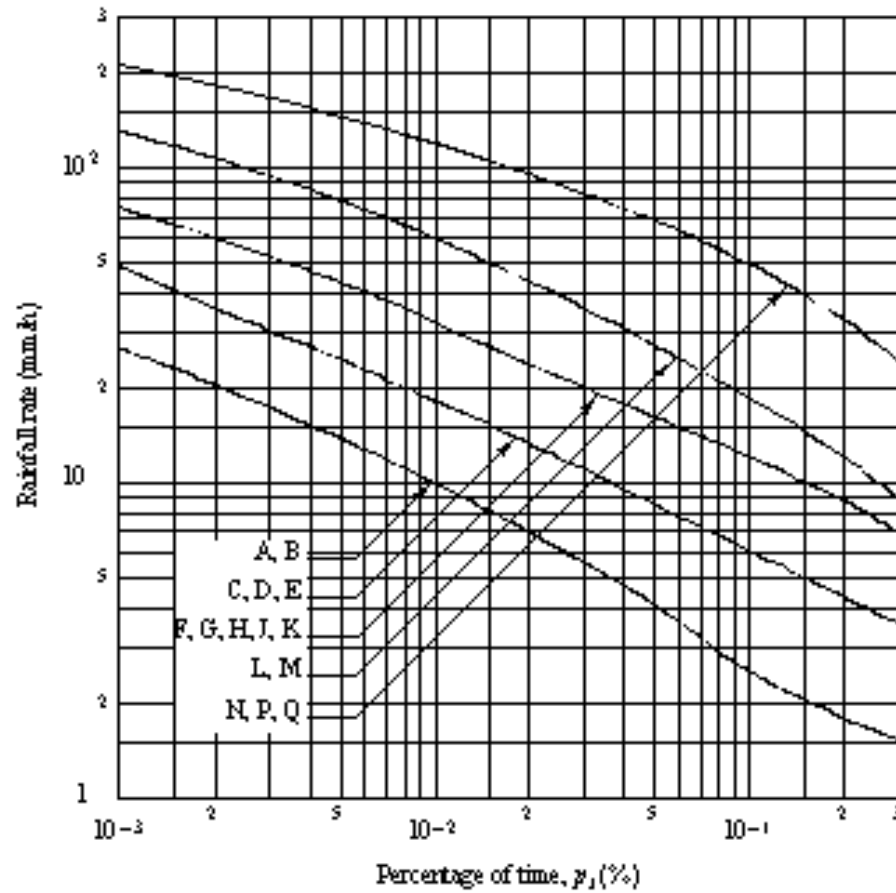
[CCIR Report 563-3, 1986]



Edwards AFB

White Sands MR

Figure A-7



Most Southern
California areas
are in Zone E

Figure A-8

Normalized total columnar content of cloud liquid water (kg/m²) exceeded for 1% of the year

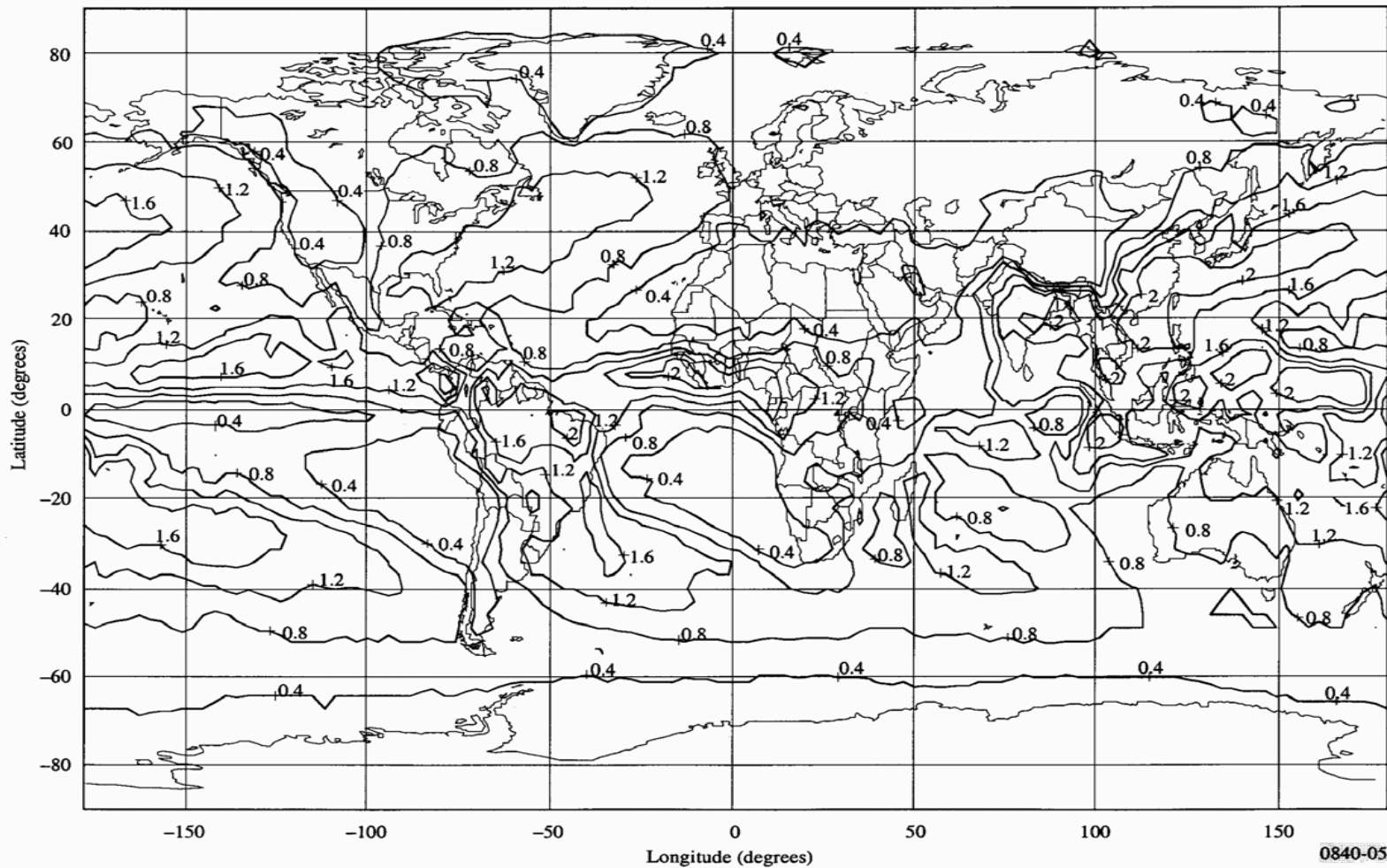


Figure A-9

Normalized total columnar content of cloud liquid water (kg/m²) exceeded for 10% of the year

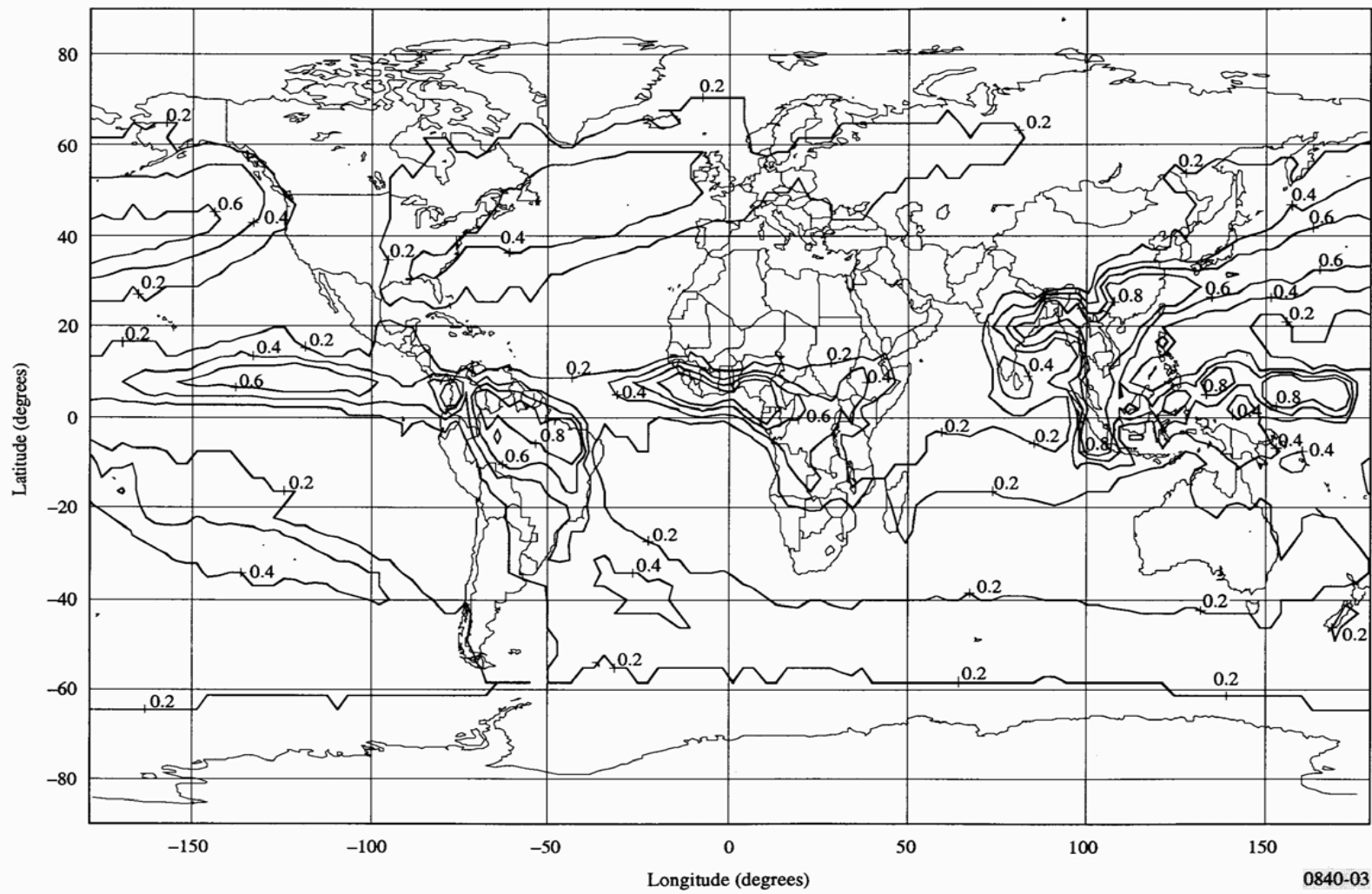


Figure A-10

Filename: S_OCCURRENCE.TXT

Average year surface duct occurrence, S_p (%)

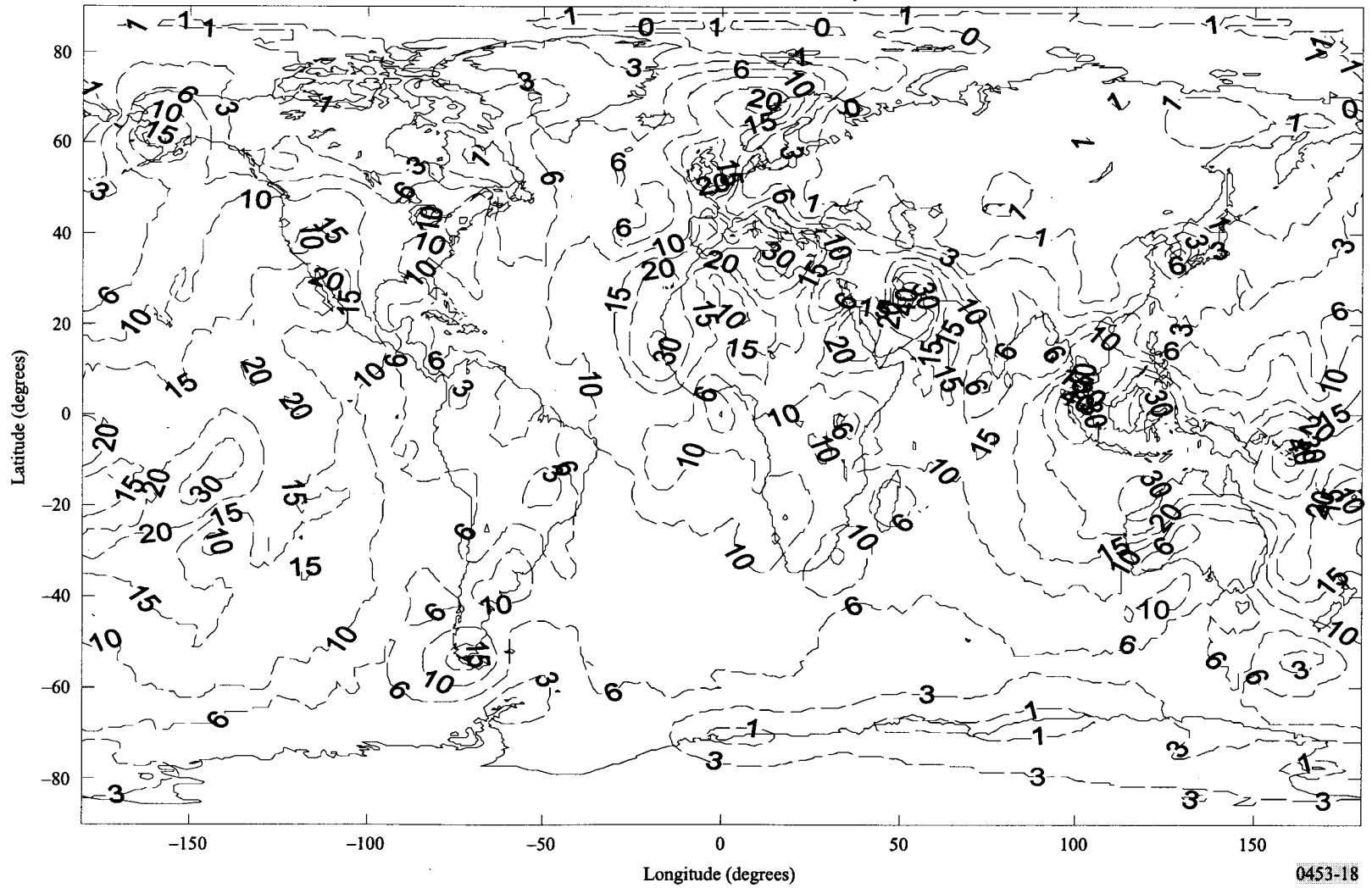


Figure A-11

0453-18

Filename: E_OCCURRENCE.TXT

Average year elevated duct occurrence, E_p (%)

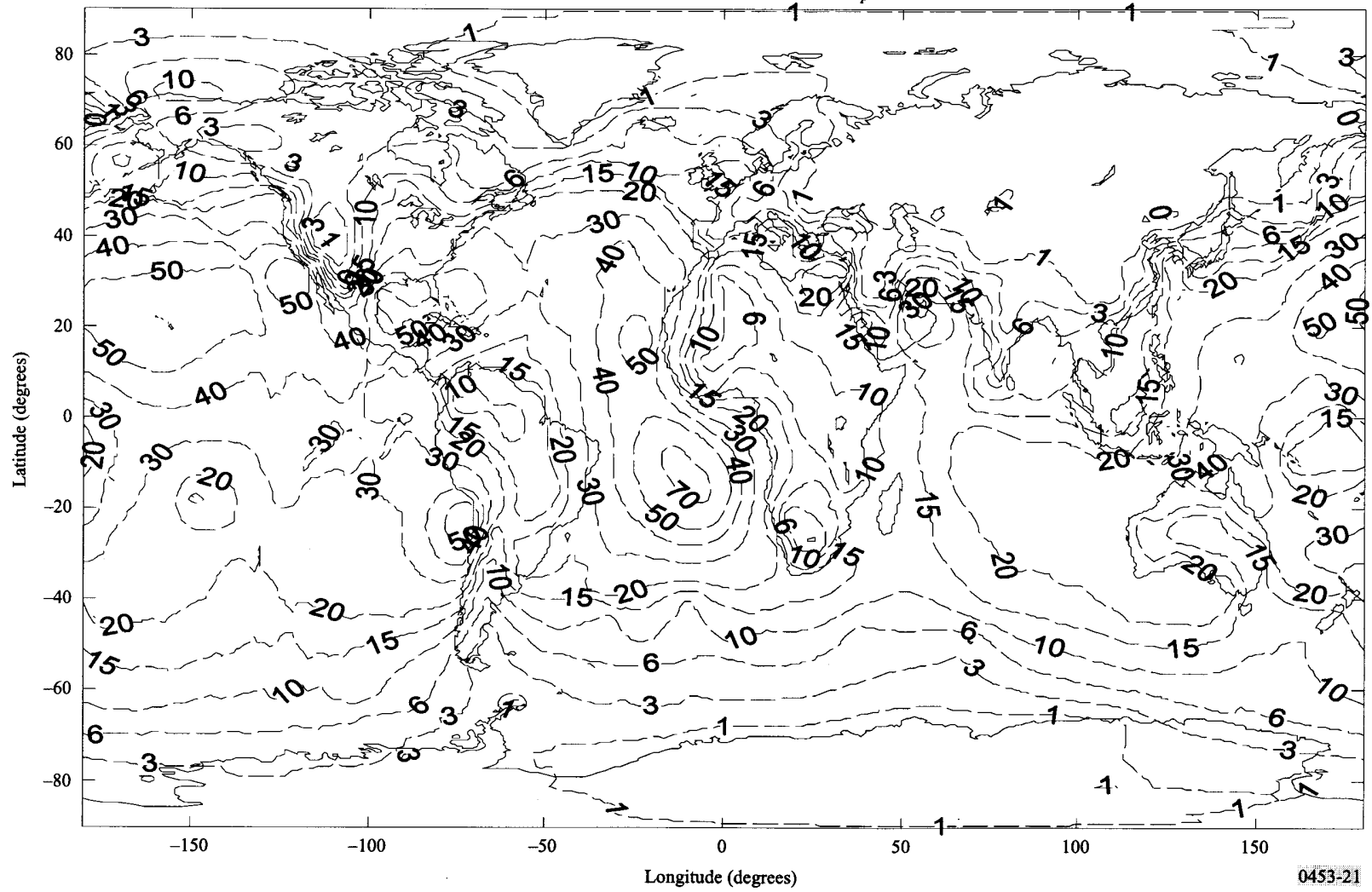


Figure A-12

Appendix II: Statement of Work

Task Description

Estimation of Microwave Power Margin Losses Due to Earth's Atmosphere in 3–30 GHz Frequency Range

Background

The Advanced Range Telemetry Project was tasked by the Department of Defense, Director Operational Test & Evaluation Central Test & Evaluation Investment Program and Test & Evaluation / Science and Technology Program, to study the technical and financial impact of moving some aeronautical telemetry (AT) operations to an unidentified band in the frequency range of 3 to 30 GHz. The majority of aeronautical telemetry (AT) links operate in the range of 1.4–2.4 GHz. One component of a comprehensive impact assessment is an authoritative determination of changes to link power margins that will be incurred as operating frequency increases. Another need is reliable identification of any new propagation anomalies that might arise at some frequencies in the range of investigation.

Estimation of Path Loss for Link Power Budget

The Friis free space equation is used to estimate distance related loss for most 1.4–2.4 GHz AT power budgets. Losses due to atmospheric absorption, clouds, fog, and precipitation are assumed to be negligible. A single lumped loss factor is normally used to compensate for fading and ducting. The compensation factor tends to be very rather conservative.

Parabolic reflector based directional receiving antennas are used in the vast majority of AT receiving sites. As operating frequency increases, it is well known that a given antenna aperture will generally compensate for increased path loss with increased gain. The 3-30 GHz study must reliably estimate upper and lower bounds on the degree to

which factors currently assumed negligible (such as atmospheric absorption and weather) will cause additional systematic and random losses at higher frequencies.

The atmospheric component study can be limited to a fairly small set of operating situations associated with two types of DOD Major Range Test Facility Bases (MRTFBs), i.e., desert range operations and sea range operations. Table 1 is a preliminary list of AT link situations seen at most of the ranges:

Table 1

Link Configuration Parameter	Significant Values
Receive antenna height above ground level (AGL)	(1) 50-100 foot tower mount. (2) 1500 foot elevation above average local terrain (hillside or hilltop site).
Transmit antenna height	10–100,000 feet AGL
Operating distances (slant range)	10 to 350 km
Receive antenna main lobe boresight angle to horizon (grazing angle)	Range: -5° to zenith
Percentage of time receive antenna grazing angle is at or below stated level	(1) 98%, 20° (2) 85%, 5°

Weather Conditions

Flight test operations tend to be conducted in clear weather conditions for a variety of reasons. However, even though visual flight rules (VFR) conditions may exist in a given operation area, this does not mean the RF links operate exclusively with clear line of sight (LOS) conditions. High altitude, long range links often peer through light to moderate cloud cover. In addition, sea range operations are often subject to significant ducting phenomenon due to marine layer moisture and temperature profile anomalies. At least two of the main “desert” ranges, namely Edwards Air Force Base and White Sands Missile Range frequently experience inversion layers. There is no historic or anecdotal evidence to indicate that overland inversion layers have a significant impact on 1.4–2.4

GHz propagation, but we need to know if these meteorological conditions will become a factor at higher frequencies.

Study Requirements

1. In cooperation with Advanced Range Telemetry Project (ARTM) staff representatives, establish a limited set of link scenarios to serve as useful benchmark comparison paths.
2. In cooperation with ARTM staff representatives, establish benchmark weather cases that will be applied to each scenario established in item 1.
3. Estimate upper and lower bounds on systematic and random path attenuation components at 3,6,12, 24 GHz, and any additional frequencies that might be identified as significant departure frequencies for non-uniform increases to loss factors.
4. Document study with a formal report of assumptions and findings.

Appendix III: Bibliography

1. Prediction procedure for the evaluation of microwave interference between stations on the surface of the earth at frequencies above about 0.7 GHz, Recommendation ITU-R P.452-9, 1999.
2. Determination of the coordination area of an earth station operating with a geostationary space station and using the same frequency band as a system in a terrestrial service, Recommendation ITU-R IS.847-1, 1993.
3. Radiometric estimation of atmospheric attenuation, ITU-R P.1322-9, 1999.
4. The radio refractive index: its formula and refractivity data, ITU-R P.453-9, 2001.
5. Calculation of free-space attenuation, ITU-R P.525, 1999
6. Propagation data required for the evaluation of coordination distances in the frequency range 100 MHz to 105 GHz, Recommendation ITU-R P.620-4, 1999.
7. Attenuation by Atmospheric Gases, Recommendation ITU-R P.676-4, 1999.
8. Propagation by diffraction, Recommendation ITU-R P.526-8, 2003.
9. Propagation data and prediction methods required for the design of terrestrial line-of-sight systems, ITU-R P.530-10, 2003.
10. Propagation prediction techniques and data required for the design of trans-horizon radio-relay systems, ITU-R P.517, 2003.
11. Propagation data and prediction methods required for the design of Earth-space telecommunication systems, ITU-R P.618, 2003.
12. Propagation data required for the evaluation of interference between stations in space and those on the surface of the Earth, ITU-R P.619, 2003.
13. Effects of tropospheric refraction on radiowave propagation, ITU-R P.834-4, 2003.
14. Water vapour: surface density and total columnar content, ITU-R P.836, 2003.
15. Characteristics of precipitation for propagation modeling, ITU-R P.837, 2003.
16. Specific attenuation model for rain for use in prediction methods, ITU-R P.838, 2003.
17. Attenuation due to clouds and fog, ITU-R P.840, 2003.
18. Mathematical model of average and related radiation patterns for line-of-sight point-to-point radio-relay system antennas for use in certain coordination studies and

interference assessment in the frequency range from 1 GHz and to about 70 GHz, Recommendation ITU-R F.1245-1, 2000.

19. Flock, W.L., Propagation effects on satellite systems at frequencies below 10 GHz, *A handbook for satellite systems design*, NASA Reference Publication 1102, 1987.
20. CCIR, Scattering by precipitation, Report 882-1, in Vol. V, *Propagation in Non-ionized Media*, Recommendations and Reports of the CCIR, 1886, Geneva: Intl. Telecomm. Union, 1986.
21. Radio Regulations, Appendix S7, Method for the determination of the coordination area around an earth station in frequency bands between 1 GHz and 40 GHz shared between space and terrestrial radiocommunication services (Former Appendix 28), Edition, 1990, Revised, 1997.
22. Rice, P.L., et al., Transmission loss predictions for tropospheric communication circuits, Vol. I, National Bureau of Standards, US Department of Commerce, Washington, DC, Technical Note 101, January, 1, 1967.
23. Rice, P.L., et al., Transmission loss predictions for tropospheric communication circuits, Vol. II, National Bureau of Standards, US Department of Commerce, Washington, DC, Technical Note 101, January, 1, 1967.